Calcium Transport and Regulation in Male and Female Rat Kidney

by

Shervin Hakimi

A thesis
presented to the University of Waterloo
in fulfillment of the
thesis requirement for the degree of
Master of Mathematics
in
Applied Mathematics

Waterloo, Ontario, Canada, 2023

Author's Declaration

This thesis consists of material all of which I authored or co-authored: see Statement of Contributions included in the thesis. This is a true copy of the thesis, including any required final revisions, as accepted by my examiners.

I understand that my thesis may be made electronically available to the public.

Statement of Contributions

This thesis contains research work that is based on a manuscript in preparation. Shervin Hakimi contributed to the design of the mathematical model, wrote the computational code, ran the simulations, analyzed the data, interpreted the results, prepared the figures, and drafted and revised the manuscript. Anita Layton contributed to the design of the mathematical model, analyzed the data, interpreted the results, and drafted and revised the manuscript.

Abstract

Calcium is an essential mineral that plays a critical role in many biological processes, such as muscle contraction, nerve function, and bone health. However, maintaining the right balance of calcium in the body is crucial since both high and low levels can have harmful effects. To ensure this balance, the kidney plays a crucial role in regulating calcium homeostasis by reabsorbing calcium in specific segments of the nephron, including the proximal tubule, thick ascending limb, and the late part of the distal convoluted tubule and connecting tubule, and controlling the amount of calcium that is excreted in the urine.

This thesis focuses on the computational modelling of renal epithelial calcium handling and sex differences of this process in male and female rat kidneys. Renal epithelial isolated cell models with emphasis on calcium transport are discussed and expanded to a nephron model for both male and female models. Sex differences were observed in the permeability of the proximal tubule to calcium and the expression of calcium channels and pumps in the late part of the distal convoluted tubule and connecting tubule. Our results revealed lower calcium reabsorption along the proximal tubule and thick ascending limb, and higher reabsorption along the late part of the distal convoluted tubule and connecting tubule in the female rat kidney model. Furthermore, the male rat kidney model showed higher urinary calcium excretion compared to the female rat kidney model, consistent with animal experiments.

We investigated the effects of perturbations in calcium-specific channels and transporters and sodium-specific transporters on renal calcium handling in male and female rat kidneys. Our findings revealed that inhibiting sodium-specific transporters had a significant impact on renal calcium transport, whereas inhibitions of calcium-specific channels and transporters had minimal effects on sodium transport. We observed that inhibiting Na^+/H^+ exchanger 3, Na^+-K^+-$2Cl^-$ co-transporter, and Na^+-Cl^- co-transporter resulted in increased urinary calcium excretion in both male and female models, while epithelial Na^+ channel inhibition led to decreased urinary calcium excretion in both male and female models.

Acknowledgements

Not too long ago, we played *Dixit*, a creative board game, at Dr. Anita Layton's home. In this game, each player chooses an illustrated card and gives a one-word clue. Scoring is based on finding the intended card without making the clue too obvious or vague. Despite some easy and hard cards, one with a balance scale surprised everyone with its intended word, kidney. I would like to thank my supervisor, Dr. Anita Layton, not only for her constant support, expertise, and teachings on being thorough and independent, but also for reminding me that even when we are busy, we need to make time for fun. I would also like to thank her for teaching me that a lot can be learned and accomplished in a short time span.

I am grateful to my committee members, Dr. Mohammad Kohandel, Dr. Anita Layton, and Dr. Matthew Scott, for dedicating their time and expertise to reviewing my thesis.

I have received support from many friends throughout my journey, and I am thankful for all of them. Among them, there is one friend who has always been there for me through thick and thin: Mehrshad Sadria. He is a true friend who constantly pushed me to be a better version of myself in various areas of life. Not only did he sit alongside me in the lab, but we also shared many memorable moments outside of it, from long walks and discussions on research and life to ice rinks and benches. He truly is a constant source of support and a one-of-a-kind researcher.

I would also like to thank my lab members: Chris West, Melissa Stadt, Pritha Dutta, Kaixin Zheng, Delaney Smith, Stephanie Abo, Karolina Suszek, Amandeep Kaur, Chi-Chung Cheung, Matt Wiens, Karolina Suszek, William Bell, and Anderson White. I have learned something from each one of them.

Last but not least, I want to express my heartfelt gratitude to my family for their unconditional love and support throughout all stages of my life. I am truly grateful for their unwavering presence in my life.

Dedication

I dedicate this thesis to my *Noorhaye Cheshm*: my mom, dad and sister, Shirin.

Table of Contents

List of Figures

List of Tables

Chapter 1

Physiology Background

The kidneys are vital organs that play a key role in the balance of electrolytes and fluid in the body by constantly filtering the blood. Homeostasis, defined as the steady internal state of the body is maintained by the kidneys: excretion of wastes and reabsorption of crucial solutes and water are actions that are sustained by the accumulative function of the tubules in the kidney, known as the nephrons. Furthermore, the kidney is also responsible for the acid-base balance (pH) of the blood and produces hormones such as calcitriol, responsible for calcium reabsorption and erythropoietin, required for red blood cell production [43, 61]. The kidney also plays an important role in the regulation of blood pressure [7]. In this chapter, I provide the necessary physiological background and first cover the anatomy of the kidney and the structure of the nephrons, discuss the dynamics of tubular reabsorption in, and provide the motivation for understanding calcium transport and regulation in the nephron along with understanding sex differences in calcium transport.

1.1 Kidney Structure

1.1.1 Kidney Anatomy

The bean-shaped organ is located on either side of the vertebral column close to the spine [140]. The kidney consists of a solid tissue called parenchyma also known as the functional tissue. The cortex of the kidney is the outside, light-red portion of the organ, while the medulla is the interior, darker part, as can be seen in Fig. 1.1. The renal medulla comprises of several renal pyramids made out of straight blood arteries and tubular structures, giving them the appearance of being striated [19]. The papillae, which point towards

the kidney's center, make up the innermost portion of the pyramids. The renal columns are the areas surrounding the renal pyramids.

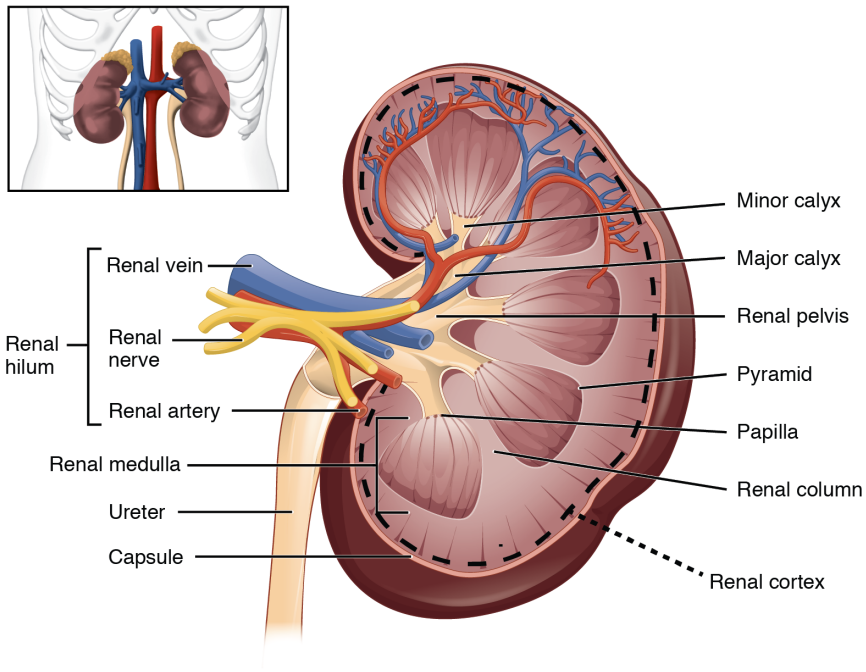

Figure 1.1: Depiction of the anatomy of the kidney. The renal cortex, medulla and papillae along with the renal pyramids and columns are presented in this figure. Figure taken from *Anatomy & Physiology* by Bige et al. [19].

1.1.2 Glomerular Filtration

Glomerular filtration is the procedure to filter blood supplied by afferent arterioles to the glomerulus (also known as the Bowman's capsule). The volume of filtrate generated by the kidneys is defined as the glomerular filtration rate (GFR), which is used to assess kidney function. The GFR varies between genders and is controlled by renal blood flow, glomerular capillary pressure, and filtration coefficient [128]. The glomerular capillaries' surface area and the filtration barrier's permeability both affect the filtration coefficient [153]. The fenestrated endothelium of the glomerular capillaries, the basement membrane, and the

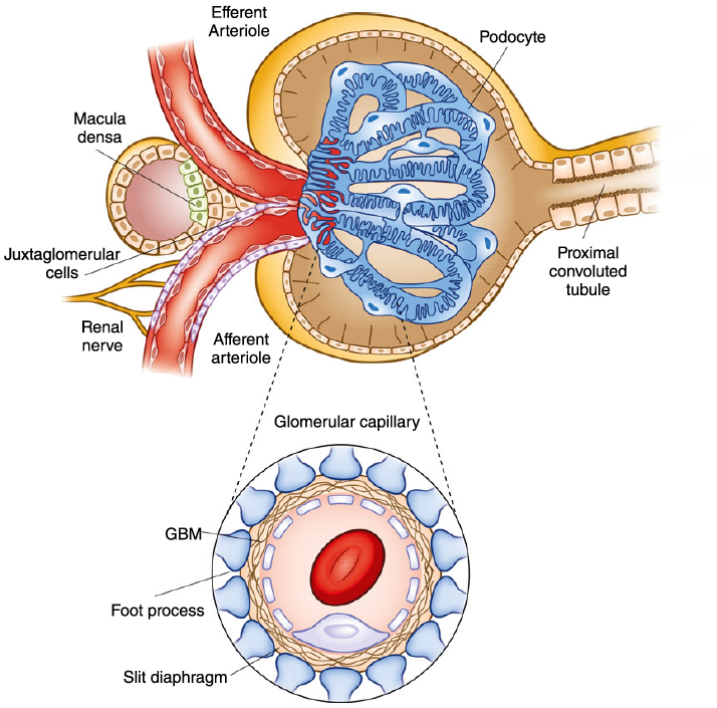

Figure 1.2: The glomerulus or Bowman's capsule. The layers that make up the filtration barrier are depicted. The outermost layer is composed of the visceral epithelial cells, the podocytes, the glomerular basement membrane and finally the fenestrated endothelial cells. The figure is taken from Ref. [112].

podocytes make up the three layers that make up the filtration barrier (see Fig. 1.2) and stymies the passage of large molecules such as proteins into the urine [112].

1.1.3 Nephron Structure

Nephron Segments

Each kidney is composed of renal tubules called nephrons which are thousands in rats and millions in humans [63, 17]. The nephron is responsible for filtering and processing the blood and reabsorbing and secreting key solutes [7]. Each nephron consists of the Bowman's capsule and a tubular system. The filtered blood enters the tubular system, beginning with the proximal tubule, which is divided into the proximal convoluted tubule

(also known as the S1-S2 segment), and the proximal straight tubule (also known as the S3 segment). Following the proximal tubule is the loop of Henle, which consists of the descending limb, thin ascending limb and thick ascending limb. The subsequent segments are the distal convoluted tubule and the connecting tubule. At the end is the collecting duct which consists of the cortical collecting duct, outer medullary collecting duct and the inner medullary collecting duct [7]. The collecting duct collects the fluids of several nephrons together. The structure of the kidney along with its respective segments is represented in Fig. 1.3. Each of these segments plays a specific role in solute and water reabsorption:

Superficial and Juxtumadullary Nephrons

Nephrons are categorized as superficial or juxtamedullary based upon the location of the glomerulus: superficial nephrons have glomeruli located near the surface of the kidney and give rise to a loop of Henle that only penetrates the outer medulla and is shorter than the juxtamedullary nephron, wheareas the juxtamedullary has both a longer loop of Henle and penetrates deep into the renal medulla [100]. The number of nephrons in rats is 36,000 and only 1/3 of the nephrons in the rat kidney are juxtumadullary nephrons (i.e., 24,000 superficial nephron and 12,000 juxtumedullary nephron) [149].

1.2 Epithelial Cell Structure

The filtered fluid (also referred to as the ultrafiltrate) enters the tubule and is carried along the lumen (see Fig 1.4). The lumen is in contact with a lining of epithelial cells that are adjacent to the blood (also referred to as the interstitium). The cells are juxtaposed with each other and are separated by the lateral interspace. The cells are confined by their membranes which allows selective influx and efflux of solutes and water, mediated by channels and transporters (see below) localized at the membranes of the cells. The membrane facing the lumen is referred to as the apical membrane and the membrane facing the interstitium is the basolateral interface. Water and solutes are also transported through the lateral interspace: specific proteins such as the claudin family [48], located at this lining between the lumen and the lateral interspace (also known as the tight junction), have selective permeability to solutes, leading to the transport of water and solutes. The transported elements via the tight junction are then transported to the interstitium through the basement membrane. The transport of water and solutes through the cell is referred to as transcellular transport, and transport through the lateral interspace as the paracellular pathway (details described below).

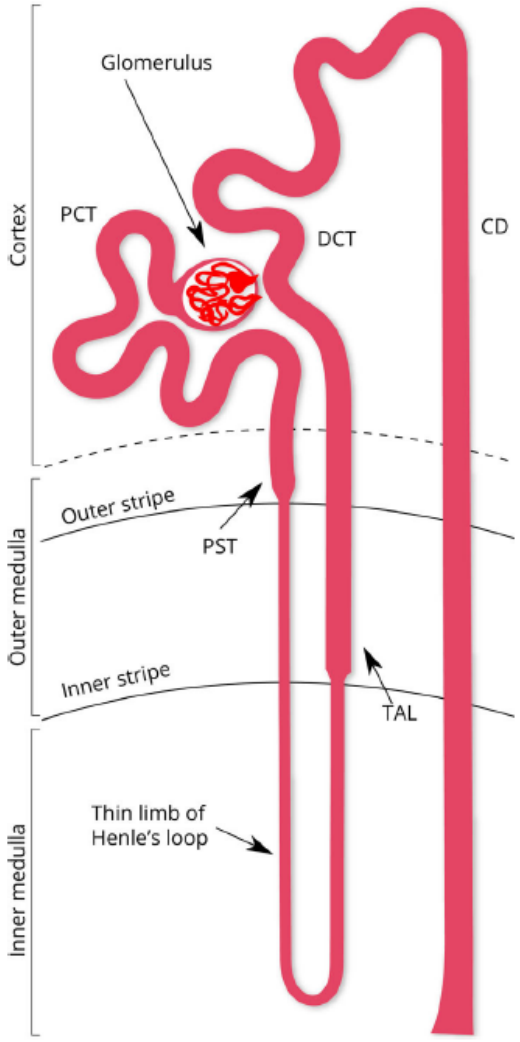

Figure 1.3: Representation of the nephron segments. PCT, proximal convoluted tubule; PST, proximal straight tubule; TAL, thick ascending limb; DCT, distal convoluted tubule; CD, collecting duct. Figure is taken from Kumaran et al., 2020 [74]

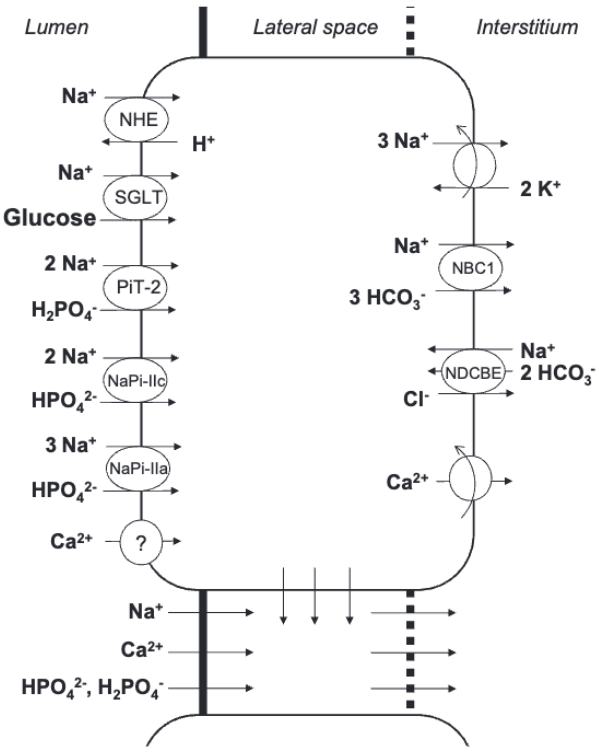

Figure 1.4: Sample cell representation (proximal tubule cell used as an example). Representing the main compartments (Lumen, Cell, Interstitium and Lateral interspace) and the channels and transporters. Lumen is the space where the ultrafiltrate is carried along the nephron, the interstitium is the blood and the lateral interspace is the space between the cells. Figure taken from Ref. [47].

1.3 Tubular Reabsorption and Secretion

Tubular reabsorption is the process of transporting filtered solutes and water from the filtrate back into the interstitium, whereas tubular secretion is the process by which certain substances (i.e, hydrogen ions, creatinine, and drugs) are transported from the interstitium into the renal tubules to be excreted in the urine. In the following section, we will describe the processes of how key solutes and water are reabsorbed along the nephron.

1.3.1 Mechanisms of Tubular Reabsorption and Secretion

All segments of the nephron participate in solute reabsorption, while some also contribute to excretion (i.e, proximal tubule, distal convoluted tubule). There are several types of transport depending on the concentration gradient between the compartments and the type of enzyme:

- **Primary Active Transport:** Primary active transport, is a type of transport process that uses energy derived from the hydrolysis of adenosine triphosphate (ATP) to move solutes against their concentration gradient across the membrane. This means that the movement of solutes is from an area of lower concentration to an area of higher concentration, which is opposite to the direction of diffusion. The sodium–potassium pump also known as the Na^+-K^+-ATPase is one of the most important active transporters. This pump is a ubiquitous enzyme located at the basolateral membrane and extrudes 3 sodium (Na^+) ions out of the cell and pumps 2 potassium (K^+) ions into cells. Its activity results in low intracellular and high extracellular Na^+ concentration. This concentration gradient allows the influx of Na^+ and also other solutes via secondary active transport (see below).
- **Secondary Active Transport:** Secondary active transport is the movement of the ions down their gradient coupled with the transport of other substances against their gradient by a shared carrier. This process still consumes ATP to generate that gradient, but the energy is not directly used to move the molecule across the membrane. Two types of secondary active transport exist: co-transport (also known as symport) and exchange (also known as antiport). Co-transport is defined as when both solutes are transported in the same direction, whereas for exchange the directions are opposite. Sodium is the driving ion for many cotransporters, such as the Na^+-K^+-$2Cl^-$ cotransporter and exchangers such as the Na^+/H^+ exchanger. The Na^+/H^+ exchanger also contributes to the excretion of hydrogen ions.
- **Passive Transport:** Passive transport require cellular energy. Solutes move down their respective concentration gradient. Examples of this transport include convection and diffusion.
  - **Convection:** Convection is the transport of a solute by the movement of fluid (in our case water) down a hydrostatic, osmotic, and oncotic pressure gradient and requires nonzero paracellular permeabilities to water and solutes.
  - **Diffusion and Electrodiffusion:** For non-charged particles diffusion is the movement of solutes from areas with high concentration to low concentration in

order to decrease the concentration gradient.
Electrodiffusion, refers to the movement of ions under the influence of both a concentration gradient and electric potential difference across membranes.

Furthermore, water and solutes can go through two main pathways:

- **Transcellular Transport:** Transcellular transport is mediated by channels and transporters located at the apical membrane of the cells. Channels are membrane-spanning water-filled pores which allow the passive diffusion of solutes down their electrochemical gradients whenever the regulatory gate is open. Transporter proteins are transmembrane proteins that move ions across the membrane against their concentration gradient. Transcellular transport can be active, secondary active, or passive.
- **Paracellular Transport:** The tight junction has selective pore-forming cation and anion-specific proteins, allowing the diffusion of solutes by electrodiffusive and convection. All paracellular transport are passive.

1.4 Motivation: Renal Calcium Handling

Proper functioning of nerve, smooth, skeletal and muscle cells hinges on the maintenance of calcium homeostasis. ∼99% of calcium is stored in the bone matrices and is dynamically released into the bloodstream following parathyroid hormone (PTH) release when extracellular calcium is depleted. The kidney plays a vital role in regulating calcium reabsorption and in its whole body homeostasis. Due to calcium's highly reactive nature, its extracellular abundance can result in complications such as bone mineral deficiency causing osteoporosis, and the formation of kidney stones as a result of hypercalcemia. On the other hand, impairment in reabsorption or excess loss of calcium may cause neurological complications [125] and chronic kidney disease (CKD) [101]. Renal diseases, certain medications and hormonal changes can affect the metabolism, expression and activity of calcium-specific transporters, and thus alter the transepithelial calcium transport along the nephron [90]. Calcium is mainly reabsorbed in the proximal tubule, thick ascending limb, and late part of the distal tubule along with the connecting tubule. In the proximal tubule and thick ascending limb, calcium is mainly reabsorbed through the paracellular pathway, whereas along the later part of the distal convoluted tubule, calcium is reabsorbed transcellular by the calcium-specific transporter, transient receptor potential cation channel subfamily V member 5 [102].

1.4.1 Sex Differences in Renal Calcium Handling

The influence of sex hormones on the development of female and male-specific traits and on the structure and function of sex-specific organs is well understood. Recent studies have shown the key roles of sex hormones in regulating the structure and function of nearly every tissue and organ in the mammalian body [21]. In particular, new data has pointed out sex differences in kidney function [139]. There are major sex differences in renal blood flow and kidney function. Given these morphological and hemodynamic differences assess the extent to which individual sex differences in morphology or transporter activities contribute to the observed difference in calcium transport along the superficial nephron.
It is well established that sex steroid deficiency induces bone loss, leading to osteoporosis, and increased risk for osteoporotic fractures [6]. However, it is less clear whether sex steroids affect renal calcium transport directly. There are several arguments for the kidney as an important target of sex steroid action related to calcium transport: it has been observed in humans and mice that males have a higher calcium excretion compared to females [64]. Also, estrogen deficiency in postmenopausal women is associated with increased serum calcium levels and increased urinary loss of calcium, and this hypercalcemia and hypercalciuria can be restored with estrogen replacement therapy [108]. Various segments of the nephron exhibit androgen receptors (AR) and estrogen receptors (ER) [26]. AR receptors are expressed in both males and females, however, there have been conflicting observations of where the AR is localized: some in vivo and ex vivo experiments have shown a predominant presence of this receptor in the glomeruli and the distal segments [115]. Whereas other experiments have shown that AR is predominantly expressed along PT in isolated mouse and rat cell models. The two isoforms of the estrogen receptors, ERα and ERβ are expressed in both males and females [68]. The expression of ERα has been observed in the brush border membrane of PT cells and cortical CD (CCD) in female mice. ERβ is observed in mesangial cells in both genders, with a higher expression in females, and in podocytes which are only expressed in females [44]. Fig. 1.5 provides an illustration depicting the distribution of androgen receptors (AR) and estrogen receptors (ER) along the nephron.

To specifically address the effects of sex differences on renal handling several animal experiments have been implemented. An ex vivo experiment on rabbit kidneys has shown that estradiol-enhanced perfusion of the PT increases calcium transport [57]. It has been stipulated that estradiol might alter claudin functionality, allowing more calcium permeability.

No known sex differences have been investigated along the TAL. The presence of the both AR and ER are conflicting as there are yet to be understood. In one experiment on the effects of androgen deficiency on renal handling, renal calcium excretion of orchidectomized

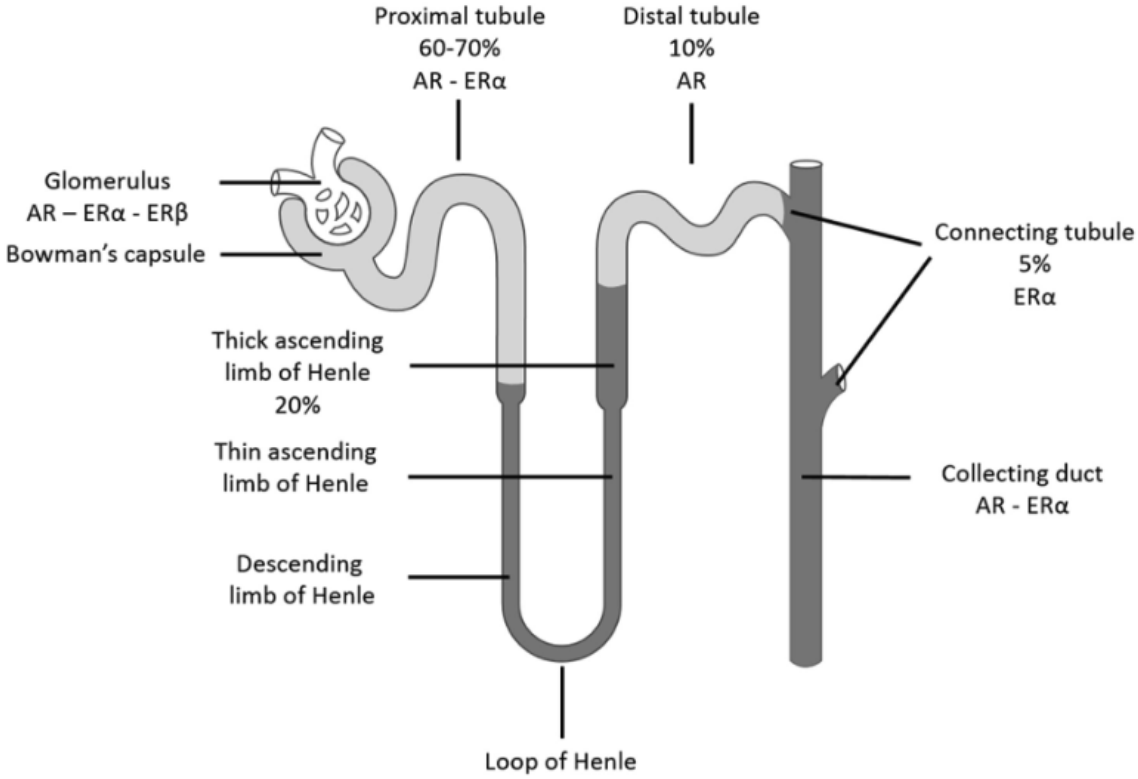

Figure 1.5: Diagram of the nephron, with the sites of expression of androgen (AR) and estrogen receptors (ERa and ERb). The amount of calcium reabsorption for each segment of each tubular segment is also illustrated. Figure taken from Ref. [70].

mice has been compared to sham-operated and testosterone enhance mice. Immonubolting assessments have shown that testosterone-depleted mice have significantly lower TRPV5 expression compared to the control group, showing the necessity of the functionality of sex hormones in the proper functioning of this protein [64]. There are sex differences between female and male rats in terms of TRPV5 expression: female rats have both higher TRPV5 mRNA and TRPV5 protein expression compared to male rats [64].
In order to address the sex differences mentioned earlier, modifications have been made to the paracellular calcium permeability and transcellular channel activity, including the proximal tubule (PT) with S3 segment, of the nephron. Additionally, in the late segment of the distal convoluted tubule and the connecting tubule, adjustments have been made to TRPV5, NCX1, and PMCA based on experimental findings in mice that showed higher expression levels of these proteins along the female DCT2-CNT segments.

1.4.2 Objectives of Thesis

The aims of this thesis are to understand calcium transport and regulation along the superficial nephron and assess the effects of calcium-specific and sodium-specific inhibition on calcium reabsorption. We also want to understand sex differences in renal calcium handling by incorporating this solute into the epithelial solute and water transport model for both male [79] and female rats [65] which will be described in detail in the following chapters.

Chapter 2

Isolated Cell Models: Investigating Ca^{2+} Transport in Renal Epithelial Cells

In this chapter, I present a mathematical model for simulating solute and water transport in the isolated renal epithelial cells, which builds upon existing published models [144, 150, 143, 147, 149, 79, 82]. Specifically, I extend the model to incorporate calcium transport. The isolated cell model serves as a foundation for more comprehensive computational tubular models and allows for a thorough analysis of perturbations and alterations in model parameters, to yield a better understanding for the dynamics of water and solute transport in a specific cell type of a nephron segment. Equations that describe the conservation of mass and membrane transport are described, together with a discussion of sex differences in rats. Additionally, I describe equations for calcium transport in the isolated cell model and present results and sensitivity analysis for calcium transport.

2.1 Introduction

Simulating solute and water transport in renal epithelial isolated cells involves mathematically representing the epithelial cell, incorporating the principles of biological kinetics and fluid dynamics, such as conservation equations, volume transport, electroneutrality, and the dynamics of various types of transporters, including those specific to calcium and other solutes. This understanding of the biological cell is then translated into mathematical models that account for the transport of water and 16 solutes, including Na^+, K^+, Cl^-, HCO_3^-,

$H_2CO_3^-$, CO_2, NH_3, NH_4^+, HPO_4^{2-}, $H_2PO_4^-$, H^+, HCO_2^-, H_2CO_2, urea, glucose, along with Ca^{2+}. In isolated cell experiments, the luminal and interstitium concentrations of these solutes, including calcium, are fixed. In the computational cell model, the concentrations and fluxes of these solutes within the cell and lateral interspace are computed and can be compared with animal microperfusion experiments. A schematic diagram of the thick ascending limb cell model is given in Fig. 2.1 as an example. In the following sections, I describe the conservation equations and the water and solute transport equations, along with calcium transport-specific equations and simulation results.

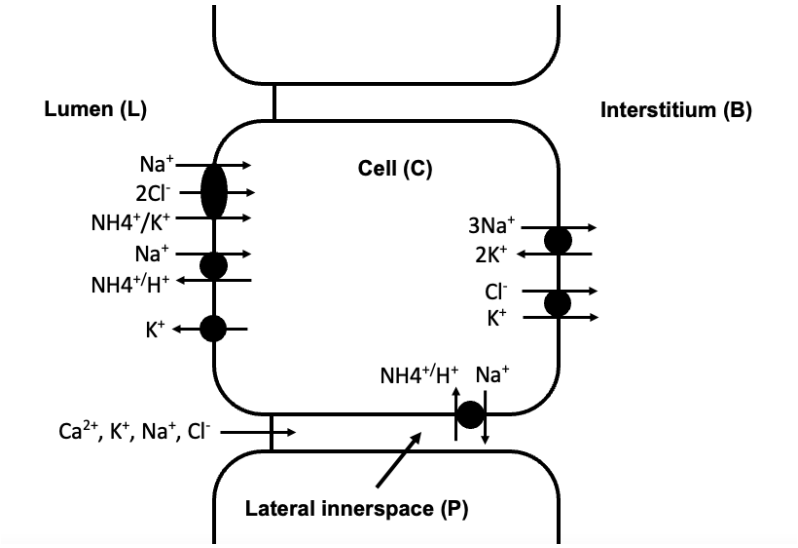

Figure 2.1: A schematic diagram of the medullary thick ascending limb cell, depicting the lumen and interstitium, lateral innerspace and the cell compartment. The luminal and interstitial concentrations are assumed known a priori [149].

2.2 Conservation of Mass Equations

Conservation of Volume. Cell i has four distinct compartments: the lumen (L), the cell (C), the lateral interspace (P), and the interstitium (S). Volume conservation in the C and P compartments in each cell i at steady state is expressed by the following equations:

$$\begin{aligned} J^i_{v,\mathrm{LC}} + J^i_{v,\mathrm{SC}} + J^i_{v,\mathrm{PC}} &= 0 \\ J^i_{v,\mathrm{LP}} + J^i_{v,\mathrm{SP}} + J^i_{v,\mathrm{CP}} &= 0 \end{aligned} \tag{2.1}$$

Here, $J^i_{v,ab}$ is the volume flux, taken positive from compartment a to b.

Conservation Of Mass Equations For Non-reacting Solutes. Conservation of non-reacting solute k in steady state for compartments C, and P in cell i is given as:

$$\begin{aligned} J^i_{k,\mathrm{LC}} + J^i_{k,\mathrm{BC}} + J^i_{k,\mathrm{PC}} &= 0 \\ J^i_{k,\mathrm{LP}} + J^i_{k,\mathrm{BP}} + J^i_{k,\mathrm{CP}} &= 0 \end{aligned} \tag{2.2}$$

where $J^i_{k,\mathrm{ab}}$ denotes the solute flux from compartment a to compartment b.

Conservation Of Mass Equations For Reacting Solutes. Equations related to reacting solutes are described in terms of their buffers. The reactions for H^+, HCO_3^- and CO_2 for instance, are:

$$H^+ + HCO_3^- \rightleftharpoons H_2CO_3 \underset{k_1}{\overset{k_2}{\rightleftharpoons}} H_2O + CO_2 \tag{2.3}$$

where k_1 and k_2 are the forward and backward reaction rates, respectively. The following set of equations describes the conservation of reacting solutes:

$$\begin{aligned} \hat{J}^i_{\mathrm{CO}_2,m} + \hat{J}^i_{\mathrm{HCO}_3^-,m} + \hat{J}^i_{\mathrm{H_2CO_3},m} &= 0 \\ \hat{J}^i_{\mathrm{HPO}_4^{2-},m} + \hat{J}^i_{\mathrm{H_2PO}_4^-,m} &= 0 \\ \hat{J}^i_{\mathrm{NH_3},m} + \hat{J}^i_{\mathrm{NH}_4^+,m} &= 0 \\ \hat{J}^i_{\mathrm{HCO}_2^-,m} + \hat{J}^i_{\mathrm{H_2CO_2},m} &= 0 \end{aligned} \tag{2.4}$$

where $m = C, P$, $\hat{J}^i_{k,\mathrm{C}} \equiv J^i_{k,\mathrm{LC}} + J^i_{k,\mathrm{BC}} + J^i_{k,\mathrm{PC}}$ and $\hat{J}^i_{k,\mathrm{P}} \equiv J^i_{k,\mathrm{LP}} + J^i_{k,\mathrm{BP}} + J^i_{k,\mathrm{CL}}$. Furthermore, the buffer pairs are assumed to be in equilibrium:

$$\mathrm{pH}^i_m = \mathrm{pK}_A - \log \frac{C^i_{A,m}}{C^i_{B,m}} \tag{2.5}$$

pK_A is the negative logarithm of the acid dissociation constant, K_A. $C^i_{k,m}$ denotes the concentration of solute k in compartment m and pH^i_m is the pH of compartment m. The buffer pairs (A,B) are (HCO_3^-, H_2CO_3), $(HPO_4^{2-}, H_2PO_4^-)$, (NH_3, NH_4^+), and (HCO_2^-, H_2CO_2). pH^i_m is given by the conservation of hydrogen ion:

$$\sum_k \hat{J}^i_{k,m} = 0 \tag{2.6}$$

where the summation index k is taken over the solutes H^+, NH_4^+, $H_2PO_4^-$, H_2CO_3, and H_2CO_2.

Conservation of Ionic Charge. As we deal with ions, we need to maintain electroneutrality within each compartment $m = C, P$:

$$\sum_k z_k C_{k,m} = 0 \tag{2.7}$$

where z_k represents the valence of solute k.

2.3 Water and Solute Transport Equations

Volume Transport. Volume fluxes are mediated by aquaporins (AQP) and are calculated using the Kedem-Katchalsky equation:

$$J^i_{v,ab} = A^i_{ab} L^i_{p,ab} \left(\sigma^i_{ab} \Delta\pi^i_{ab} + \Delta P^i_{ab} \right) \tag{2.8}$$

where A^i_{ab} denotes the area separating compartments a and b, $L^i_{p,ab}$ represents the hydraulic permeability, $\Delta\pi^i_{ab} \equiv RT \sum \Delta C^i_{ab}$ represents the osmotic pressure gradient, where RT is the product of the gas constant and thermodynamic temperature, and $\sum \Delta C^i_{ab}$ represents the osmolarity difference. σ^i_{ab} represents the reflective coefficient, and ΔP^i_{ab} denotes the hydrostatic pressure gradient.

Solute Transport. As discussed in the previous chapter, the solute flux terms encompass a multitude of components that elucidated in the following lines:

Convective Flux or Solvent Drag. Solvent drag is a phenomenon in which solutes are carried along with the solvent (in this case, water) as it moves through a permeable membrane, driven by hydrostatic, osmotic, and oncotic pressure gradients:

$$\left(1 - \sigma^i_{k,ab}\right) \bar{C}^i_{k,ab} J^i_{v,ab} \tag{2.9}$$

In this equation, $\sigma^i_{k,ab}$ represents the reflection coefficient of solute k for the membrane between components a and b, and

$$\bar{C}^i_{k,ab} = \frac{C^i_{k,a} - C^i_{k,b}}{\ln C^i_{k,a} - \ln C^i_{k,b}} \tag{2.10}$$

represents the mean concentration of solute k between the compartments a and b for cell i.

Electrodiffusive Flux. The electrodiffusive flux is a combination of the diffusive flux, which is driven by the concentration gradient, and the electrostatic flux, which is driven by the electric potential gradient across the membrane. For charged ions specifically, the electrodiffusive flux is given by the Goldman-Hodgkin-Katz equation:

$$h^i_{k,ab}\zeta^i_{k,ab}\left(\frac{C^i_{k,a} - C^i_{k,b}\exp\left(-\zeta^i_{k,ab}\right)}{1 - \exp\left(-\zeta^i_{k,ab}\right)}\right) \tag{2.11}$$

In this equation, $h^i_{k,ab}$ represents the permeability of solute k between the compartments a and b, and $\zeta^i_{k,ab}$ is defined as:

$$\zeta^i_{k,ab} = \frac{z_k F}{RT}\Delta V^i_{ab} \tag{2.12}$$

where z_k is the solute valence, F is Faraday's constant, and ΔV^i_{ab} denotes the electrical potential difference between the compartments a and b. For an uncharged solute, the diffusive flux is written as:

$$h^i_{k,ab}\left(C^i_{k,a} - C^i_{k,b}\right) \tag{2.13}$$

Coupled Transport. Several forms of coupled transport are present in the nephron, including the antiporter Na^+/H^+ exchanger and the symporter Na^+/Cl^-. To illustrate this concept, we utilize the approach developed in Refs. [77, 145, 59].

In Fig. 2.2, the solutes A, B, and C respectively represent Na^+, H^+, and NH_4^+ , in which the last two bind competitively to the transporter. X represents the empty transporter. i denotes the internal face of the membrane, and e represents the external face of the membrane. The key assumption of the model is that ion binding is very rapid relative to membrane transport. To simplify the notation below, concentrations are denoted by lowercase letters. For instance, a represents the concentration of A, and ax represents that of

the complex AX. We make use of the assumption that binding reactions are instantaneous, resulting in:

$$K_a = \frac{a^i x^i}{(ax)^i} = \frac{a^e x^e}{(ax)^e}, \quad K_b = \frac{b^i x^i}{(bx)^i} = \frac{b^e x^e}{(bx)^e}, \quad K_c = \frac{c^i x^i}{(cx)^i} = \frac{c^e x^e}{(cx)^e}$$

where K_a, K_b, and K_c represent equilibrium constants. The total amount of carrier (x_T) is conserved, therefore:

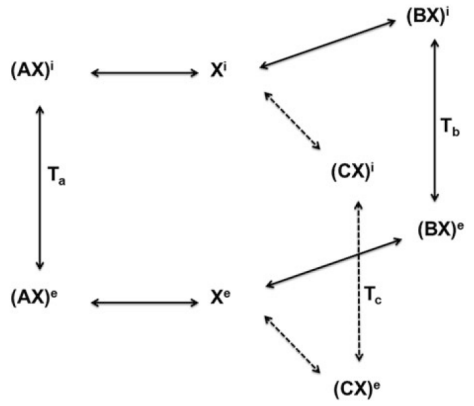

Figure 2.2: Model representation of the Na^+/H^+ exchanger. A, B, C are Na^+, H^+ and NH_4^+ , respectively and they bind to the empty carrier, X. The resulting complexes are transported across the membrane.

$$x^i + (ax)^i + (bx)^i + (cx)^i + x^e + (ax)^e + (bx)^e + (cx)^e = x_T \tag{2.14}$$

In addition, the flux of the carrier in one direction must be counterbalanced by that in the other direction so that there is zero net flux:

$$T_a(ax)^i + T_b(bx)^i + T_c(cx)^i = T_a(ax)^e + T_b(bx)^e + T_c(cx)^e \tag{2.15}$$

where T_k represents the transport rate of solute k. Here, the forward and backward rates across membranes are taken to be equal:

$$\alpha \equiv \frac{a}{K_a}, \beta \equiv \frac{b}{K_b}, \gamma \equiv \frac{c}{K_c}.$$

Note that $(ax)^i = a^i x^i / K_a = \alpha^i x^i, (bx)^i = \beta^i x^i$. We can rewrite Eq. 2.14 and Eq.2.15 to:

$$\begin{aligned} x^i \left[1 + \alpha^i + \beta^i + \gamma^i\right] + x^e \left[1 + \alpha^e + \beta^e + \gamma^e\right] &= x_T, \\ -x^i \left[T_a\alpha^i + T_b\beta^i + T_c\gamma^i\right] + x^e \left[T_a\alpha^e + T_b\beta^e + T_c\gamma^e\right] &= 0. \end{aligned}$$

This system of equations can be solved for x^i and x^e. The determinant equals:

$$\begin{aligned} \Sigma = \left(1 + \alpha^i + \beta^i + \gamma^i\right)\left(T_a\alpha^e + T_b\beta^e + T_c\gamma^e\right) + \\ \left(1 + \alpha^e + \beta^e + \gamma^e\right)\left(T_a\alpha^i + T_b\beta^i + T_c\gamma^i\right). \end{aligned}$$

And we have:

$$\begin{aligned} x^i &= x_T \left(T_a\alpha^e + T_b\beta^e + T_c\gamma^e\right)/\Sigma, \\ x^e &= x_T \left(T_a\alpha^i + T_b\beta^i + T_c\gamma^i\right)/\Sigma. \end{aligned}$$

We can now calculate the flux of each ion across the carrier. The net outward flux of solute A is given by:

$$J_a = T_a(ax)^i - T_a(ax)^e = T_a\left(\alpha^i x^i - \alpha^e x^e\right)$$

Substituting the equations and rearranging, we arrive at:

$$J_a = \frac{x_T T_a}{\Sigma}\left[T_b\left(\alpha^i\beta^e - \alpha^e\beta^i\right) + T_c\left(\alpha^i\gamma^e - \alpha^e\gamma^i\right)\right]$$

The net outward fluxes of B and C are equal to:

$$\begin{aligned} J_b &= \frac{x_T T_b}{\Sigma}\left[T_a\left(\beta^i\alpha^e - \beta^e\alpha^i\right) + T_c\left(\beta^i\gamma^e - \beta^e\gamma^i\right)\right], \\ J_c &= \frac{x_T T_c}{\Sigma}\left[T_a\left(\gamma^i\alpha^e - \gamma^e\alpha^i\right) + T_b\left(\gamma^i\beta^e - \gamma^e\beta^i\right)\right]. \end{aligned}$$

By knowing the binding equilibrium constants, the transport rates, and the total amount of carrier, the fluxes are calculated as a function of internal and external concentrations of A, B, and C. The model parameters are usually not measured directly in practice but are instead derived by fitting the model equations to experimental kinetics data. However, due

to the number of parameters often exceeding the number of independent measurements, further assumptions need to be made: for instance, one of the transport rates could be assumed constant, or the internal and external binding affinities could be considered to be equal.

Active Transport (ATP-Driven). We will also discuss the mathematical modelling of Na^+-K^+-ATPase. This ubiquitous pump provides the majority of energy for secondary active transport by the extrusion of $3Na^+$ ions and the influx of $2K^+$ ions, resulting in low intracellular Na+ concentration and a high intracellular K^+ concentration. We can compute ionic fluxes across the Na^+-K^+-ATPase by assuming that the binding of each ion to the enzyme is an independent process. Considering that the binding of one intracellular Na^+ion to the free enzyme, E, to form the complex NaE is a first-order, reversible reaction:

$$Na^+ + E \overset{k^{on}_{NaE}/k^{off}_{NaE}}{\longleftrightarrow} NaE$$

where k^{on}_{NaE} and k^{aff}_{NaE} are the association and dissociation kinetic constants for this reaction, respectively. The rate of NaE formation is given by:

$$\frac{dC_{NaE}}{dt} = k^{on}_{NaE} C^i_{Na} C_E - k^{off}_{NaE} C_{NaE} \tag{2.16}$$

C^i_{Na}, C_E and C_{NaE} are the intracellular concentration of Na^+, the concentration of E and NaE, respectively. $C^{\text{sot}}_E = C_E + C_{NaE}$ is defined as the total concentration of enzyme remains constant. Therefore, Eq. 2.16 can be rewritten as:

$$\begin{aligned}\frac{dC_{NaE}}{dt} &= k^{an}_{NaE} C^i_{Na} \left(C^{tat}_E - C_{NaE}\right) - k^{off}_{NaE} C_{NaE+} \\ &= k^{on}_{NaE} C^i_{Na} C^{tot}_E - \left(k^{on}_{NaE} C^i_{Na} + k^{off}_{NaE}\right) C_{NaE}.\end{aligned}$$

At steady state, we therefore have:

$$C_{NaE} = \frac{C^{tot}_E C^i_{Na}}{C^i_{Na} + K^i_{Na}} \tag{2.17}$$

where $K^i_{Na} = k^{off}_{NaE}/k^{on}_{NaE}$ is the dissociation constant of the NaE complex. Eq. 2.17 means that the probability (p_{Na}) of having one Na^+ion bound to one pump unit is proportional to $C^i_{Na}/\left(C^i_{Na} + K^i_{Na}\right)$. If all 3 Na^+ binding sites have the same affinity and there is no cooperativity between them (i.e., assumed to be independent), the probability of having

$3Na^+$ ions bound to the complex is p_{Na}^3. Similarly, p_K is proportional to $C_K^e/\left(C_K^e + K_K^e\right)$ where C_K^e is the external K^+concentration and K_K^e denotes the dissociation of the KE complex. Therefore, the probability of having 2 extracellular K^+ ions bound to the pump is ${p_K}^2$. Thus, the flux of Na^+ions across the pump can be expressed as:

$$J_{Na}^{NaK} = J_{Na}^{NaK,\max}\left[\frac{C_{Na}^i}{C_{Na}^i + K_{Na}^i}\right]^3\left[\frac{C_K^e}{C_K^e + K_K^e}\right]^2,$$

$J_{Na}^{NaK,\max}$ is the maximum efflux of Na^+ions at steady state. For K^+ions the flux is:

$$J_K^{NaK} = -(2/3)J_{Na}^{NaK}$$

Garay and Garrahan [54] found that the apparent Na^+affinity of the pump increases linearly with intracellular K^+levels:

$$K_{Na}^i = K_{Na}^{NaK}\left(1 + C_K^i/a_{NaK}\right)$$

where $K_{\mathrm{Na}}^{\mathrm{NaK}}$ and a_{NaK} are both constants. Similarly, the apparent K^+affinity is altered by extracellular Na^+ [129], such that:

$$K_K^e = K_K^{NaK}\left(1 + C_{Na}^e/b_{NaK}\right).$$

In the kidney, K_{Na}^{NaK} and K_K^{NaK} are taken as 0.2 and 0.1mM, and a_{NaK} as b_{NaK} as 8.33 and 18.5 mM, respectively. Thus, under typical conditions ($C_K^i \sim C_{Na}^e \sim 150$mM), the apparent affinity of the pump for $Na^+$and $K^+$is on the order of 4 and 1 mM, respectively.

2.4 Sex-specific Parameters

The original epithelial solute and transport models were developed for the male rat kidney [82, 34]. However, animal experiments have shown specific sex differences in rat kidneys. In female rat kidneys, the single nephron glomerular filtration rate (SNGFR), which refers to the rate at which blood is filtered through the glomeruli, is lower compared to male rat kidneys. Additionally, the kidney mass of a female rat is approximately half that of an age-matched male rat [97]. Conversely, the glomerulus population is similar in both sexes, and the urinary volume output is not substantially different [105]. Further animal

experiments [139] have explored sex differences in the abundance of channels and transporters (see Fig. 2.3). Based on these experiments, female rat nephrons in the proximal tubule (including S3), express greater Na^+/H^+ exchanger 3 (NHE3) phosphorylation and higher distribution of NHE3 at the base of the microvilli and have lower transport area, lower abundance of Na^+-Picotransporter 2 (NaPi2), aquaporin-1 (AQP1), and expression of specific members of the claudin family (i.e., claudin-2), responsible for the paracellular permeability of solutes. These differences result in lower Na^+ and HCO_3^- reabsorption and increased volume flow from the proximal tubule of a female rat kidney [139]. Along the thick ascending limb (TAL) of the female rat, the Na^+-K^+-$2Cl^-$ cotransporter, K^+-Cl^- (KCC), and Na^+-K^+-ATPase have higher activities. Furthermore, distal segments of the female rat kidney exhibit a higher abundance of Na^+-Cl^- cotransporter (NCC), claudin-7, and epithelial Na^+ channel (ENaC) α- and γ-subunits [139]. These differences are also associated with a lower fasting plasma K^+ concentration in females compared to male rats. All non-calcium-specific sex differences have been summarized in Table 2.8.

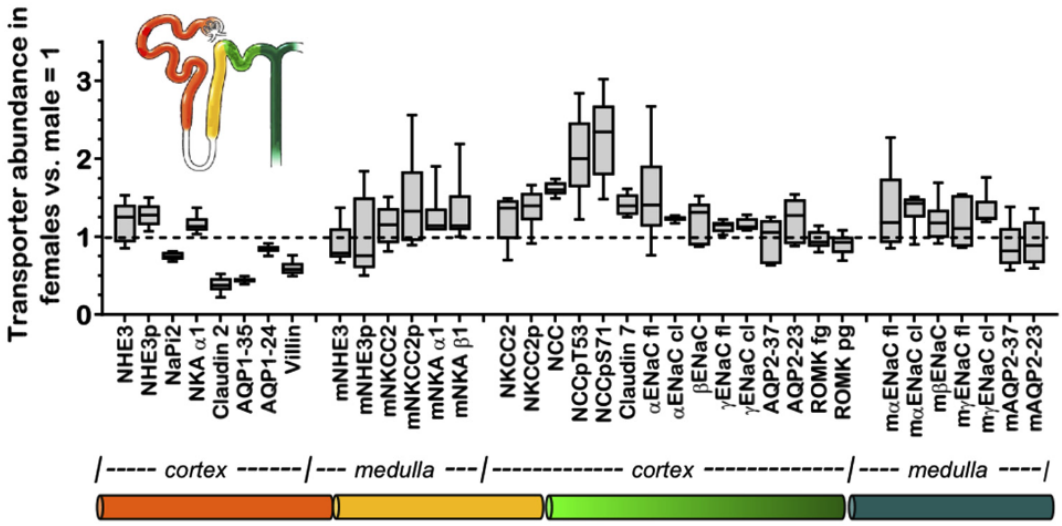

Figure 2.3: Abundance differences of key transporters, channels, and aquaporins between male and female rat kidneys: NHE3, Na^+/H^+ exchanger 3; NaPi2, Na^+-P_i cotransporter 2; NKA α1, Na^+-K^+-ATPase α1-catalytic subunit; AQP, aquaporin water channel subunit; NKCC2, Na^+-K^+-2Cl cotransporter isoform 2; NCC, Na^+-Cl^- cotransporter; pS71 and pT53, phosphorylation sites associated with activation; ENaC, epithelial Na^+ channel; fl, full-length form; cl, cleaved forms; ROMK, renal outer medullary K^+ channel. Figure taken from Ref. [65].

2.5 Equations Specific to Calcium Transport

I have extended the published epithelial solute and water transport models to include calcium transport. Calcium is reabsorbed in the proximal tubule (PT), the thick ascending limb (TAL), and the last 1/3 part of the distal convoluted tubule, also referred to as DCT2, as well as the connecting tubule (CNT) where calcium is reabsorbed transcellularly. An illustration of a nephron, along with the cell models of the segments in which calcium reabsorption occurs, is depicted in Fig. 2.4. In this section, I describe the equations specific to calcium transport in PT, TAL, and DCT2-CNT.

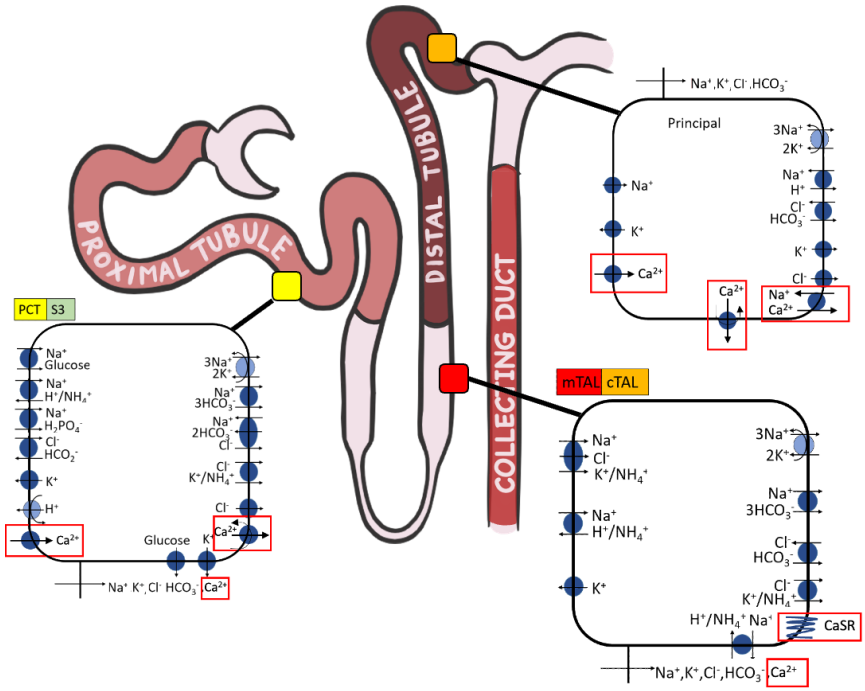

Figure 2.4: Illustration of a nephron with the main segments in which calcium reabsorption occurs. Calcium-related elements are depicted in red boxes. PCT, proximal convoluted tubule; mTAL, medullary thick ascending limb; cTAL, cortical thick ascending limb. The principal cell of the CNT tubule is represented (calcium-specific channels and transporters in DCT2 are similar to CNT). Illustration made by Karolina Suszek (collecting duct added by Melissa Stadt).

2.5.1 Proximal Tubule Cell Equations

Calcium is mainly reabsorbed via the paracellular pathway in PT cell. The paracellular flux of calcium consists of electrodiffusive fluxes driven by the concentration gradient and difference in electric potential along with convective flux, which is driven by volume transport. Furthermore, the L-type calcium channel located at the apical membrane of the PT cells allows transcellular reabsorption of Ca^{2+} along this segment. The apical permeability to calcium is an adjusted value and is taken so that the transcellular flux of calcium is equal to 15% of total calcium reabsorption. Recent transcriptomic data [87] indicates that Ca^{2+} extrusion in the cell is mainly mediated by plasma membrane Ca^{2+}-ATPase (PMCA), and the contribution of Na^+/Ca^{2+} exchanger (NCX1) is neglected. In Fig. 2.5, a depiction of this cell model is shown. Calcium flux from the lumen to the compartments M ($M = C, P$) can be described as the sum of convective and electrodiffusive fluxes.

$$J_{\mathrm{Ca}}^{LM} = J_{\mathrm{V}}^{LM}\left(1-\sigma_{\mathrm{Ca}}^{LM}\right)\overline{\mathrm{C}}_{\mathrm{Ca}} + h_{\mathrm{Ca}}^{LM}\zeta_{\mathrm{Ca}}^{LM}\left(\frac{\mathrm{C}_{\mathrm{Ca}}^{\mathrm{L}} - \mathrm{C}_{\mathrm{Ca}}^{M}\exp\left(-\zeta_{\mathrm{Ca}}\right)}{1-\exp\left(-\zeta_{\mathrm{Ca}}^{\mathrm{L}}\right)}\right) \tag{2.18}$$

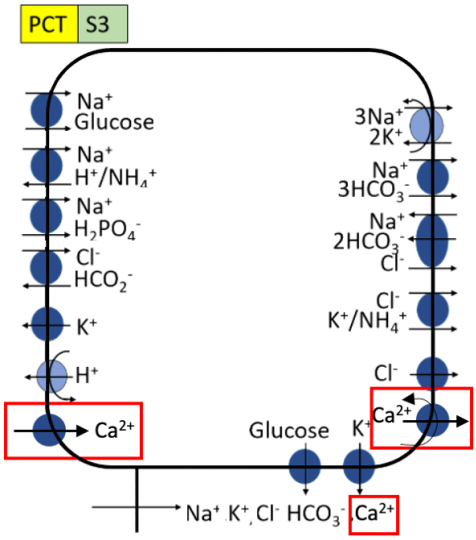

Figure 2.5: Isolated PT cell with Ca^{2+} specific elements highlighted in red boxes. Ca^{2+} is predominantly reabsorbed via the paracellular pathway. Ca^{2+} is extruded by PMCA located at the basolateral membranes. PCT, proximal convoluted tubule; S3, proximal straight tubule.

Parameter	Value (Reference)	
	Male	Female
Permeability to Ca^{2+}:		
Tight Junction	20×10^{-5} cm/s [53]	100×10^{-5} cm/s (*)
Basement Membrane	60×10^{-5} cm/s [92]	60×10^{-5} cm/s (**)
Apical Cell Membrane	0.005×10^{-5} cm/s (*)	0.03×10^{-5} cm/s (*)
PMCA maximum flux, $J_{Ca}^{PMCA,\max}$	0.5×10^{-9} $mmol \cdot cm^{-2} \cdot s^{-1}$ (*)	2.5×10^{-9} $mmol \cdot cm^{-2} \cdot s^{-1}$ (*)
PMCA affinity to Ca^{2+}, $K_{m,PMCA}$	75.6 nM [134]	75.6 nM (**)
Reflection coefficient of tight junction to Ca^{2+}	0.89 [106]	0.89 (**)

Table 2.1: Calcium-specific parameters of PT (S3 included) cell for male and female rat kidneys. The basement membrane permeability is calculated based on Na^+ permeability which is based on a Ca^{2+}-to-Na^+ free diffusivity ratio of 7.93:13 for all the segments [154]. Values presented in (*) are adjusted and values presented in (**) denote that the parameter is the same for both male and female models.

PMCA is mathematically modeled as:

$$J_{\mathrm{Ca}}^{\mathrm{PMCA}} = J_{\mathrm{Ca}}^{\mathrm{PMCA,max}} \left[\frac{\mathrm{C}_{\mathrm{Ca}}^{\mathrm{C}}}{K_{m,PMCA} + \mathrm{C}_{\mathrm{Ca}}^{\mathrm{C}}} \right] \tag{2.19}$$

In Eq. 2.19, $J_{\mathrm{Ca}}^{\mathrm{PMCA,max}}$ represents the maximum PMCA flux, $K_{m,PMCA}$ denotes the affinity of the pump to Ca^{2+}, and $\mathrm{C}_{\mathrm{Ca}}^{\mathrm{C}}$ represents the cellular calcium concentration in millimoles per liter (mM).

In ex-vivo experiments on rabbit PT cells, it has been observed that estradiol enhances Ca^{2+} reabsorption [57]. I have adjusted transcellular and paracellular permeability and $J_{\mathrm{Ca}}^{\mathrm{PMCA,max}}$ in the female model accordingly to reflect the differences between the sexes. Table 2.1 summarizes the Ca^{2+}-related parameters for the PT segment in both sexes.

2.5.2 Thick Ascending Limb Cell Equations

Along the TAL, calcium reabsorption is entirely paracellular [4]. Since this segment is impermeable to water, the paracellular flux is solely electrodiffusive, driven by the positive transepithelial voltage (ΔV_{te}), which is defined as the voltage difference between the lumen and the interstitium. The activity of Na^+-K^+-ATPase results in a low intracellular Na^+ concentration and a high extracellular Na^+ concentration, creating a transepithelial concentration gradient. This concentration gradient allows for the transcellular reabsorption

of Na^+, K^+, Cl^-, and NH_4^+ via NKCC2. The high intracellular concentration and low extracellular concentration of K^+ also facilitate apical recycling of K^+ to the lumen via the apical potassium channel, resulting in a positive ΔV_{te}. Furthermore, micropuncture experiments conducted on both the medullary thick ascending limb (mTAL) and cortical thick ascending limb (cTAL) have shown heterogeneity in terms of calcium permeabilities in this segment, with cTAL exhibiting considerably higher permeability to Ca^{2+} [151]. Regarding Ca^{2+} transport, no specific sex difference has been observed along the TAL [70]. Figure 2.6 represents a schematic diagram of the cell model for this segment.

Parameter	Value (Reference)	
	Male	Female
CaSR parameters (tight junction Ca^{2+} permeability):		
Maximum half concentration, EC_{50}^n	1.25 mM [38]	1.25 (**)
Hill function coefficient, n	4 [14]	4 (**)
Inhibitory coefficient, α_λ	-4/7 [96]	-4/7 (**)
Tight junction permeability in the absence of Ca^{2+}, λ^*	12×10^{-5} cm/s [96]	12×10^{-5} cm/s (**)
CaSR parameters (effect on ROMK and NKCC2):		
Inhibitory coefficient for NKCC2 activity, α_{NKCC2}	-0.84 [141]	-0.84 (**)
Inhibitory coefficient for potassium channel activity , α_{ROMK}	-0.5 [123]	-0.5 (**)

Table 2.2: Calcium-specific parameters of TAL cell for male and female rats. Values presented in (*) are adjusted and values presented in (**) denote that the parameter is the same for both male and female models.

Calcium Sensing Receptor (CaSR)

One key protein expressed at the basolateral membrane of the TAL cell is the calcium-sensing receptor (CaSR). This protein modulates the paracellular permeability of tight junctions to Ca^{2+} based on the interstitial concentration of calcium. Its main purpose is to regulate Ca^{2+} reabsorption in response to changes in serum calcium concentrations. Parathyroid hormone (PTH) plays a crucial role in this dynamic process, as it stimulates an increase in Ca^{2+} reabsorption. To mathematically model the effect of CaSR, a steep inverse gradient function with a fourth-order Hill function is considered, following a similar approach as described in Ref. [46].:

$$\lambda = \lambda^* \left[1 + \alpha_\lambda \left(\frac{\left[\mathrm{Ca}^{2+}\right]_i^n}{\left[\mathrm{Ca}^{2+}\right]_i^n + \mathrm{EC}_{50}^n} \right) \right] \tag{2.20}$$

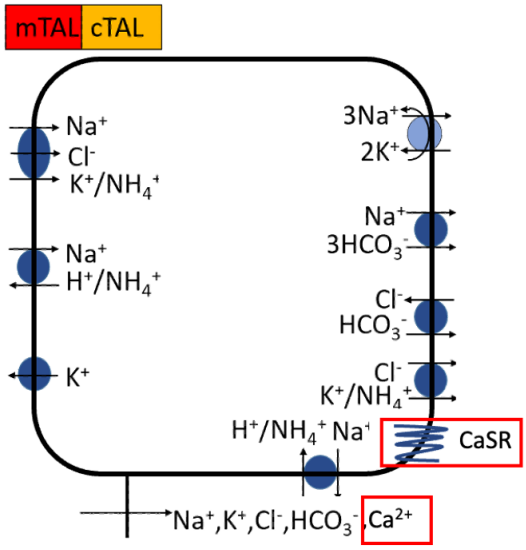

Figure 2.6: Isolated TAL cell with Ca^{2+} specific elements highlighted in red boxes. Ca^{2+} is entirely reabsorbed via the paracellular pathway. CaSR at the basolateral membrane adjusts Ca^{2+} permeability based on the interstitial Ca^{2+} concentration. mTAL, medullary thick ascending limb; cTAL, cortical thick ascending limb.

In Eq. 2.20, The parameter λ^* represents the original permeability of tight junctions in the absence of Ca^{2+}. The value of α_λ determines whether CaSR exerts inhibitory or excitatory effects, with a negative value indicating inhibitory effects and a positive value indicating excitatory effects (i.e., CaSR's effect on tight junction permeability of Ca^{2+} is inhibitory). i is either the lumen ($i = L$) or the interstitium ($i = S$), depending on where CaSR is localized (i.e, for TAL it is localized at the basolateral membrane). n is the Hill function coefficient and equals 4, and EC_{50}^n is the maximum half concentration and is equal to 1.25 mM. CaSR also affects the activity of non-calcium-specific channels and transporters: In vivo experiments on rats have shown that by increasing Ca^{2+} from 1.1 to 5 mM, there is an $\sim$84% decrease in renal outer medullary potassium channel (ROMK) activity. In another in vivo experiment with calcimimetic treatment on male mice, NKCC2 phosphorylation decreased by $\sim$50%, without changing NKCC2 expression levels [16]. The parameter values of the effects of CaSR on ROMK and NKCC2 are given in Table 2.9. CaSR is also expressed along the apical membranes of DCT, and inner and outer medullary cells of the collecting duct which will be described in Section. 2.5.4.

2.5.3 Late Distal Tubule and Connecting Tubule Cell Equations

The CNT contains three types of cells: a principal cell and two intercalated cells. Only the principal cells of the CNT express calcium-specific proteins. In DCT2-CNT, calcium reabsorption occurs entirely via the transcellular pathway, facilitated by the transient receptor potential vanilloid subtype V (TRPV5) protein located at the apical membrane of the cells. The isolated cell model is similar to Bonny and Edwards's isolated DCT2-CNT cell rat model [23]. Two basolateral proteins, PMCA and NCX1, work in tandem to facilitate the extrusion of Ca^{2+} ions from the cell. Additionally, animal experiments have provided evidence that TRPV5 is predominantly expressed along DCT2 and to a lesser extent in CNT [94]. Our model also takes into account this expression pattern.

TRPV5. The permeability properties of TRPV5 are experimentally determined as conductance. Therefore, the TRPV5 $Ca2^{2+}$ flux is computed using the modified form of Ohm's law:

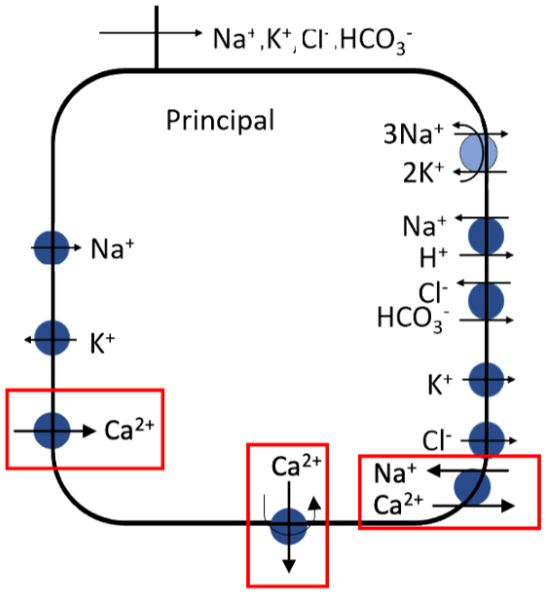

Figure 2.7: Isolated CNT principal cell with Ca^{2+} specific elements highlighted in red boxes (similar channels and transporters for DCT2). Ca^{2+} is reabsorbed transcellularly via TRPV5 and is extruded by PMCA and NCX1 located at the basolateral membranes.

$$J_{\mathrm{Ca}}^{\mathrm{TRPV5}} = f_{\mathrm{Ca}}^{\mathrm{TRPV5}} \cdot \frac{N_{\mathrm{TRPV5}} \times g_{\mathrm{TRPV5}} \left[\Delta\Psi^{\mathrm{LC}} - E_{\mathrm{Ca}}^{\mathrm{LC}}\right]}{2F} \tag{2.21}$$

N_{TRPV5} is the TRPV5 channel density, g_{TRPV5} is the channel conductance which its value hinges on the intracellular pH (pHi) and extracellular pH (pHe), $\Delta\Psi^{\mathrm{LP}} = \Psi^{\mathrm{L}} - \Psi^{\mathrm{C}}$ is the electric potential difference across the apical membrane, and $E_{\mathrm{Ca}}^{\mathrm{LPr}}$ is the Nernst potential of Ca^{2+} which is defined as:

$$E_{\mathrm{Ca}}^{\mathrm{LC}} = \frac{RT}{2F} \ln\left(\frac{\mathrm{C}_{\mathrm{Ca}}^{\mathrm{C}}}{\mathrm{C}_{\mathrm{Ca}}^{\mathrm{L}}}\right) \tag{2.22}$$

In the aforementioned equation, f_{Ca}^{TRPV5} takes into account the Ca^{2+} induced inhibition of TRPV5 activity, whereas the effects of pH are embedded in the conductance. The inhibition term is calculated as:

$$f_{\mathrm{Cai}}^{\mathrm{TRPV5}} = \frac{1}{1 + (\mathrm{C}_{\mathrm{Ca}}^{\mathrm{C}}/\mathrm{C}_{\mathrm{inhib}}^{\mathrm{TRPV5}})} \tag{2.23}$$

where in the above equation, intracellular Ca^{2+} concentration for half-maximal block is denoted as $\mathrm{C}_{\mathrm{inhib}}^{\mathrm{TRPV5}}$. We also take into account that the channel conductance is a function of the pHe and pHi which has three states: closed (C), sub-conductive (S), and fully conductive (F). We assume that these states do not alter other properties of TRPV5 and only affect the conductance. The equations of these transitions based on the states can be written as:

$$C \xrightarrow{k_1 k_2} S \xrightarrow{k_3/k_4} F \tag{2.24}$$

The channel can be in each of these states with a probability of P_J, in which $J = C, S, F$. The relation of these probabilities can be written as:

$$\begin{aligned} \frac{\partial P_C}{\partial t} &= -k_1^{\mathrm{TRPV5}} P_C + k_2^{\mathrm{TRPV5}} P_S \\ \frac{\partial P_F}{\partial t} &= -k_4^{\mathrm{TRPV5}} P_F + k_3^{\mathrm{TRPV5}} P_S \\ P_S &= 1 - P_C - P_F \end{aligned} \tag{2.25}$$

Solving for steady state, the simplified relation between the probabilities is given by:

$$\begin{aligned} P_S &= \frac{k_1 k_4}{k_1 k_4 + k_2 k_4 + k_3 k_1} \\ P_F &= \frac{k_1 k_3}{k_1 k_4 + k_2 k_4 + k_3 k_1} \end{aligned} \tag{2.26}$$

The value for the channel conductance is computed based on the probabilities:

$$g_{TRPV5} = P_F g_f + P_S g_S \tag{2.27}$$

The $k_{2,3}^{TRPV5}$ terms are a function of pHi and their relation along with the other k terms is given as:

$$k_1^{\text{TRPV5}} = 42.7 \text{ s}^{-1} \tag{2.28}$$

$$k_2^{\text{TRPV5}} = \begin{cases} 55.9 + \frac{173.3-55.9}{7.0-7.4}(\text{pHi} - 7.4) & \text{if pHi} < 7.4 \\ 55.9 + \frac{30.4-55.9}{8.4-7.4}(\text{pHi} - 7.4) & \text{if pHi} \geq 7.4 \end{cases} \tag{2.29}$$

$$\begin{aligned} k_3^{\text{TRPV5}} &= 0.1684 \cdot \exp(0.6035 \cdot \text{pHi}) \\ k_4^{\text{TRPV5}} &= 58.7 \text{ s}^{-1} \end{aligned} \tag{2.30}$$

And the g_F and g_S values are computed as:

$$\begin{aligned} g_F &= g_F^* + \frac{g_F^*}{g_F^* + g_S^*} \left(\frac{91 - 58}{7.4 - 5.4} \right) (\text{pHe} - 7.4) \\ g_S &= g_S^* + \frac{g_S^*}{g_F^* + g_S^*} \left(\frac{91 - 58}{7.4 - 5.4} \right) (\text{pHe} - 7.4) \end{aligned} \tag{2.31}$$

where the g_F^* and g_S^* are the reference conductances when $\text{pH}_\text{e} = \text{pH}_\text{i} = 7.4$. The conductance plot based on the pH_e and pH_i is given in Fig. 2.8.

Sex differences exist between female and male rats in TRPV5 expression: female rats exhibit higher levels of both TRPV5 mRNA and TRPV5 protein expression compared to male rats, as reported in a study by Hsu et al. [64]. Accordingly, the values in the female model have been adjusted to reflect these differences.

PMCA. The mathematical modeling of of PMCA in DCT2-CNT cells is similar to that of PMCA in PT, as given in Eq. 2.19, with differences in affinity and maximum flux. Detailed parameters for DCT2-CNT are summarized in Table 2.3.

NCX1. The NCX1.3 isoform is the predominant isoform of NCX1 in DCT2-CNT cells. However, due to the absence of existing kinetic models for NCX1.3, the current model utilizes the NCX1.1 isoform, which is the predominant isoform in cardiac cells. The computation of fluxes related to NCX1 is as follows:

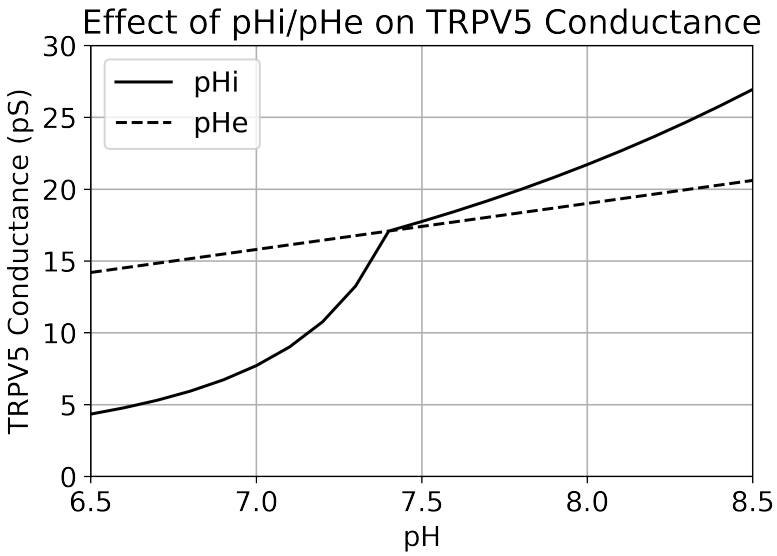

Figure 2.8: Conductance of TRPV5 is a function of both pHi and pHe. In each of these plots one of the pHs is fixed to the reference value of 7.4 and the other pH is altered accordingly. As we can see pHi has a nonlinear function whereas for pHe we have a linear change.

$$J_{\mathrm{Ca}}^{\mathrm{NCX1}} = J_{\mathrm{Ca}}^{\mathrm{NCX1,max}} \left(\frac{\left(\mathrm{C}_{\mathrm{Ca}}^{\mathrm{C}}/K_{\mathrm{m,NCX1}}\right)^2}{1+\left(\mathrm{C}_{\mathrm{Ca}}^{\mathrm{C}}/K_{\mathrm{m,NCX11}}\right)^2} \right) \times \left(\frac{\Phi_R \left(\mathrm{C}_{\mathrm{Na}}^{\mathrm{S}}\right)^3 \mathrm{C}_{\mathrm{Ca}}^{\mathrm{C}} - \Phi_F \left(\mathrm{C}_{\mathrm{Na}}^{\mathrm{C}}\right)^3 \mathrm{C}_{\mathrm{Ca}}^{\mathrm{S}}}{\mathrm{G}\left(1+k_{\mathrm{sat}}\Phi_R\right)} \right) \tag{2.32}$$

$$J_{\mathrm{Na}}^{\mathrm{NCX1}} = -3 \times J_{\mathrm{Ca}}^{\mathrm{NCX1}} \tag{2.33}$$

$$\Phi_R = \exp\left[(\gamma-1)\Psi^{\mathrm{C}}F/RT\right] \tag{2.34}$$

$$\Phi_F = \exp\left[\gamma\Psi^{\mathrm{C}}F/RT\right] \tag{2.35}$$

where in the above equations:

$$
\begin{aligned}
G = & \left(\mathrm{C}_{\mathrm{Na}}^{\mathrm{S}}\right)^3 \mathrm{C}_{\mathrm{Ca}}^{\mathrm{C}} + \left(\mathrm{C}_{\mathrm{Na}}^{\mathrm{C}}\right)^3 \mathrm{C}_{\mathrm{Ca}}^{\mathrm{S}} + {K_{\mathrm{mNao}}}^3 \mathrm{C}_{\mathrm{Ca}}^{\mathrm{C}} + K_{\mathrm{mCao}} \left(\mathrm{C}_{\mathrm{Na}}^{\mathrm{C}}\right)^3 \\
& + {K_{\mathrm{mNai}}}^3 \mathrm{C}_{\mathrm{Ca}}^{\mathrm{S}} \left(1 + \mathrm{C}_{\mathrm{Ca}}^{\mathrm{C}} / K_{\mathrm{mCai}}\right) \\
& + K_{\mathrm{mCai}} \left(\mathrm{C}_{\mathrm{Na}}^{\mathrm{S}}\right)^3 \left(1 + \left(\mathrm{C}_{\mathrm{Na}}^{\mathrm{C}}\right)^3 / {K_{\mathrm{mNai}}}^3\right)
\end{aligned} \tag{2.36}
$$

Parameter	Value (Reference)	
	Male	Female
PMCA parameters:		
PMCA maximum flux, $J_{Ca}^{PMCA,\max}$	$4.0 \times 10^{-9}\ mmol \cdot cm^{-2} \cdot s^{-1}$ (*)	$4.5 \times 10^{-9}\ mmol \cdot cm^{-2} \cdot s^{-1}$ (*)
PMCA affinity to Ca^{2+}, $K_{m,PMCA}$	42.6 nM [134]	42.6 nM (**)
TRPV5 parameters:		
Channel density, N_{TRPV5}	DCT2: 20×10^6 1/cm^2 (*) CNT: 5×10^6 1/cm^2 (*)	DCT2: 35×35^6 1/cm^2 Based on [64] CNT: 8.75×10^6 1/cm^2 Based on [64]
Intracellular [Ca^{2+}] for half-maximal block, C_{inhib}^{TRPV5}	74 nM [134]	74 nM (**)
NCX1 parameters:		
NCX1 maximum flux, $J_{Ca}^{NCX1,\max}$	$2,500 \times 10^{-9}\ mmol \cdot cm^{-2} \cdot s^{-1}$ (*)	$2,750 \times 10^{-9}\ mmol \cdot cm^{-2} \cdot s^{-1}$ (**)
NCX1 affinity to Ca^{2+}, $K_{m,NCX1}$	0.125 μM [67]	0.125 μM (**)
Constant for voltage dependence, γ	0.35 [67]	0.35 (**)
Internal Ca^{2+} half-saturation constant, $K_{m,Cai}$	3.59 μM [67]	3.59 μM (**)
External Ca^{2+} half-saturation constant, $K_{m,Cao}$	1.3 mM [67]	1.3 mM (**)
Internal Na^+ half-saturation constant, $K_{m,Nai}$	12.29 mM [67]	12.29 mM (**)
External Na^+ half-saturation constant, $K_{m,Nao}$	87.5 mM [67]	87.5 mM (**)
CaSR parameters (effect on NCC):		
Excitatory coefficient for NCC activity , α_{NCC}	0.5 [16]	0.5 (**)

Table 2.3: Calcium-specific parameters of DCT2-CNT cell for male and female rats. Values presented in (*) are adjusted and values presented in (**) denote that the parameter is the same for both male and female models.

Effect of Ca^{2+} *on other transporters.* An increase in the intracellular concentration of Ca^{2+} from approximately 150 nM to 100 μM significantly reduces the open probability of ENaC, while not affecting its conductance. To accurately capture this effect, the following equation has been utilized:

$$
f_{\mathrm{Cai}}^{\mathrm{ENaC}} = \begin{cases} \sqrt{(150/\mathrm{C}_{\mathrm{Ca}}^{\mathrm{C}})} & \text{if } \mathrm{C}_{\mathrm{Ca}}^{\mathrm{C}} > 150\text{nM} \\ 1 & \text{if } \mathrm{C}_{\mathrm{Ca}}^{\mathrm{C}} \leq 150\text{nM} \end{cases} \tag{2.37}
$$

CaSR is also expressed at the apical membrane of DCT cells. In vivo experiments on male mice have revealed the effects of CaSR in increasing NCC activity. However, other functions of this protein are not yet fully understood [16].

2.5.4 Other Segments

The short descending limb (SDL) has negligible calcium permeability, and therefore we assume no calcium transport occurs in this segment [120]. Along the collecting duct segments, namely the cortical collecting duct (CCD), outer medullary cortical duct (OMCD), and inner medullary cortical duct (IMCD), there is minimal paracellular permeability that promotes limited paracellular transport without transcellular transport [116]. CaSR is also present in the medullary segments of the collecting ducts, specifically located on the apical membrane of inner medullary collecting duct (IMCD) cells and the apical membrane of type A intercalated cells of the outer medullary collecting duct (OMCD). In IMCD, CaSR increases apical water permeability by increasing luminal Ca^{2+} concentrations. In OMCD cells, an increase in luminal Ca^{2+} levels enhances H^+ transport in the type A cells [124, 117, 46]. The effects of CaSR in these segments have been implemented, and all the respective parameters are summarized in Table. 2.4. Furthermore, all the parameters are also summarized in Table 2.9.

Parameter	Value (Reference)	
	Male	Female
Permeability to Ca^{2+}		
Tight Junction	20×10^{-5} cm/s [27]	20×10^{-5} cm/s (**)
Basement Membrane	4.5×10^{-5} cm/s [92]	4.5×10^{-5} cm/s (**)
CaSR parameters:		
Promoting coefficient for apical HATPase activity of type A OMCD cells, α_{HATP}	+2 [118]	+2 (**)
Inhibitory coefficient for apical water permeability of IMCD cells, α_{pf}	-3/8 [123]	-3/8 (**)

Table 2.4: Calcium-specific parameters along cortical duct (CD) segments for male and female rats. Values presented in (*) are adjusted and values presented in (**) denote that the parameter is the same for both male and female models.

2.6 Simulation Results

2.6.1 Proximal Tubule Cell

Baseline Results. Similar luminal and interstitial concentrations for both male and female renal epithelial isolated PT cell models are assumed (summarized in Table. 2.5). The total flux of Ca^{2+} (J_{Ca}^{Total}) in the male model is predicted to be 4.81 $pmol \cdot min^{-1} \cdot mm^{-1}$. The paracellular flux of calcium (J_{Ca}^{Para}) and the transcellular flux of calcium (J_{Ca}^{Trans}) are equal to 3.98 $pmol \cdot min^{-1} \cdot mm^{-1}$ and 0.82 $pmol \cdot min^{-1} \cdot mm^{-1}$, respectively. J_{Ca}^{Para} makes up 78% of the total calcium flux, which is consistent with a previously published male rat PT model [47]. Electrodiffusive flux accounts for the majority of the paracellular flux (76%), driven by the lumen-to-lateral interspace concentration gradient of calcium and the positive ΔV_{te} (1.03 mV). In the female model, the total flux of calcium in the isolated PT cell is slightly lower at 4.23 $pmol \cdot min^{-1} \cdot mm^{-1}$. Paracellular flux amounts to 81% of the total flux and is equal to 3.42 $pmol \cdot min^{-1} \cdot mm^{-1}$, with electrodiffusive flux making up 74% of this flux. Lower NHE3 expression in the female model results in a ΔV_{te} (0.88 mV) lower than the male model.

Solute	Lumen Concentration (mM)	Interstitium Concentration (mM)
Na^+	142.67	144
K^+	5.89	4.9
Cl^-	129.7	118.8
HCO_3^-	14.28	24.8
H_2CO_3	4.3×10^{-3}	4.3×10^{-3}
CO_2	1.48	1.5
HPO_4^{2-}	2.78	3.00
$H_2PO_4^-$	1.44	0.89
Urea	10.05	8.0
NH_3	0.014	0.018
NH_4^+	1.69	0.78
H^+	8.2×10^{-5}	4.75×10^{-5}
HCO_2^-	1.97	0.99
H_2CO_2	0.0009	0.0002
Glucose	0.97	5
Ca^{2+}	1.36	1.25

Table 2.5: Luminal and interstitium concentrations of the renal epithelial isolated PT cell model for both male and female models.

Sensitivity Analysis. The paracellular permeability of Ca^{2+} (P_{Ca}^{Para}), the transcellular permeability of Ca^{2+} (P_{Ca}^{Trans}), the expression level of NHE3, and the paracellular permeability of Na^+ (P_{Na}^{Para}) were altered by increasing and decreasing these parameters by 20%. The relative changes in transcellular and paracellular Ca^{2+} fluxes were computed and shown in Fig. 2.9. The choice of NHE3 expression and P_{Na}^{Para} is based on findings from isolated rat PT cell experiments, which reveal that alterations in Na^+ transport are associated with parallel changes in Ca^{2+} transport [51]. Perturbing P_{Ca}^{Para} by +20% and -20% has minimal effect on J_{Ca}^{Trans} in both sexes. However, increasing this parameter results in an increase in J_{Ca}^{Para} and vice versa. Increasing P_{Ca}^{Trans} leads to an increase in J_{Ca}^{Trans} in both sexes, while for J_{Ca}^{Para}, increasing P_{Ca}^{Trans} decreases the total paracellular flux. Over-expression of NHE3 has a minor effect on J_{Ca}^{Trans}, while it mainly increases the paracellular flux by enhancing ΔV_{te}. On the other hand, increasing P_{Na}^{Para} has a negligible effect on the transcellular flux, but higher P_{Na}^{Para} results in increased paracellular reabsorption of Na^+, leading to a lower ΔV_{te}, resulting in a reduced J_{Ca}^{Para}.

2.6.2 Isolated Thick Ascending Limb Cell Results

Baseline Results. Luminal and interstitial compositions of the renal epithelial isolated cTAL cell in both male and female models are similar to a published TAL model [46]; see Table. 2.6. Calcium reabsorption is entirely paracellular. Since this segment is impermeable to water the paracellular flux is solely electrodiffusive. The total paracellular flux of calcium in the male model is equal to 1.67 $pmol \cdot min^{-1} \cdot mm^{-1}$, driven by the positive ΔV_{te} (7.37 mV). The female isolated cTAL cell model exhibits a lower calcium flux equal to 1.25 $pmol \cdot min^{-1} \cdot mm^{-1}$, resulting from a less positive ΔV_{te} (5.24 mV).

The positive ΔV_{te} is a consequence of the simultaneous reabsorption of sodium chloride (NaCl) in parallel with the apical recycling of K^+. Therefore, the impact of modifying luminal concentrations of NaCl and KCl can be evaluated in terms of their effect on Ca^{2+} flux. A decrease in the luminal concentration of NaCl ([NaCl]) leads to a reduction in paracellular Na^+ reabsorption in both the male and female models, resulting in an increase in ΔV_{te} (see Fig. 2.10a). Increased ΔV_{te} due to decreased luminal [NaCl] are consistent with *in vitro* animal experiments conducted on isolated cTAL cells of the rat kidney [98]. Furthermore, our results reveal that luminal NH_4^+ concentration ($[NH_4^+]$) significantly impacts ΔV_{te} in both male and female models, with the male model aligning with previous studies such as Ref. [148], where a decrease in luminal $[NH_4^+]$ leads to increased apical K^+ recycling and a more positive ΔV_{te} and an increased J_{Ca}^{Total} (see Fig. 2.10b).

Additionally, decreasing the luminal KCl concentration ([KCl]) results in a higher transcellular K^+ concentration gradient, an increased apical K^+ recycling and subsequently

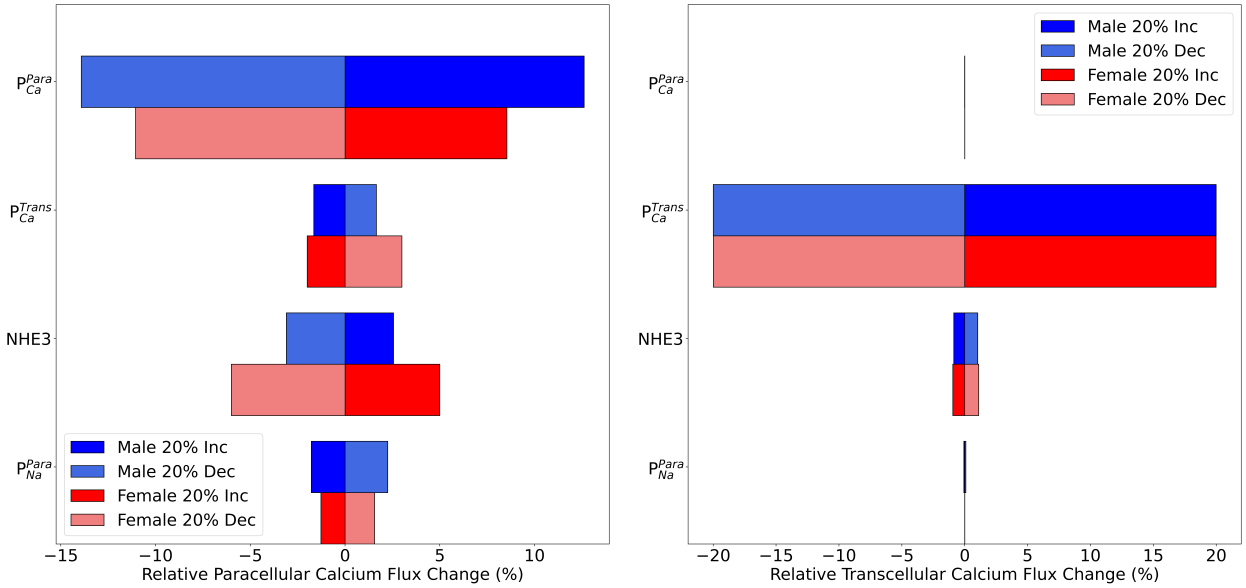

(a) (b)

Figure 2.9: Sensitvity analysis of the relative change in paracellular (a) and transcellular (b) flux of calcium for the isolated renal epithelial PT cell by altering P_{Ca}^{Para}, P_{Ca}^{Trans}, expression of NHE3, P_{Na}^{Para}, one at a time for male and female models. Blue bars are predicted responses for the male model; red bars, are for the female model. Darker and lighter bars correspond to a 20% increase (Inc) and a 20% decrease (Dec)in model parameters, respectively.

elevated ΔV_{te}, in both male and female models (see Fig. 2.11a). The female model exhibits higher sensitivity to luminal [KCl] compared to the male model. Additionally, lower luminal $[NH_4^+]$ results in higher K^+ uptake via NKCC2 due to the competitive binding of NH_4^+ and K^+ to the NKCC2 splice variants. The increased ΔV_{te} results in higher J_{Ca}^{Total} in both sexes, as shown in Fig. 2.11b.

Sensitivity Analysis. P_{Ca}^{Para}, the expression level of Na^+-K^+-$2Cl^-$ (NKCC2) splice variant A and B (NKCC2A and NKCC2B), NHE3, P_{Na}^{Para}, the permeability of the apical renal outer medullary K^+ channel (ROMK), the expression levels of K^+-Cl^- (KCC), and Na^+-K^+-ATPase are altered by +20% and -20% (see Fig. 2.12). Increasing P_{Ca}^{Para} results in an increase in J_{Ca}^{Total} in both sexes. Increased NKCC2A and NKCC2B result in a higher K^+ uptake and higher apical K^+ recycling, leading to a higher ΔV_{te} and thus a higher J_{Ca}^{Total} in both male and female models. J_{Ca}^{Total} is less sensitive to apical NHE3 expression compared

Solute	Lumen Concentration (mM)	Interstitium Concentration (mM)
Na^+	144	144
K^+	5.0	5.0
Cl^-	122.9	122.9
HCO_3^-	25	25
H_2CO_3	4.41×10^{-3}	4.41×10^{-3}
CO_2	1.5	1.5
HPO_4^{2-}	2.00	2.00
$H_2PO_4^-$	0.60	0.60
Urea	5.00	5.00
NH_3	14.7×10^{-3}	14.7×10^{-3}
NH_4^+	0.99	0.99
H^+	4.75×10^{-5}	4.75×10^{-5}
HCO_2^- (*)	0.99	0.99
H_2CO_2 (*)	2.00×10^{-4}	2.00×10^{-4}
Glucose (*)	5.0	5.0
Ca^{2+}	1.25	1.25

Table 2.6: Luminal and interstitium concentrations of the renal epithelial isolated cTAL cell for male and female models similar to the isolated cTAL cell in a published TAL model [46]. Solutes with (*) are not included in the published TAL model. Cortical medullary concentrations have been assumed for these solutes.

to the other parameters, and over-expression of NHE3 results in a slightly increased J_{Ca}^{Total}. Increased P_{Na}^{Para} allows increased paracellular Na^+ reabsorption, leading to a less positive ΔV_{te}, and lower J_{Ca}^{Total} in both sexes. Increased ROMK expression results in a higher apical K^+ recycling and a higher ΔV_{te} in both male and female models. Increased KCC expression results in a higher efflux of K^+ from the cell and a lower transcellular K^+ gradient, resulting in a lower ΔV_{te} and thus lower J_{Ca}^{Total}. Na^+-K^+-ATPase activity results in a high intracellular K^+ concentration and a low intracellular Na^+ concentration. In the male model increasing Na^+-K^+-ATPase expression results in a higher transcellular K^+ gradient and a higher J_{Ca}^{Total}. In the female model increasing Na^+-K^+-ATPase activity results in a high Na^+ transcellular concentration gradient, but a lesser apical uptake of K^+ and apical K^+ recycling, leading to a lower J_{Ca}^{Total}.

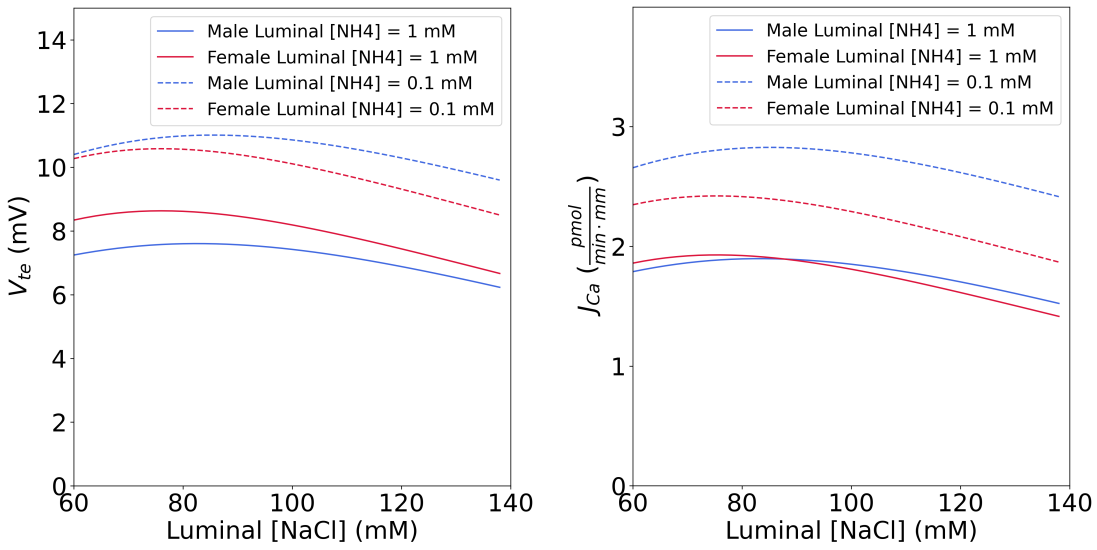

(a) (b)

Figure 2.10: Effect of altering luminal NaCl concentrations on (a) V_{te} and (b) J_{Ca} for male and female models. Blue lines are the results for the male model; red bars, are for the female model. Solid and dotted lines correspond to a luminal $[NH_4^+]$ of 1 mM and 0.1 mM, respectively.

2.6.3 Isolated DCT2-CNT Cell Model Results

Baseline Results. Luminal and interstitial compositions similar to a previously published isolated CNT cell model are used [23]; see Table 2.7. Calcium reabsorption occurs exclusively through the transcellular pathway mediated by TRPV5. In the male model, the calcium flux is equal to 2.23 $pmol \cdot min^{-1} \cdot mm^{-1}$, consistent with observed values from in vitro experiments on CNT principal cells of male rabbits [20]. In contrast, the transcellular flux in the female model is considerably higher compared to the male model, predicted to be 3.41 $pmol \cdot min^{-1} \cdot mm^{-1}$, which is attributed to the higher expression level of TRPV5 in the female model compared to the male model. Basolateral extrusion of calcium occurs via NCX1 and PMCA, with NCX1 accounting for 68% and 71% of the total extrusion of calcium from the cell in male and female models, respectively, while the remaining portion is attributed to PMCA.

Sensitivity Analysis. The expression levels of TRPV5, NCX1, PMCA, and ENaC are altered by +20% and -20%, and the predicted relative change in J_{Ca}^{Total} is evaluated in

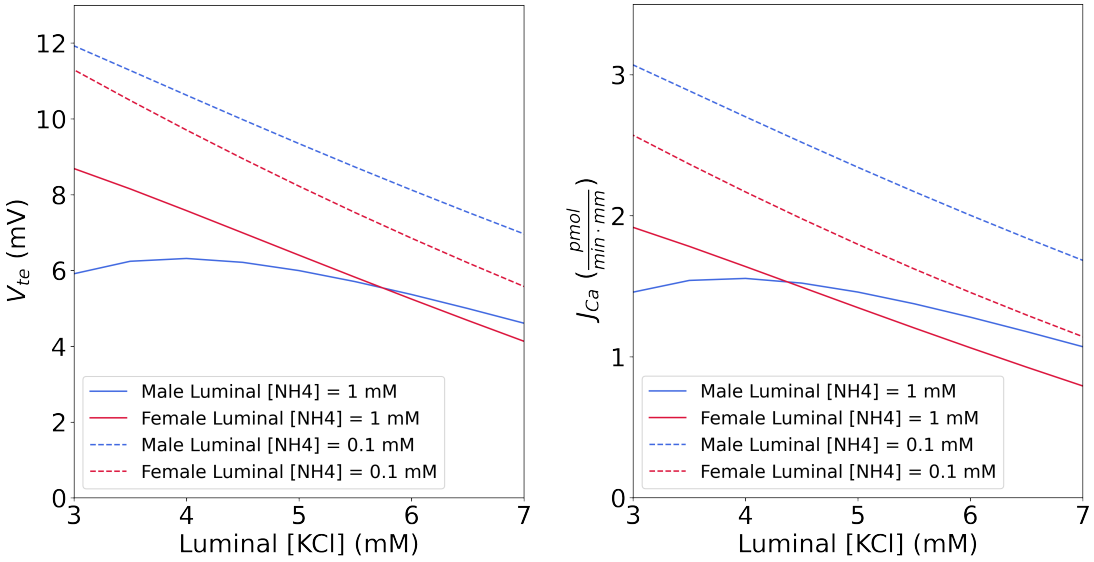

(a) (b)

Figure 2.11: Effect of altering luminal KCl concentrations on (a) V_{te} and (b) J_{Ca} for male and female models. Blue lines are the results for the male model; red bars, are for the female model. Solid and dotted lines correspond to a luminal $[NH_4^+]$ of 1 mM and 0.1 mM, respectively.

male and female models (see Fig. 2.13). Decreasing the expression of TRPV5, NCX1, and PMCA results in a decrease in J_{Ca}^{Total}, and vice versa. However, when the expression of ENaC is decreased, an increase in J_{Ca}^{Total} is observed. This is because the reduction in ENaC expression leads to cellular hyperpolarization, resulting in an increased transcellular voltage that drives the influx of calcium via TRPV5, without altering the conductance of the channel due to minimal changes in pHi and pHe.

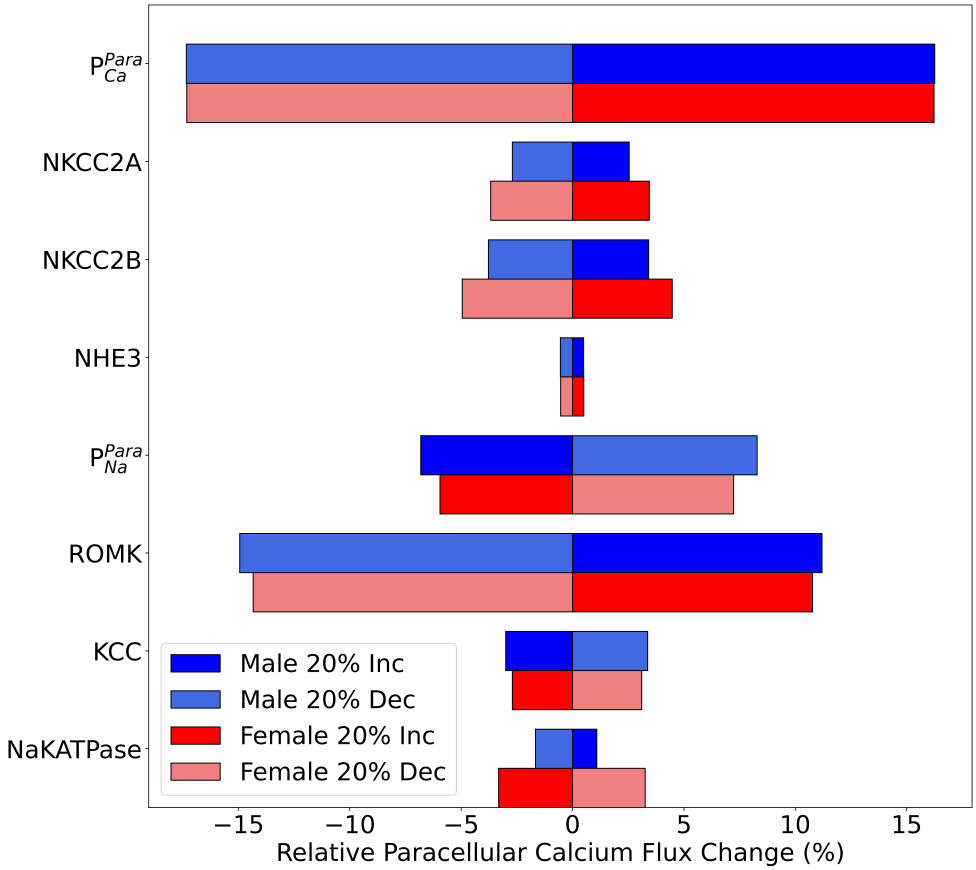

Figure 2.12: Sensitivity analysis of the relative change in paracellular calcium flux in the isolated renal epithelial cTAL cell. P_{Ca}^{Para}, NKCC2A, NKCC2B, NHE3 expression, P_{Na}^{Para}, ROMK channel permeability, KCC, and Na^+-K^+-ATPase have been altered by +20% and -20%, one at a time, for male and female models. Blue bars are predicted responses for the male model; red bars, are for the female model. Darker and lighter bars correspond to a 20% increase (Inc) and a 20% decrease (Dec) in model parameters, respectively.

Solute	Lumen Concentration (mM)	Interstitium Concentration (mM)
Na^+	65.0	144
K^+	2.00	5.00
Cl^-	56.9	123.9
HCO_3^-	8.00	24.0
H_2CO_3	3.53×10^{-3}	3.53×10^{-3}
CO_2	1.2	1.2
HPO_4^{2-}	2.23	2.08
$H_2PO_4^-$	1.67	0.52
Urea	30.00	5.00
NH_3	18.8×10^{-3}	3.52×10^{-3}
NH_4^+	3.16	0.20
H^+	1.76×10^{-4}	3.064×10^{-8}
HCO_2^- (*)	0.99	0.99
H_2CO_2 (*)	2.00×10^{-4}	2.00×10^{-4}
Glucose (*)	5.0	5.0
Ca^{2+}	0.70	1.70

Table 2.7: Luminal and interstitium concentrations of the renal epithelial isolated CNT cell in a male and female model similar to a published isolated CNT model [23]. Solutes with (*) are not included in the published CNT model. Cortical medullary concentrations have been assumed for these solutes.

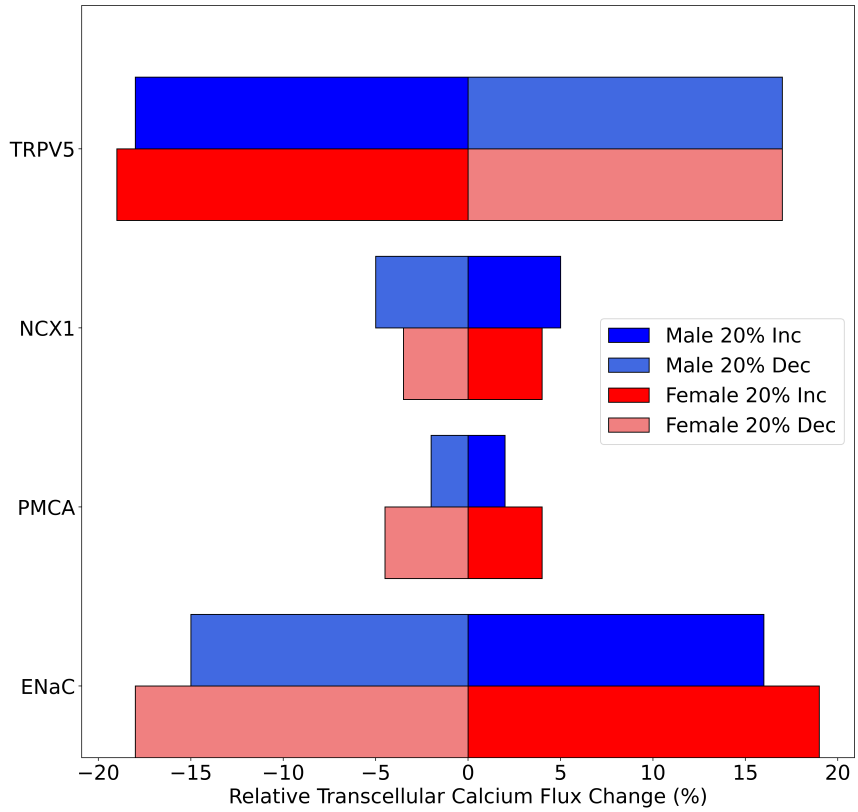

Figure 2.13: Sensitivity analysis on relative change in transcellular flux of calcium in the isolated renal epithelial principal CNT cell for both male and female models. TRPV5, NCX1, PMCA, and ENaC expression levels have been altered by +20% and -20% for male and female models, one at a time, and the relative change in calcium flux is predicted. Blue bars are predicted responses for the male model; red bars, are for the female male. Darker and lighter bars correspond to a 20% increase (Inc) and a 20% decrease (Dec)in model parameters, respectively.

Parameter	Female-to-Male Ratio	Parameter	Female-to-Male Ratio
PCT		S3	
NHE3 activity	0.83		0.83
NaPi2	0.75		0.75
$P_{\rm Na}, P_{\rm Cl}$ (paracellular)	0.4		0.4
P_f (transcellular)	0.64		0.64
	SDL		
$P_{\rm Na}, P_{\rm Cl}$ (transcellular)	0.5		
P_f (transcellular)	2		
mTAL		cTAL	
NKCC2 activity	2		2
KCC activity	1.5		1.5
$Na^+ - K^+$-ATPase activity	2		2
Na^+/H^+exchanger	0.8		0.8
$Na^+ - HPO_4^{2-}$ cotransporter	0.8		0.8
$Na^+ - HCO_3^-$cotransporter	0.8		0.8
$P_{\rm Na}, P_{\rm Cl}$ (paracellular)	0.9		
DCT		CNT	
NCC activity	1.6		
$Na^+ - K^+ -$ ATPase activity	2		2
Na^+/H^+exchanger	0.85		0.9
$Na^+ - HPO_4^{2-}$ cotransporter	0.85		0.9
ENaC activity	2		1.3
$P_{\rm N}, P_{\rm Cl}$ (paracellular)	1.4		1.4
P_f (transcellular)	2		1.5
CCD		OMCD	
$Na^+ - K^+$-ATPase activity	1.5		1.1
$H^+ - K^+$-ATPase activity	1		1.5
Na^+/H^+exchanger	0.9		0.9
$Na^+ - HPO_4^{2-}$ cotransporter	0.9		0.9
ENaC activity	1.5		1.2
$P_{\rm Na}, P_{\rm Cl}$ (paracellular)	1.4		1
$P_{\rm K}$(apical)	0.7		1.2
$P_{\rm f}$ (transcellular)	2		2
IMCD		Morphology	
$Na^+ - K^+$-ATPase activity	1.2	PCT, S3	
$H^+ - K^+ -$ ATPase activity	1.5	Length	0.8
$K^+ - Cl^-$cotransporter	1.2	Diameter	0.8
NaKCl2 activity	0.6	Distal segments	
$P_{\rm Na}, P_{\rm Cl}$ (paracellular)	0.5	Length	0.85
$P_{\rm K}$(apical)	2	Diameter	0.85
$P_{\rm Na}$ (apical)	0.5	Hemodynamics	
$P_{\rm f}$ (transcellular)	2	SNGFR	0.8
$P_{\rm urea}$ changing fraction	0.89		

Table 2.8: NaPi2, $Na^+ - P_i$ cotransporter 2; $P_{\rm Na}$, Na^+permeability; $P_{\rm Cl}$, Cl^-permeability; $P_{\rm f}$, water permeability; SDL, short descending limb; NKCC2, $Na^+ - K^+ - Cl^-$cotransporter isoform 2; KCC, $K^+ - Cl^-$cotransporter; ENaC, epithelial Na^+channel; $P_{\rm K}$, K^+permeability; NaKCl2, $Na^+ - K^+ - Cl^-$cotransporter isoform 1; $P_{\rm urea}$, urea permeability; PCT, proximal convoluted tubule; S3, proximal straight tubule; mTAL, medullary thick ascending limb; cTAL, cortical thick ascending limb; DCT, distal convoluted tubule; CNT, connecting tubule; CCD, cortical collecting duct; OMCD, outer medullary collecting duct; IMCD, inner medullary collecting duct; SNGFR, single nephron glomerular filtration rate. Values are from Ref. [65].

Parameter	Value (Reference)	
	Male	Female
PT:		
Permeability to Ca^{2+}		
Tight Junction	20×10^{-5} cm/s [53]	100×10^{-5} cm/s (*)
Basement Membrane	60×10^{-5} cm/s [92]	60×10^{-5} cm/s (**)
Apical Cell Membrane	0.005×10^{-5} cm/s (*)	0.03×10^{-5} cm/s (*)
PMCA maximum flux, $J_{Ca}^{PMCA,\max}$	0.5×10^{-9} $mmol \cdot cm^{-2} \cdot s^{-1}$ (*)	2.5×10^{-9} $mmol \cdot cm^{-2} \cdot s^{-1}$ (*)
PMCA affinity to Ca^{2+}, $K_{m,PMCA}$	75.6 nM [134]	75.6 nM (**)
Reflection coefficient of tight junction to Ca^{2+}	0.89 [106]	0.89 (**)
TAL:		
CaSR parameters (tight junction Ca^{2+} permeability):		
Maximum half concentration, EC_{50}^{n}	1.25 mM [38]	1.25 (**)
Hill function coefficient, n	4 [14]	4 (**)
Inhibitory coefficient, α_λ	-4/7 [96]	-4/7 (**)
Tight junction permeability in the absence of Ca^{2+}, λ^*	12×10^{-5} cm/s [96]	12×10^{-5} cm/s (**)
CaSR parameters (effect on ROMK and NKCC2):		
Inhibitory coefficient for NKCC2 activity, α_{NKCC2}	-0.84 [141]	-0.84 (**)
Inhibitory coefficient for potassium channel activity , α_{ROMK}	-0.5 [123]	-0.5 (**)
DCT2-CNT:		
PMCA parameters:		
PMCA maximum flux, $J_{Ca}^{PMCA,\max}$	4.0×10^{-9} $mmol \cdot cm^{-2} \cdot s^{-1}$ (*)	4.5×10^{-9} $mmol \cdot cm^{-2} \cdot s^{-1}$ (*)
PMCA affinity to Ca^{2+}, $K_{m,PMCA}$	42.6 nM [134]	42.6 nM (**)
TRPV5 parameters:		
Channel density, N_{TRPV5}	DCT2: 20×10^6 1/cm^2 (*) CNT: 5×10^6 1/cm^2 (*)	DCT2: 35×35^6 1/cm^2 Based on [64] CNT: 8.75×10^6 1/cm^2 Based on [64]
intracellular [Ca^{2+}] for half-maximal block, C_{inhib}^{TRPV5}	74 nM [134]	74 nM (**)
NCX1 parameters:		
NCX1 maximum flux, $J_{Ca}^{NCX1,\max}$	$2,500 \times 10^{-9}$ $mmol \cdot cm^{-2} \cdot s^{-1}$ (*)	$2,750 \times 10^{-9}$ $mmol \cdot cm^{-2} \cdot s^{-1}$ (**)
NCX1 affinity to Ca^{2+}, $K_{m,NCX1}$	0.125 μM [67]	0.125 μM (**)
Constant for voltage dependence, γ	0.35 [67]	0.35 (**)
Internal Ca^{2+} half-saturation constant, $K_{m,Cai}$	3.59 μM [67]	3.59 μM (**)
External Ca^{2+} half-saturation constant, $K_{m,Cao}$	1.3 mM [67]	1.3 mM (**)
Internal Na^{+} half-saturation constant, $K_{m,Nai}$	12.29 mM [67]	12.29 mM (**)
External Na^{+} half-saturation constant, $K_{m,Nao}$	87.5 mM [67]	87.5 mM (**)
CaSR parameters (effect on NCC):		
Excitatory coefficient for NCC activity , α_{NCC}	0.5 [16]	0.5 (**)
CD segments:		
Permeability to Ca^{2+}		
Tight Junction	20×10^{-5} cm/s [27]	20×10^{-5} cm/s (**)
Basement Membrane	4.5×10^{-5} cm/s [92]	4.5×10^{-5} cm/s (**)
CaSR parameters:		
Promoting coefficient for apical HATPase activity of type A OMCD cells, α_{HATP}	+2 [118]	+2 (**)
Inhibitory coefficient for apical water permeability of IMCD cells, α_{pf}	-3/8 [123]	-3/8 (**)

Table 2.9: Calcium-specific parameters for all the segments along the nephron. Values presented in (*) are adjusted and values presented in (**) denote that the parameter is the same for both male and female models. PT, proximal tubule; TAL, thick ascending limb; DCT2, late part of distal convoluted tubule; CNT, connecting tubule; CD, collecting duct; OMCD, outer medullary collecting duct; IMCD, inner medullary collecting duct.

Chapter 3

Nephron Model: Baseline Results

This chapter expands the renal epithelial isolated cell models to a nephron model and provides a comprehensive analysis of calcium transport along the superficial rat nephron, with a specific focus on male and female differences. Baseline results for epithelial solute and water transport in the nephron model are simulated for 16 different solutes. A detailed description of calcium reabsorption along the superficial nephron in male and female rat kidneys is provided, with an emphasis on the contribution of paracellular and transcellular transport, as well as the role of Na^+ transport in driving calcium transport. Notable sex differences are observed, with lower calcium delivery and transport rates in the proximal tubule and thick ascending limb, but higher rates in the late distal convoluted tubule and connecting tubule in female rats compared to males. These findings highlight the significance of considering sex-specific differences in nephron function and calcium handling.

3.1 Introduction to the Nephron Model

We develop sex-specific models of epithelial transport along a superficial nephron, based on the isolated renal epithelial cell models presented in Chapter 2. The superficial nephron model encompasses various segments. It starts from Bowman's capsule and includes the proximal tubule (PT), short descending limb (SDL), thick ascending limb (TAL), which is further divided into the medullary thick ascending limb (mTAL) and the cortical thick ascending limb (cTAL), distal convoluted tubule (DCT), connecting tubule (CNT), cortical collecting duct (CCD), outer medullary collecting duct (OMCD), and inner medullary collecting duct (IMCD). Each nephron segment is represented as a rigid tubule lined by a layer of epithelial cells, with apical and basolateral transporters that vary according to

cell type. That is, individual nephron segments are constructed by lining up a series of specific cell models, with the exception of CNT, CCD, and OMCD segments. CNT and CCD segments are composed of three types of cells: principal cells, alpha cells, and beta cells (also known as intercalated cells). On the other hand, the OMCD segment expresses only alpha cells and principal cells. The schematic representation of the superficial nephron model can be found in Fig. 3.1.

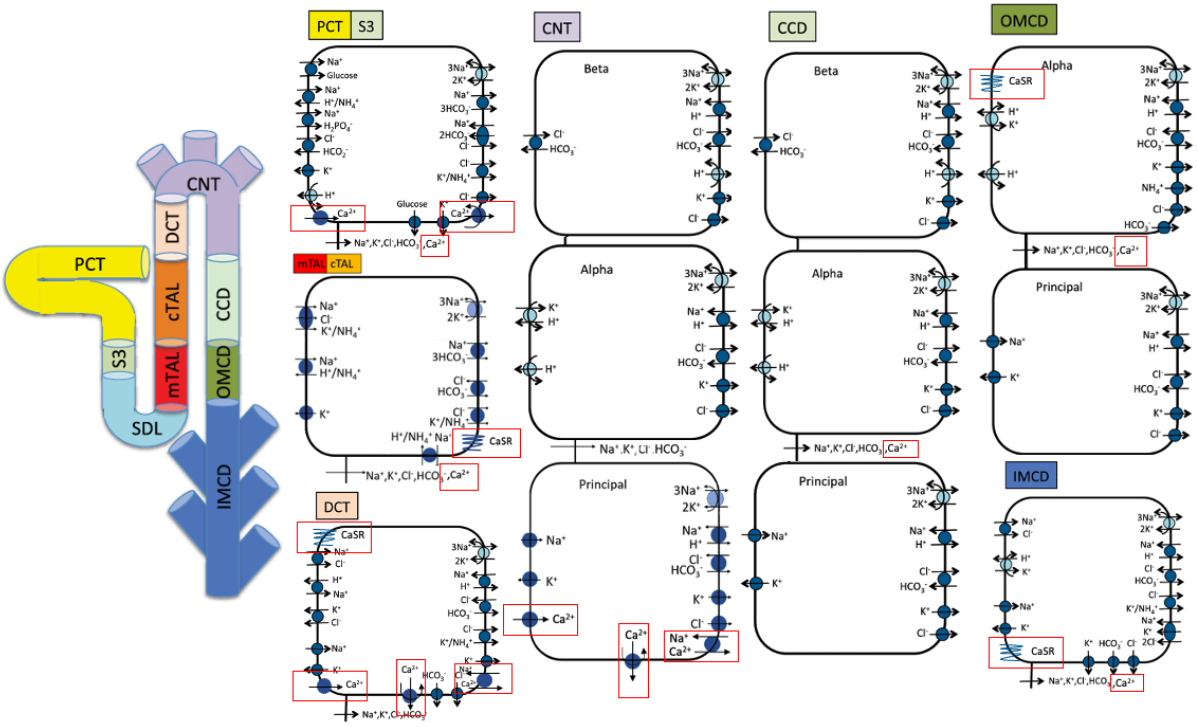

Figure 3.1: Schematic representation of the superficial nephron model. The diagram only displays Na^+, K^+, and Cl^- transporters. PCT, proximal convoluted tubule; S3, proximal straight tubule; mTAL, medullary thick ascending limb; cTAL, cortical thick ascending limb; DCT, distal convoluted tubule; CNT, connecting tubule; CCD, cortical collecting duct; OMCD, outer medullary collecting duct; IMCD, and inner medullary collecting duct. Illustration is taken from Ref. [65].

3.2 Neprhon Model Equations

In the nephron model, we need to ensure that the conservation of volume and conservation of mass equations in the lumen are satisfied. This should be done in conjunction with the equations that describe the conservation of mass and conservation of volume equations in the renal epithelial isolated cell model within the cell and lateral inner space compartments, as elaborated in Chapter 2. In this section, I provide a detailed description of these equations in the lumen.

3.2.1 Conservation of Mass Equations

Conservation of Volume. Tubular fluid flow is described by the pressure-driven Poiseuille flow. Within the lumen of a non-coalescing tubule (i.e., all segments excluding CNT and IMCD, explained below), the conservation of volume is given by:

$$\frac{dQ^i}{dx} = 2\pi r^i \hat{J}_v^i \tag{3.1}$$

where Q^i is the luminal volume flow, r^i is the luminal radius, and $\hat{J}_v^i \equiv J_{v,LC}^i + J_{v,LP}^i$ denotes overall (transcellular and paracellular) volume flux.

Conservation Equations for Non-reacting Solutes. Similarly, the conservation equation of solute k in lumen for a non-reacting solute is given by:

$$\frac{d}{dx}\left(Q^i C_{k,L}^i\right) = 2\pi r^i \hat{J}_k^i \tag{3.2}$$

where $\mathrm{C}_{k,L}^i$ is the luminal concentration of solute k and $\hat{J}_k^i \equiv J_{k,LC}^i + J_{k,LP}^i$ denotes the respective solute flux.

Conservation Equations for Reacting Solutes. For reacting solutes, conservation is applied to the total buffers in lumen which are as follows:

$$\begin{aligned}
\frac{d}{dx}\left(Q^i C_{\mathrm{CO_2},L}^i + Q^i C_{\mathrm{HCO_3},L}^i + Q^i C_{\mathrm{H_2CO_3},L}^i\right) &= \hat{J}_{\mathrm{CO_2},L}^i + \hat{J}_{\mathrm{HCO_3},L}^i + \hat{J}_{\mathrm{H_2CO_3},L}^i \\
\frac{d}{dx}\left(Q^i C_{\mathrm{HPO_4},L}^i + Q^i C_{\mathrm{H_2PO_4,\ L}}^i\right) &= \hat{J}_{\mathrm{HPO_4},L}^i + \hat{J}_{\mathrm{H_2PO_4},L}^i \\
\frac{d}{dx}\left(Q^i C_{\mathrm{NH_3},L}^i + Q^i C_{\mathrm{NH_4},L}^i\right) &= \hat{J}_{\mathrm{NH_3},L}^i + \hat{J}_{\mathrm{NH_4},L}^i
\end{aligned} \tag{3.3}$$

Pressure Equations. The hydrostatic pressure in the lumen of cell i, denoted as P^i, is related to Q^i and r^i by:

$$\frac{dP^i}{dx} = -\frac{8\mu Q^i}{\pi \left(r^i\right)^4} \tag{3.4}$$

where μ is the luminal fluid viscosity.

Conservation of Mass Equations for Coalescing Segments. CNT and IMCD segments coalesce with other nephrons (see Fig. 3.1). To capture this phenomenon in the model the equations are modified by scaling luminal water and solute flows by the tubule population ω_i similar to Ref. [82]. In these segments, the conservation of luminal fluid and non-reacting solutes is given by:

$$\begin{aligned} \frac{d}{dx}\left(\omega^i Q^i\right) &= \hat{J}^i_{v,L} \\ \frac{d}{dx}\left(\omega^i Q^i C^i_{k,L}\right) &= \hat{J}^i_{k,L} \end{aligned} \tag{3.5}$$

The equations for reacting solutes are also modified similarly. The convergence of the connecting tubules is described by ω_{CNT}, which denotes the fraction of connecting tubules remaining at coordinate x^{CNT}:

$$\omega^{CNT}(x^{CNT}) = 2^{-2.32x^{CNT}/L^{CNT}} \tag{3.6}$$

where L^{CNT} denotes the CNT length and x^{CNT} denotes the distance from the CNT inlet. Eq. 3.6 is formulated such that at the end of the connecting tubule, 10% of the population remain. These remaining CNT cells converge into the CCD.

The IMCD cells coalesce in a similar manner. Let $\omega^{IMCD}(\mathrm{x})$ denote the number of IMCD cells along the superficial nephron:

$$\omega^{\mathrm{IMCD}}\left(x^{\mathrm{IMCD}}\right) = 0.2 \times \left(1 - 0.95\left(\frac{x^{\mathrm{IMCD}}}{L^{\mathrm{IMCD}}}\right)^2\right) \exp^{-2.75\times x^{\mathrm{IMCD}}/L^{\mathrm{IMCD}}} \tag{3.7}$$

where L^{IMCD} denotes the IMCD length and x^{IMCD} denotes the distance from its inlet.

Flow-dependant Tubular Transport. The PT is lined with specialized epithelial cells called brush border cells, which have microvilli that increase their surface area for absorption, resulting in reabsorption along PT that varies proportionally to SNGFR. To model

flow-dependent epithelial transport, we utilize a similar approach as in Ref. [150]. Specifically, the PT is assumed to be compliant (i.e., non-compliant segments have constant r^i) with the radius given by:

$$r_{\mathrm{PT}} = r^0_{\mathrm{PT}} \left(1 + \mu_{\mathrm{PT}} \left(P_{\mathrm{PT}} - P^0_{\mathrm{PT}}\right)\right) \tag{3.8}$$

where r^0_{PT} is reference radius, P^0_{PT} the reference, and μ_{PT} characterizes tubular compliance. To account for the modulation of transporter density by luminal flow, we determine the microvillous torque as:

$$\tau_{\mathrm{PT}} = \frac{8\mu Q_{\mathrm{PT}} l_{\mathrm{PT,mv}}}{r^2_{\mathrm{PT}}} \left(1 + \frac{l_{\mathrm{PT,mv}} + \delta_{\mathrm{PT,mv}}}{r_{\mathrm{PT}}} + \frac{l^2_{\mathrm{PT,mv}}}{2r^2_{\mathrm{PT}}}\right) \tag{3.9}$$

where $l_{PT,mv}$ is the microvillous length and $\sigma_{PT,mv}$ denotes the height above the microvillous tip where drag is considered. The density of apical and basolateral transporters in proximal tubule cells is scaled by:

$$Scale = 1 + s \left(\frac{\tau_{\mathrm{PT}}}{\tau^0_{\mathrm{PT}}} - 1\right) \tag{3.10}$$

where the reference torque τ^0_{PT} is evaluated at the reference flow set to the inflow of PT (i.e., $\sim$45 nl/min).

Moreover, within the cell compartment, we have ammonia genesis (i.e, ammonia is generated) along PT at a rate of $\mathrm{Q^i(NH4^+)}$, resulting in the following conservation equation for ($\mathrm{NH3}$, $\mathrm{NH4^+}$):

$$\hat{J}^i_{\mathrm{NH_3},C} + \hat{J}^i_{\mathrm{NH_4^+},C} = \mathrm{Q^i(NH4^+)} \tag{3.11}$$

The CNT and CCD are also known to exhibit flow-dependent transepithelial transport. We added a simple representation of that flow dependence by scaling apical $\mathrm{Na^+}$ permeability in the CNT and CCD similar to Ref. [80], respectively, by τ_{CNT} and τ_{CCD}, given by:

$$\tau_{\mathrm{CNT}} = 1 + 3\left(\frac{Q_{\mathrm{CNT}}}{Q^0_{\mathrm{CNT}}} - 1\right), \quad \tau_{\mathrm{CCD}} = 1 + 3\left(\frac{Q_{\mathrm{CCD}}}{Q^0_{\mathrm{CCD}}} - 1\right) \tag{3.12}$$

where $\mathrm{Q^0_{CNT}}$ and $\mathrm{Q^0_{CCD}}$ are the reference flows.

Conservation of Charge. Furthermore, the condition of no net current into the lumen must be met, as represented by the given equation:

$$\sum_k z_k F \left(J_k^{CL} + J_k^{PL} \right) = 0 \tag{3.13}$$

where J_k^{CL} and J_k^{PL} denote the flux of solute k from the cellular and paracellular space to the lumen, respectively.

3.2.2 Numerical Solution

The tubular nephron model consists of a set of coupled differential-algebraic equations that need to be solved with appropriate boundary conditions. In our epithelial transport model, we have focused on steady-state conditions, where the time derivatives in all conservation equations have been set to zero. This means that there is no net accumulation of fluid or solute within any of the compartments. To spatially discretize the differential equations in our nephron model, we divided each segment into a discrete set of 200 grid points, referred to as cells, except for the PT, which is divided into 175 cells for the PCT and 25 cells for the S3 segment. Spatial derivatives in the lumen are approximated using a forward-finite difference scheme. To perform numerical simulations, boundary conditions must first be specified. The concentrations in the interstitium solution are fixed, while the luminal fluid composition, pressure, and flow rate at the PT inlet are specified. The output of each segment is then used as the input for the following segment.

Moving axially along the tubular axis, at each cell i (see Fig. 3.2), the variables that need to be solved are the 16 solute concentrations, electric potential, volume in the lumen, lateral interspace, and the epithelial cell compartments. The set of coupled nonlinear equations is comprised of the equations and fluxes introduced in Chapter 2 and the aforementioned sections in Chapter 3. By integrating the conservation equations, the steady-state values of solute concentrations, volume, and electrical potential in the epithelial cell compartments, lateral interspace, and tubular lumen can be determined as a function of position along the tubular axis. The system of algebraic equations obtained can be expressed as $F(x) = 0$, where $F(x)$ is a function that describes the relationships between the variables at each point along the tubular axis. We have utilized Newton's method to solve the system of algebraic equations.

Newton's method convergence criterion is typically defined by specifying a threshold for the residual, which is usually set to a small value (e.g., 10^{-4} in our simulations). In

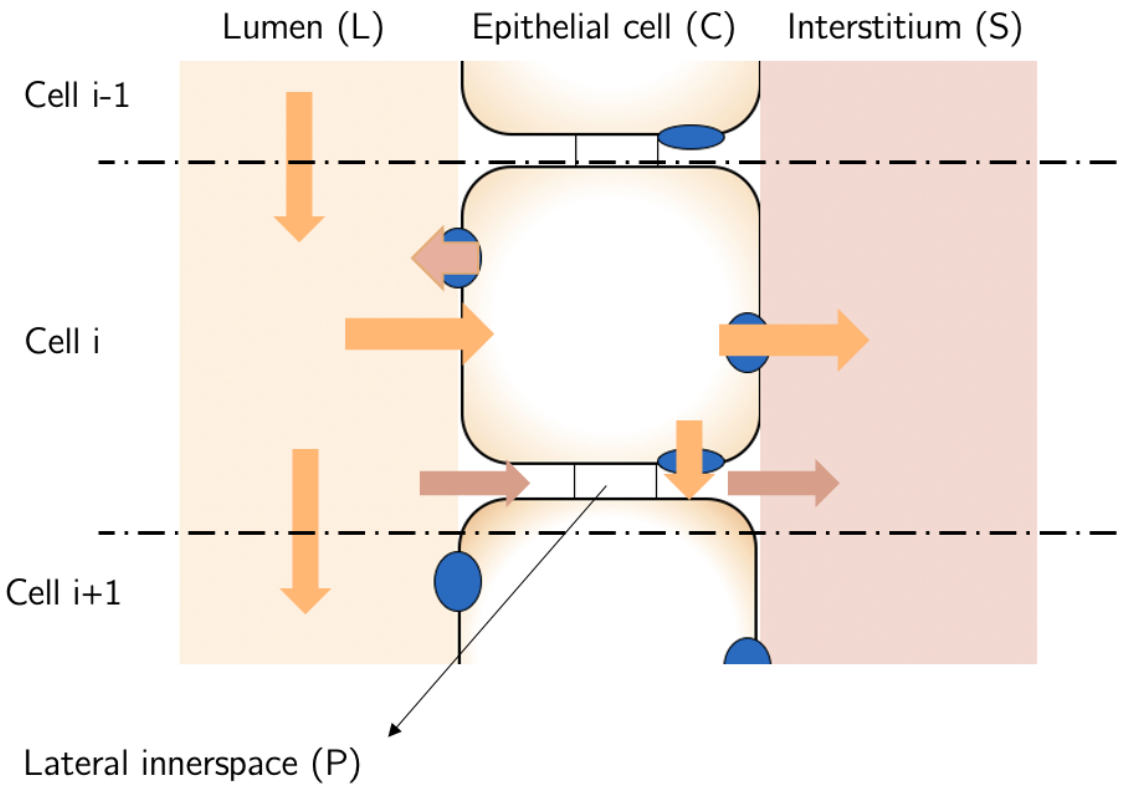

Figure 3.2: The figure shows a schematic of a sample grid point, defined as a cell along the nephron, with four compartments labelled: the lumen, the epithelial cell, the interstitium, and the lateral innerspace. The arrows in the schematic represent the transcellular and paracellular fluxes between the four compartments. In our simulations, we solve for 16 solute concentrations, volume, and electric potential in the lumen, cell, and lateral interstitial space.

addition, the number of iterations is usually limited to prevent excessive computational cost or divergence. In our simulations, we used a maximum of 500 iterations. If the convergence criterion is not met, the method may diverge or fail to converge. To facilitate convergence, we implemented a damped Newton's method. The damping parameter is manually specified for each segment and is based on the cell number, the norm of the error, and the number of iterations.

3.3 Baseline Model Results for Male and Female Rat Kidneys

Predictions of the baseline results for the neprhon model of epithelial solute and water transport, involving 16 solutes, in the superficial nephrons of male and female rat kidneys, have been obtained. The segmental delivery, which refers to the luminal solute flow at the inlet of a specific segment, for select solutes (Na^+, Ca^{2+}, K^+, Cl^-, HCO_3^-, NH_4^+, urea, Titratable Acids (TA), and luminal volume), are summarized in Fig.3.4. Furthermore, the segmental transport, defined as the total amount of reabsorption of a specific solute along the segment, is summarized in Fig.3.5. In the subsequent subsections, a detailed description of calcium reabsorption along the superficial nephron of male and female rat kidneys is provided.

3.3.1 Proximal Tubule Results

We will first discuss the results of the male rat model. Assuming a single nephron filtration rate (SNGFR) of 30 nl/min under baseline conditions, and a net amount of 24,000 superficial nephrons per rat kidney, the male model's predicted outcomes for delivery and transport of Ca^{2+} are summarized in Figs. 3.4B and 3.5B, respectively. Calcium enters the PT inlet at a rate of 0.92 μmol·min^{-1} and reabsorption along this segment is 0.63 μmol·min^{-1} which is equal to 68% of the filtered load of calcium, with paracellular transport making up 80% of the total reabsorption with remaining being transcellular reabsorption via apical calcium channels. Paracellular transport is mainly driven by electrodiffusive flux, facilitated by both the lumen-to-intracellular space concentration gradient and the transepithelial voltage difference (ΔV_{te}) with the lumen-to-intracellular space concentration gradient having a more significant role. Convective flux accounts for only 10% of total paracellular transport in PT. Proximal tubular calcium transport is driven, in large part, by Na^+ transport (see Fig. 3.5A), which establishes a lumen-positive ΔV_{te} and elevates luminal calcium concentration by driving water reabsorption. As discussed in Chapter .2, there are sex differences in terms of SNGFR. In the female rat model due to lower SNGFR (24 vs. 30 nL/min), we observe a lower delivery for all the solutes including Na^+ and Ca^{2+} at the PT inlet (82.944 μmol·min^{-1} and 0.72 μmol·min^{-1}). Similar to published results in a nephron model that does not represent Ca^{2+} transport [66], we predict a much lower fractional Na^+ (54% compared to 70%) reabsorption along PT in the female rat kidney, as a result of smaller transport area and lower NHE3 activity (see Fig. 3.5A). The reduced fractional Na^+ reabsorption and the resulting reduced water reabsorption lead to a

significantly lower Ca^{2+} reabsorption along this segment (61% compared to 68%) despite assuming that the female model PT having a higher paracellular calcium permeability relative to male, based on ex-vivo experiments on estradiol enhanced rabbit kidney PT cells [57]. Similar to the male rat model electrodiffusive paracellular flux drives calcium reabsorption along this segment, amounting to 81% of total Ca^{2+} reabsorption along PT.

3.3.2 Thick Ascending Limb Results

In the male model, calcium enters the mTAL inlet at a rate of 0.29 μmol·min^{-1}. Calcium reabsorption along the TAL is entirely paracellular and is driven by the positive ΔV_{te} established by the activity of Na^+-K^+-ATPase. This activity leads to a low intracellular concentration of Na^+ and a high extracellular concentration of Na^+, allowing for the transport of Na^+, Cl^-, K^+, and NH_4^+ via NKCC2, with the latter two solutes competing to bind to the co-transporter. Na^+-K^+-ATPase also establishes a high intracellular concentration of K^+ and a low extracellular concentration of K^+, resulting in a high transcellular gradient of K^+ and subsequent apical recycling of K^+ to the lumen via the apical potassium channel.

The mTAL segment has a higher interstitial concentration of Ca^{2+} compared to cTAL, with interstitial concentration of Ca^{2+} linearly decreasing from 2.5 mM to 1.25 mM along mTAL and remaining at 1.25 mM along cTAL (similar in both male and female models). This results in CaSR lowering the tight junction permeability of mTAL compared to cTAL, leading to less calcium reabsorption in the medullary limb compared to the cortical limb. CaSR also has a greater inhibitory effect on the activity of NKCC2 and ROMK in the mTAL limb compared to cTAL for similar reasons. However, the overall effect of CaSR on NKCC2 and ROMK is small, resulting in a decrease in activity by $\sim$2% and $\sim$3%, respectively for male and female models. In the male model, the TAL segment reabsorbs calcium at a rate of 0.20 μmol·min^{-1}, which accounts for 22% of the filtered load.

The delivery of Ca^{2+} to the mTAL inlet is slightly lower in the female model compared to the male model, at 0.28 μmol·min^{-1}. The female rat kidney has a smaller transport area along TAL, but a higher activity of NKCC2, KCC, and Na^+-K^+-ATPase, as reported in Ref. [65] and Chapter 2. This increased activity of Na^+-K^+-ATPase, combined with higher Na^+ delivery, results in a higher transcellular sodium concentration gradient. As a result, there is greater Na^+ reabsorption in the female model compared to the male model, with NKCC2 playing a more significant role in Na^+ reabsorption in TAL compared to NHE3.

The flow-dependant ammonia genesis in PT cells leads to a higher luminal concentration of NH_4^+ in the female model compared to the male model starting from the late part of PT

segment (see Fig. 3.3a). This higher concentration persists along the TAL. Despite a higher influx of Na^+ via NKCC2 in the female model, the competitive binding of NH_4^+ and K^+ results in a decreased influx of K^+. On the other hand, the higher basolateral influx of K^+ due to elevated Na^+-K^+-ATPase activity is counteracted by the increased basolateral efflux of K^+ due to higher basolateral K^+-Cl^- (KCC) activity in the female model (see Fig. 3.1 and Table. 2.8). These competing effects result in a lower intracellular K^+ concentration in the female model compared to the male model (see Fig. 3.3b). Since the apical potassium channel in both male and female models is similar, the resulting apical recycling of K^+ is lower in the female model. Consequently, this leads to a diminished lumen-positive ΔV_{te} specifically along cTAL compared to the male model, resulting in lower Ca^{2+} reabsorption in the female model (0.13 μmol·min^{-1}) compared to the male model (0.19 μmol·min^{-1}), which amounts to 18% of fractional calcium reabsorption.

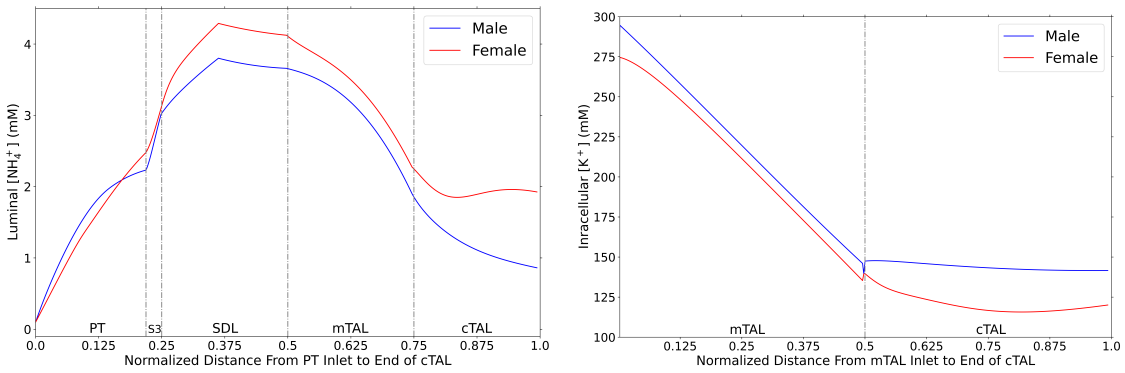

(a) (b)

Figure 3.3: (a) Luminal NH_4^+ concentration and (b) intracellular K^+ concentration in male (blue line) and female (red line) models. PT, proximal tubule; S3, proximal straight tubule; SDL, short descending limb; mTAL, medullary thick ascending limb; cTAL, cortical thick ascending limb.

3.3.3 Distal Convoluted Tubule and Connecting Tubule Results

In both male and female models, DCT and CNT are assumed to have minimal paracellular permeability to calcium, resulting in negligible paracellular calcium transport along DCT-CNT, as discussed in Section 2.5.3. Calcium reabsorption along DCT2-CNT is entirely transcellular, with DCT2 showing higher reabsorption due to significantly higher TRPV5 expression compared to CNT (in the male model, DCT2 accounts for 4.7% and

CNT accounts for 3.2% of the total fractional calcium reabsorption). NCX1 is responsible for extruding most of the calcium from the cell (78%), with the remaining portion being transported by PMCA. Influx of interstitial Na^+ via NCX1 contributes only a small fraction of total Na^+ influx (around 1%). Overall, calcium transport along DCT2-CNT leads to a total reabsorption of 0.075 μmol·min^{-1} or 7.9% fractional reabsorption of calcium in the male model. In the female model, we observe considerably higher calcium reabsorption along DCT-CNT compared to the male model (9.7% in DCT2 and 6.5% in CNT), attributed to considerably higher TRPV5 expression in the female model.

3.3.4 Collecting Duct and Calcium Excretion Results

Calcium reabsorption along CD is negligible and limited to the paracellular pathway. In the male model, urinary calcium excretion is predicted to be 0.030 μmol·min^{-1} or 3.4% of filtered load, at a concentration of 3.39 mM. We observe a similar fractional calcium excretion in the female model (3.0%) and a lower urinary calcium excretion in the female model (0.025 μmol·min^{-1}), consistent with animal experiments and human observations.

The predicted segmental reabsorption rates for male and female models have been shown to be in good agreement with the experimental measurements. Specifically, we predict that the fractional reabsorption rates for the male and female models are 68% and 62%, respectively, which are consistent with the range of 60-70% reported in the literature for the PT [102]. For TAL, the predicted rates for male and female models are 22% and 20%, respectively, which are in line with the values observed in animal experiments cited in several studies, ranging from 20-25% [3, 1, 75, 83, 137, 36, 25]. Moreover, the predicted urinary calcium excretion rates of 3.4% and 3.1% for male and female models, respectively, are consistent with the reported range of 2-5% of the filtered load in a recent publication [58]. Furthermore, the predicted urine calcium concentration values of 3.4 mM and 4.3 mM for male and female models, respectively, fall within the reported range of 0.7 to 7 mM in various studies [10, 32, 49, 135]. It is important to note that the accuracy of these predictions depends on the accuracy of the experimental measurements and assumptions made in the modelling approach.

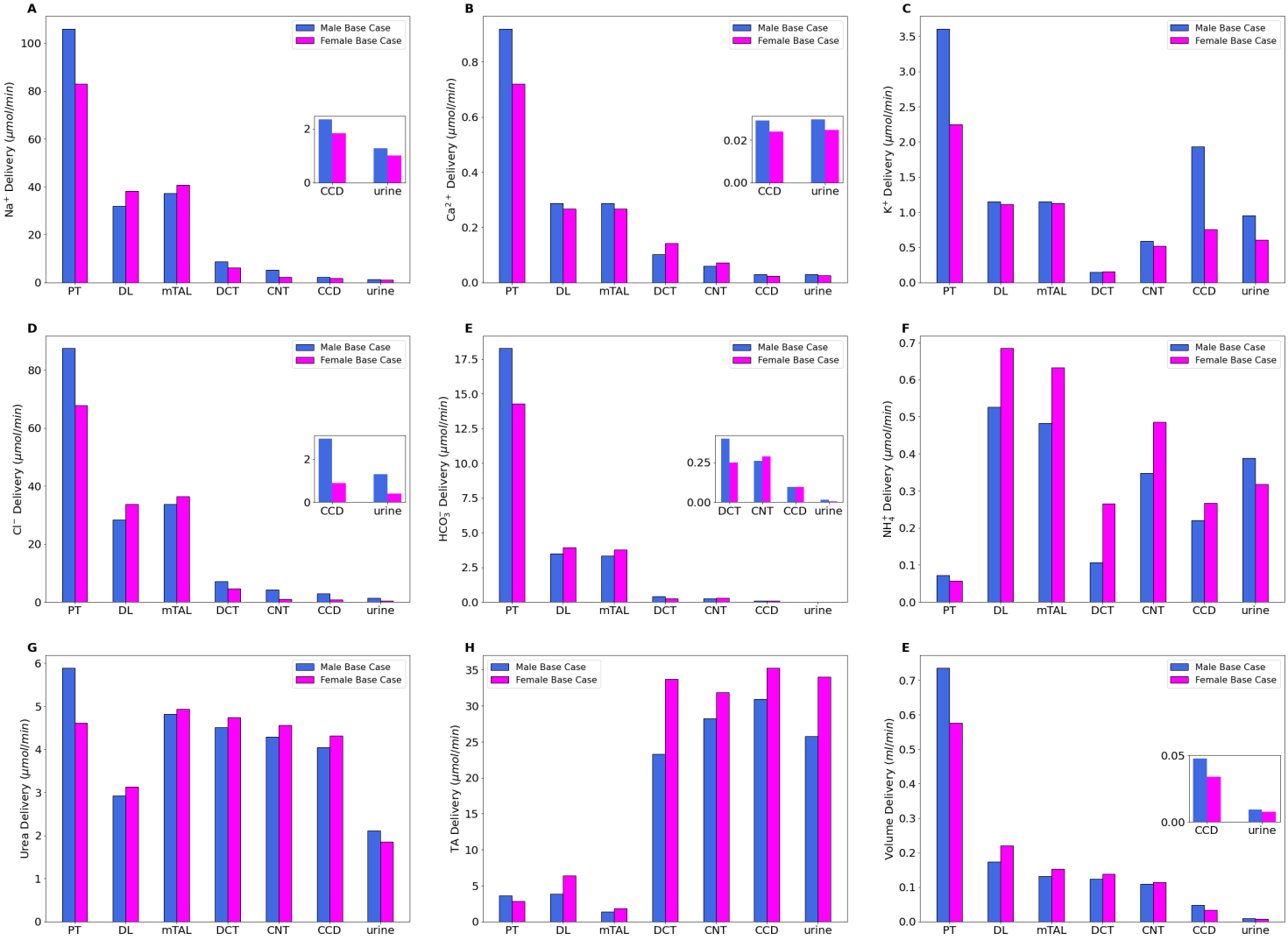

Figure 3.4: Delivery of key solutes (A–H) and fluid (G) to the beginning of individual nephron segments in male and female rats. PT, proximal tubule; DL, descending limb; mTAL, medullary thick ascending limb; DCT, distal convoluted tubule; CNT, connecting tubule; CCD, cortical collecting duct; TA, titratable acid.

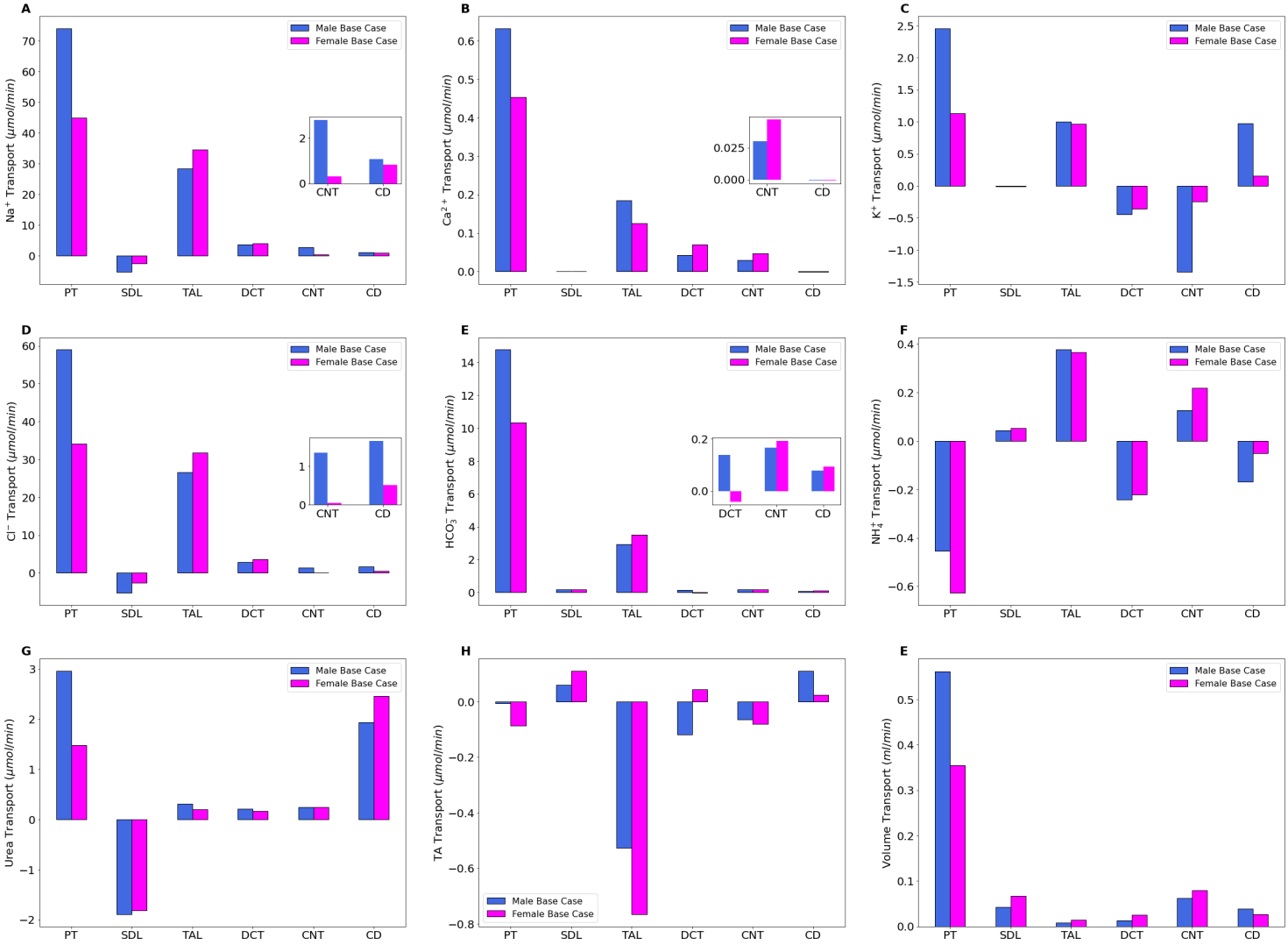

Figure 3.5: Net transport of key solutes (A–H) and fluid (E) along individual nephron segments, in male and female rats. Transport is taken positive out of a nephron segment. PT, proximal tubule; DL, descending limb; TAL, thick ascending limb; DCT, distal convoluted tubule; CNT, connecting tubule; CD, collecting duct; TA, titratable acid.

3.4 Discussion

Calcium transport along superficial nephrons in male and female rat kidneys was investigated by extending the renal epithelial isolated cell models to a nephron model. The current models have expanded previously published models for male rat kidney [79] and female rat kidney [91] to incorporate Ca^{2+} transport.

The model predicts that approximately 68% of calcium reabsorption occurs along the proximal tubule (PT), including the S3 segment, in male rats, and approximately 62% in female rats. Paracellular transport accounts for about 80% of the total reabsorption, with the remaining being transcellular transport, in superficial nephrons of both male and female rat kidneys. These values are consistent with experimental animal studies [52]. Apical L-type channels facilitate the influx of calcium through the cell membrane of PT cells. In the epithelial PT cell calcium is mainly extruded by PMCA, but the exact mechanisms of calcium extrusion within these cells are not fully understood [155]. Claudins, a family of proteins, play a crucial role in the paracellular transport of Na^+ and calcium Ca^{2+} in the PT, as PT cells are highly permeable to calcium due to the presence of pore-forming cation-specific claudin members such as claudins 2, 10a, and 17 [22]. Animal experiments have demonstrated a close coupling between paracellular transport of calcium and Na^+ transport [127]. The activity of Na^+-K^+-ATPase establishes a steep transcellular sodium gradient, resulting in a low intracellular concentration of $[Na^+]$ and a high extracellular concentration of $[Na^+]$. This gradient promotes the reabsorption of Na^+ ions primarily through the action of NHE3 [138]. The lumen positive ΔV_{te} along with the lumen-to-innerspace calcium concentration gradient, facilitates paracellular calcium transport through electrodiffusion. PT is known to be highly permeable to volume transport, allowing for calcium transport via solvent drag. However, our model predicts that only approximately 10% of total paracellular transport can be attributed to convection in both sexes, indicating a lesser role of convection in paracellular calcium transport. Some studies have reported the presence of CaSR at the apical membrane along the PT, although their function is not fully understood [2, 119]. Interestingly, elevation of interstitial PTH levels, which promotes increased calcium reabsorption in the TAL, has been found to have an inhibitory effect on calcium transport in the PT. This inhibitory effect can be attributed to the inhibitory effects of PTH on NHE3 [18].

SDL has been shown to have a very low calcium permeability [120]. In contrast, the tight junctions of TAL are considerably more permeable to calcium due to the presence of claudins-10, claudin-16 (also known as paracellin-1), and claudin-19, which facilitate paracellular transport of calcium [62]. This is further supported by our model, which predicts paracellular calcium reabsorption of approximately 22% along the TAL in the male model

and 18% in the female model, with higher reabsorption in the cortical limb compared to the medullary part, consistent with observations from animal experiments [42]. Similar to PT, calcium reabsorption in TAL is dependent on Na^+ reabsorption, and alterations in transcellular and paracellular sodium transport can significantly affect calcium reabsorption. CaSR expressed at the basolateral membrane of TAL cells acts as a regulator of paracellular calcium transport by mainly modulating claudin-16 phosphorylation based on the interstitial calcium concentration [96]. CaSR also has an inhibitory effect on the activity of non-calcium-specific channels and transporters. In vivo experiments on rats have shown that increasing calcium concentration from 1.1 to 5 mM results in an approximately 84% decrease in the activity of the renal outer medullary potassium channel (ROMK) [16]. In another in vivo experiment with the treatment of calcimimetic on male mice, phosphorylation of the sodium-potassium-chloride cotransporter (NKCC2) decreased by approximately 50%, without changing NKCC2 expression levels [16].

Studies have shown that the apical calcium channel TRPV5 is predominantly expressed along DCT2, with lower expression in CNT [94]. The model predicts a higher reabsorption along DCT2 compared to CNT in both sexes, as a result of the higher expression of TRPV5 in DCT2 in both male and female models. NCX1 account for $\sim$70% of calcium extrusion from the cell and its activity is dependent on luminal and interstitial $[Na^+]$. Paracellular transport, on the other hand, is negligible along this segment as the pore-forming cation claudins are minimally expressed [62]. CaSR is colocalized with NCC along DCT and has a small inhibitory effect on its activity, although other functions of CaSR in this segment are not yet fully understood [16]. Immunohistochemical studies on mouse kidneys have shown higher TRPV5 protein expression along the DCT2-CNT segment in female mouse kidneys compared to males [64]. Our model also takes into account this higher TRPV5 expression in the female model, and predicts a significantly greater calcium reabsorption in the female model compared to the male model, in both DCT2 and CNT segments.

Along CD, there has been reported to have no significant transcellular calcium transport and minimal paracellular permeability based on studies conducted in isolated CCD cells of rabbits [27]. Animal experiments have provided evidence of the presence of CaSR on the apical membrane of cells in the OMCD and IMCD. In isolated mouse OMCD cells, it has been shown that increased luminal $[Ca^{2+}]$ leads to elevated HATPase activity in type A cells, as observed in a study in Ref. [118]. Similarly, in perfused rat IMCD cells, CaSR has been shown to decrease apical water permeability in response to elevated luminal calcium concentration, as reported in a study by Sands et al. in 1997 [123]. These findings highlight the role of CaSR in regulating renal tubular function and its potential involvement in calcium handling in the collecting ducts.

Chapter 4

Nephron Model: Effects of Ca^{2+} and Na^{+} Transporter Inhibition

This chapter explores the effects of inhibiting calcium channels, such as TRPV5, and calcium exchangers, such as NCX1, alongside reducing paracellular calcium permeability along PT and TAL. Furthermore, the effects of inhibiting sodium transporters, such as NHE3, NKCC2, NCC, and ENaC, on calcium transport along the superficial nephron in male and female rats are investigated. The results show that NCX1 and TRPV5 inhibition, as well as a decrease in paracellular calcium permeability along TAL, lead to high urinary calcium excretion in both male and female models. Decreasing calcium permeability along PT results in slightly higher urinary calcium excretion, as the loss of calcium reabsorption along PT is compensated in TAL. Furthermore, inhibiting NHE3, NKCC2, and NCC also results in high urinary calcium excretion, while inhibiting ENaC leads to lower urinary calcium excretion in both male and female models. The chapter also discusses the differences in segmental calcium compensation between male and female models. Finally, the discussion summarizes the results and provides further insights into the implications of the findings.

4.1 Effects of Ca^{2+} Transporter Inhibition

4.1.1 TRPV5 and NCX1 Inhibition

TRPV5

The effect of complete inhibition of TRPV5 expression along DCT2-CNT on urine calcium transport was investigated in both male and female models. The delivery and transport of Na^+ and Ca^{2+} are summarized in Fig. 4.1 and Fig. 4.2, respectively.

The model results indicate that complete inhibition of TRPV5 only caused a negligible increase in Na^+ transport along DCT2-CNT (approximately 1-3% in both male and female models). As there is no transcellular reabsorption of calcium along DCT2-CNT, a significant increase in luminal calcium concentration occurred along the CD in both male and female models, leading to hypercalciuria. The higher luminal Ca^{2+} concentration along CD resulted in a slightly reduced Na^+ urine excretion due to increased Na^+ reabsorption, resulting from a more positive lumen-positive ΔV_{te} (5% in male model and 12% in female model). Furthermore, there was a significantly higher urine calcium excretion in both male and female models (see Table 4.1). Notably, the female model showed a greater increase in calcium excretion (468%) than the male model (243%), which can be attributed to the higher expression levels of TRPV5 and NCX1 in the female model.

NCX1 Inhibition

The impact of full inhibition of the basolateral NCX1 pump on calcium transport was investigated, and the segmental delivery and transport results of Na^+ and Ca^{2+} are presented in Fig. 4.3 and Fig. 4.4, respectively. Complete inhibition of NCX1 had a negligible effect on Na^+ transport along DCT2-CNT. Moreover, as discussed in Chapter 3, NCX1 predominantly extrudes Ca^{2+} from the cell along the DCT2-CNT segment, with PMCA being responsible for the remaining Ca^{2+} transport in both male and female models. Complete inhibition of NCX1 is expected to significantly decrease calcium reabsorption along DCT2-CNT in both male and female models (see Table 4.1), and PMCA does not sufficiently compensate for the lack of the other basolateral efflux pathway. The increased luminal Ca^{2+} concentration leads to a more positive lumen-positive ΔV_{te}, resulting in a slight increase in Na^+ transport along CD and a decrease in urinary Na^+ excretion (see Table, 4.1. There is a significant increase in urinary Ca^{2+} excretion, which is more noticeable in the female model (228% vs 46%) due to the higher expression of both TRPV5 and NCX1 compared to the male model.

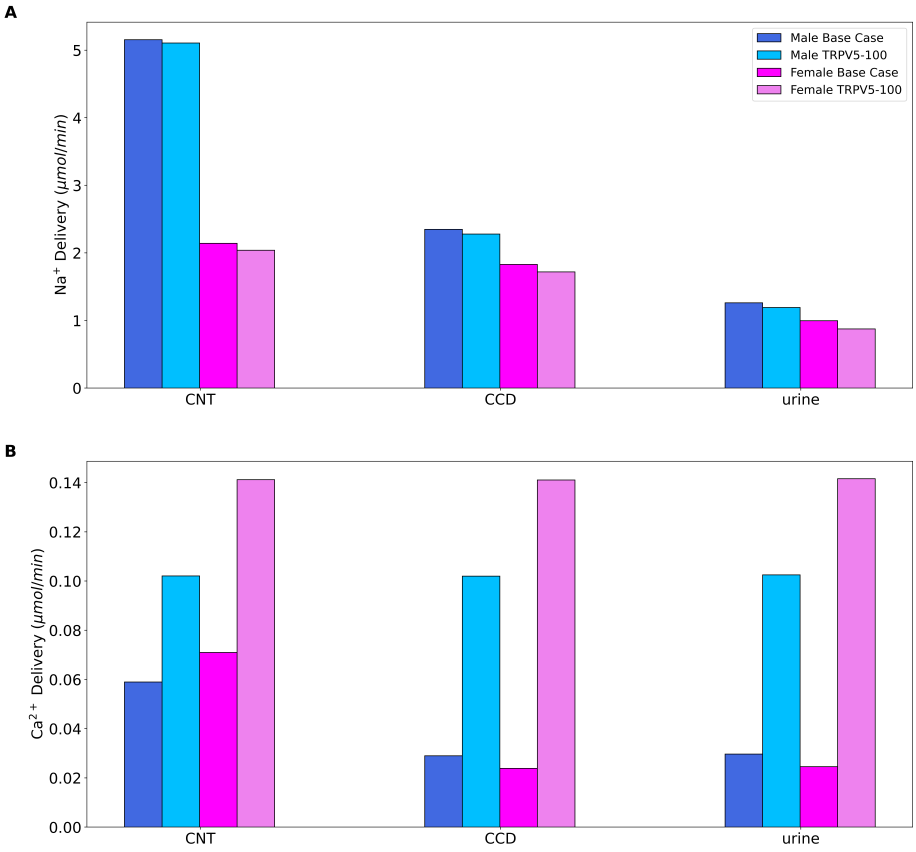

Figure 4.1: Comparison of segmental solute delivery of (A) Na^+ (B) Ca^{2+} for male and female models for base case, and for 100% inhibition in TRPV5 activity (TRPV5-100); PT, proximal tubule; DL, descending limb; mTAL, medullary thick ascending limb; DCT, distal convoluted tubule; CNT, connecting tubule; CCD, cortical collecting duct.

4.1.2 Decreasing Paracellular Calcium Permeability

Along the PT

Simulations were conducted to investigate the effects of decreasing P_{Ca}^{Para} by 50% along the PT. The delivery and transport plots are shown in Fig. 4.5 and Fig. 4.6. Decreasing P_{Ca}^{Para} by 50% has a negligible effect on Na^+ transport and urinary Na^+ excretion in both male and female models. The results indicate that decreasing P_{Ca}^{Para} along PT leads to only a slight reduction in calcium transport along this segment in both male and female models. This increased Ca^{2+} flow to the TAL, results in a higher lumen-to-lateral innerspace Ca^{2+}

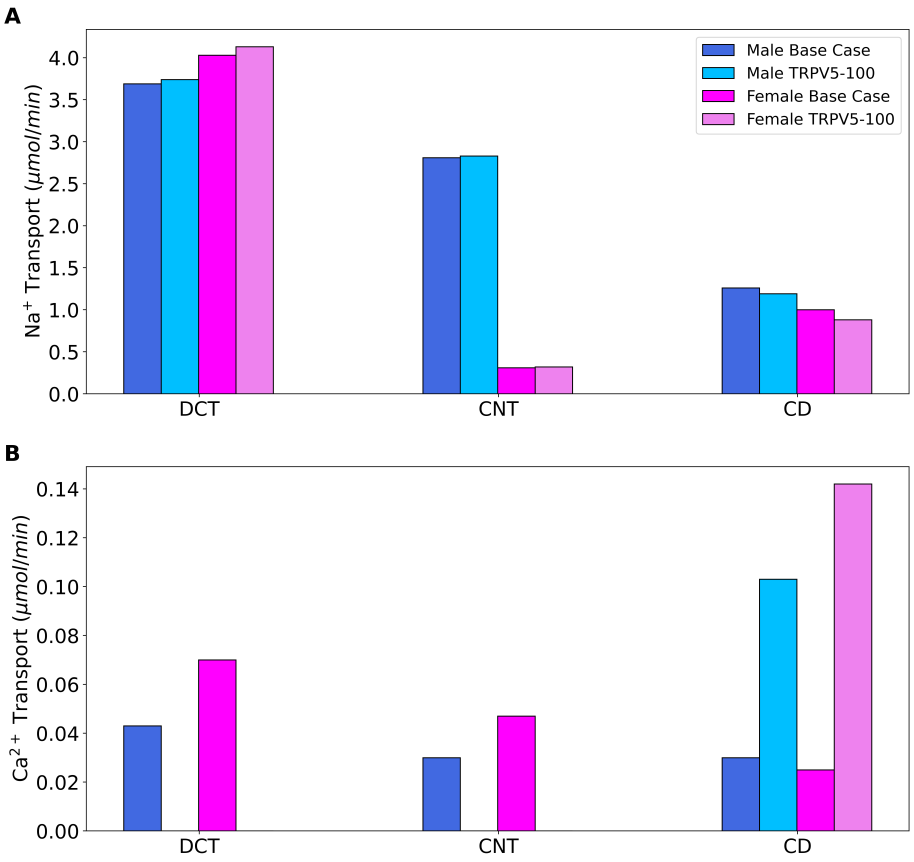

Figure 4.2: Comparison of segmental solute transport of (A) Na^+ and (B) Ca^{2+} for male and female models for the base case, and for 100% inhibition of TRPV5 activity (TRPV5-100); PT, proximal tubule; SDL, short descending limb; TAL, thick ascending limb; DCT, distal convoluted tubule; CNT, connecting tubule; CD, cortical duct.

concentration gradient, resulting in compensation in calcium reabsorption along TAL. The simulations resulted in a slight increase in calcium excretion, with male and female models showing a 16% and 4% increase, respectively.

Along the TAL

A simulation was conducted to investigate the effects of a 50% reduction in paracellular TAL permeability to Ca^{2+}. The resulting Na^+ and Ca^{2+} delivery and transport profiles are shown in Fig. 4.7 and Fig. 4.8. Decreasing paracellular TAL permeability to Ca^{2+}

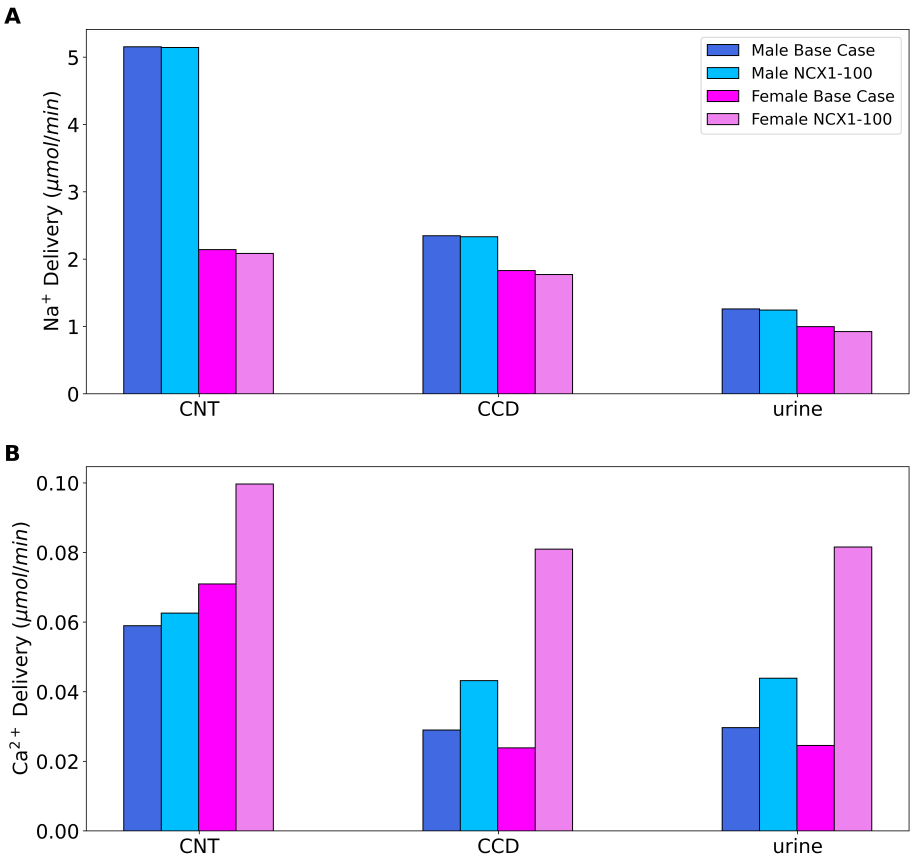

Figure 4.3: Comparison of segmental solute delivery of (A) Na^+ (B) Ca^{2+} for male and female models for base case, and for 100% inhibition of NCX1 activity (NCX1-100); PT, proximal tubule; DL, descending limb; mTAL, medullary thick ascending limb; DCT, distal convoluted tubule; CNT, connecting tubule; CCD, cortical collecting duct.

has a negligible effect on Na^+ transport and urinary Na^+ excretion (see Table. 4.1). It was observed that calcium reabsorption along DCT2-CNT cannot sufficiently compensate for the reduced reabsorption in the TAL. Furthermore, the elevated luminal Ca^{2+} concentration is insufficient to strongly stimulate transcellular calcium transport via TRPV5. Consequently, the urinary excretion of Ca^{2+} is predicted to increase by 143% in the male model and 140% in the female model.

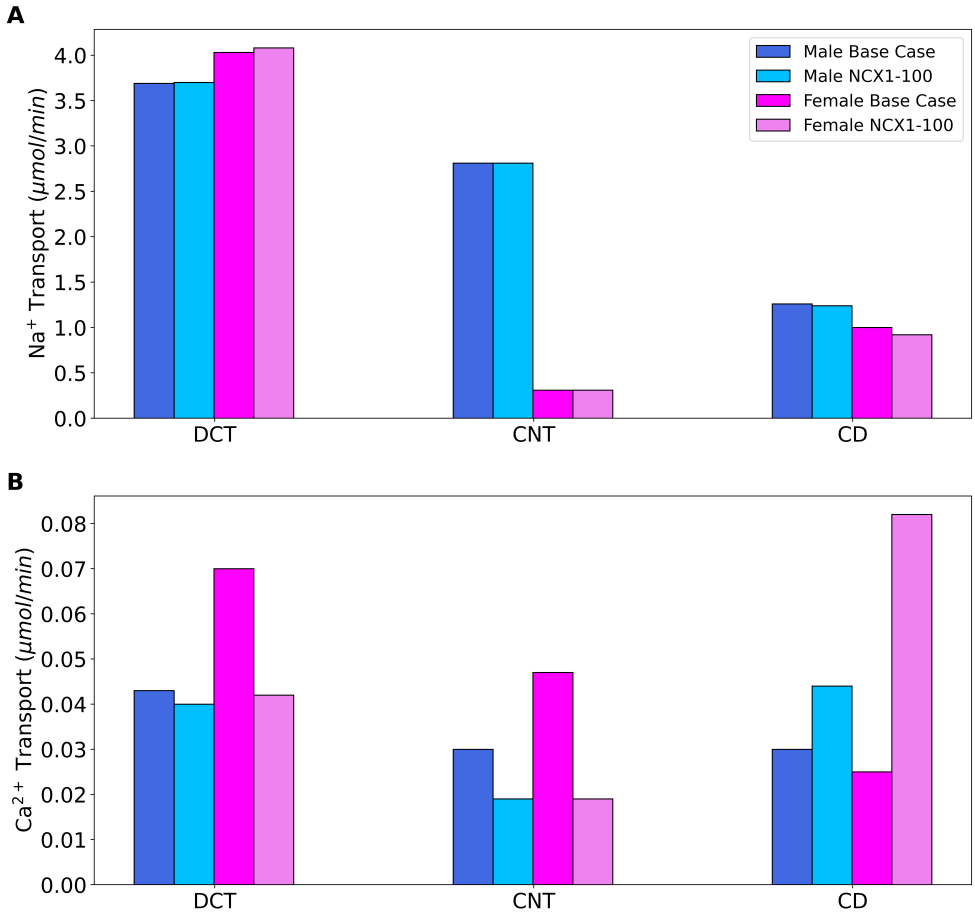

Figure 4.4: Comparison of segmental solute transport of (A) Na^+ and (B) Ca^{2+} for male and female models for the base case, and for 100% inhibition of NCX1 activity (NCX1-100); PT, proximal tubule; SDL, short descending limb; TAL, thick ascending limb; DCT, distal convoluted tubule; CNT, connecting tubule; CD, cortical duct.

4.2 Effects of Na^+ Transporter Inhibition

4.2.1 NHE3 Inhibition

The Na^+/H^+ exchanger 3 (NHE3) is present at the apical membrane of PT and TAL cells [8]. In this study, the inhibition of NHE3 was simulated at two different levels, i.e., 50% and 80%. The simulations aimed to examine the impact of the inhibition on Ca^{2+}

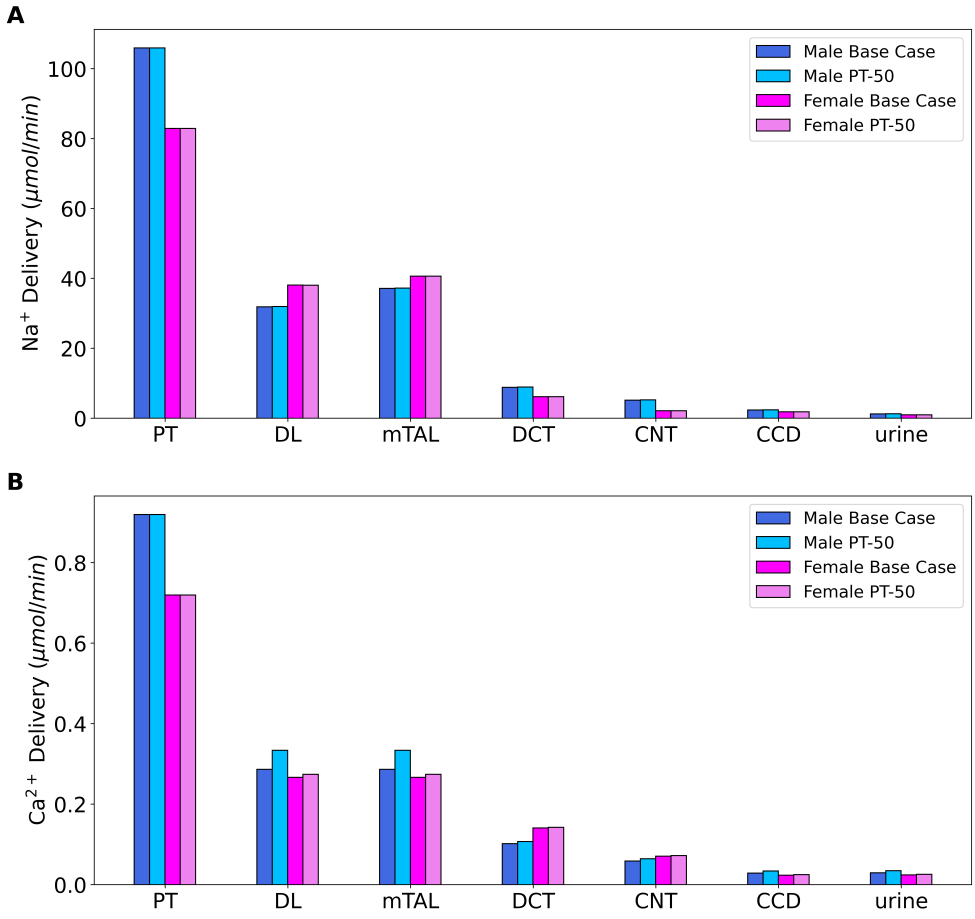

Figure 4.5: Comparison of segmental solute delivery of (A) Na^+ (B) Ca^{2+} for male and female models for base case, and for 50% decrease in paracellular permeability of Ca^{2+} along PT (PT-50); PT, proximal tubule; DL, descending limb; mTAL, medullary thick ascending limb; DCT, distal convoluted tubule; CNT, connecting tubule; CCD, cortical collecting duct.

and Na^+ transport in both male and female models. The choice to simulate 80% rather than full inhibition (i.e., 100% inhibition of NHE3) is motivated by the presence of other amiloride-sensitive Na^+/H^+ exchangers in the PT that may contribute significantly to Na^+ reabsorption along this segment, while NHE3 is the only Na^+/H^+ exchanger represented in the current model. Furthermore, NHE2 is also present at the TAL apical membranes [131]. Thus, for the simulations of 50% and 80% inhibition, NHE TAL expression was inhibited by 25% and 40% for medullary and cortical limbs, respectively. It was assumed that NHE3 was

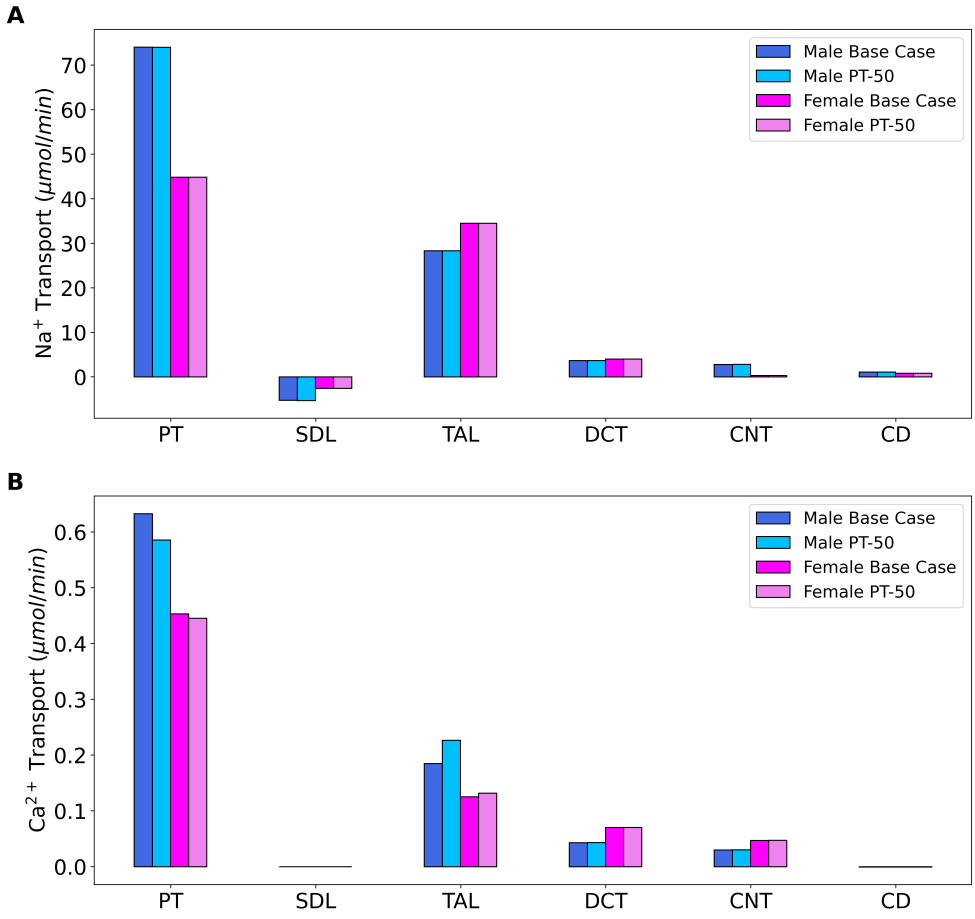

Figure 4.6: Comparison of segmental solute transport of (A) Na^+ and (B) Ca^{2+} for male and female models for the base case, and for 50% decrease in paracellular permeability if Ca^{2+} along PT (PT-50); PT, proximal tubule; SDL, short descending limb; TAL, thick ascending limb; DCT, distal convoluted tubule; CNT, connecting tubule; CD, cortical duct

inhibited for a sufficiently long time to allow changes in interstitial osmolarity to occur, but before the initiation of compensatory mechanisms. Inhibition of NHE3 led to a substantial increase in fluid delivery to the loops of Henle and CD, overwhelming the inner-medullary concentrating effect. As a result, the medullary interstitial concentrations of Na^+, K^+, Cl^-, and urea were lowered as described in Ref. [79]. Similarly, it was assumed that the interstitial concentration of calcium remained unaffected at the cortico-medullary junction and the outer-inner medullary junction, but was reduced to 3 mM (from 4 mM under baseline conditions) at the papillary tip. Furthermore, it was assumed that the increased

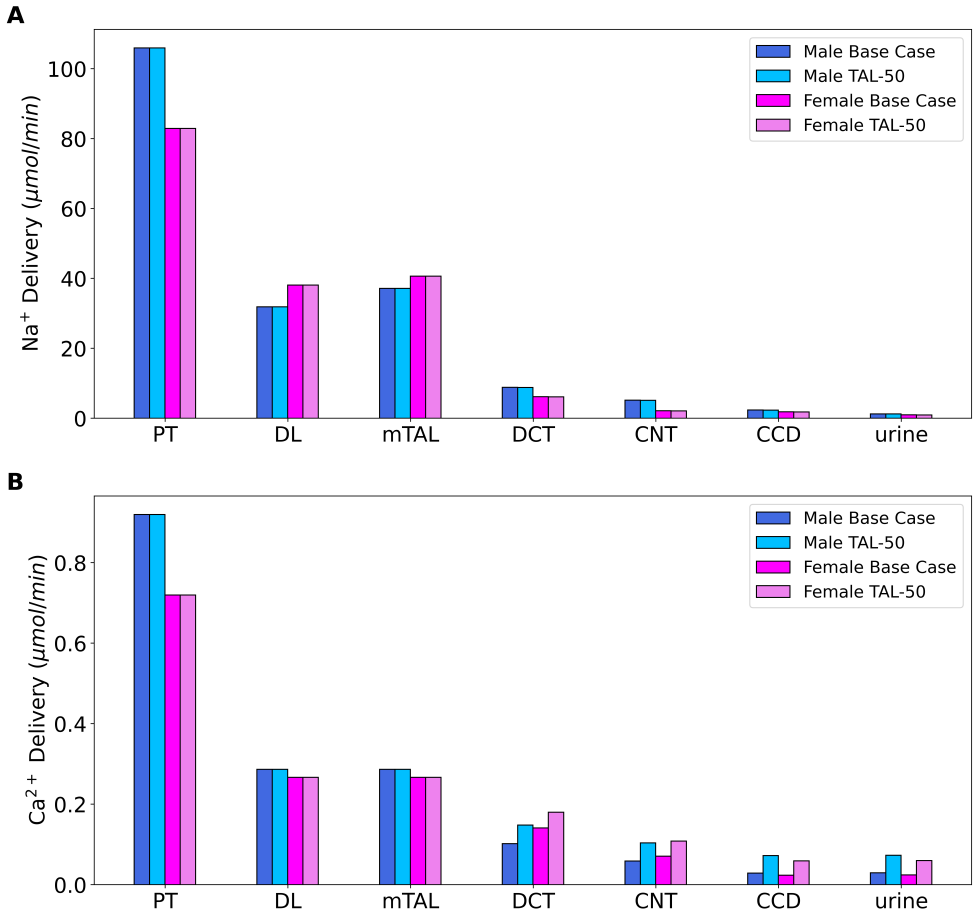

Figure 4.7: Comparison of segmental solute delivery of (A) Na^+ (B) Ca^{2+} for male and female models for base case, and for 50% decrease in paracellular permeability of Ca^{2+} along TAL (TAL-50); PT, proximal tubule; DL, descending limb; mTAL, medullary thick ascending limb; DCT, distal convoluted tubule; CNT, connecting tubule; CCD, cortical collecting duct.

delivery of NaCl to TAL would activate the tubuloglomerular feedback (TGF) [79], which is a mechanism that regulates the glomerular filtration rate in the kidney. As a result, SNGFR was decreased accordingly by 8% and 30% with 50% and 80% inhibition, respectively.

The predicted segmental deliveries of Na^+ and Ca^{2+} are shown in Figs. 4.9A and 4.9B for both male and female models, respectively. NHE3 inhibition indirectly reduces Ca^{2+} reabsorption along the PT segment by substantially decreasing Na^+ reabsorption, resulting

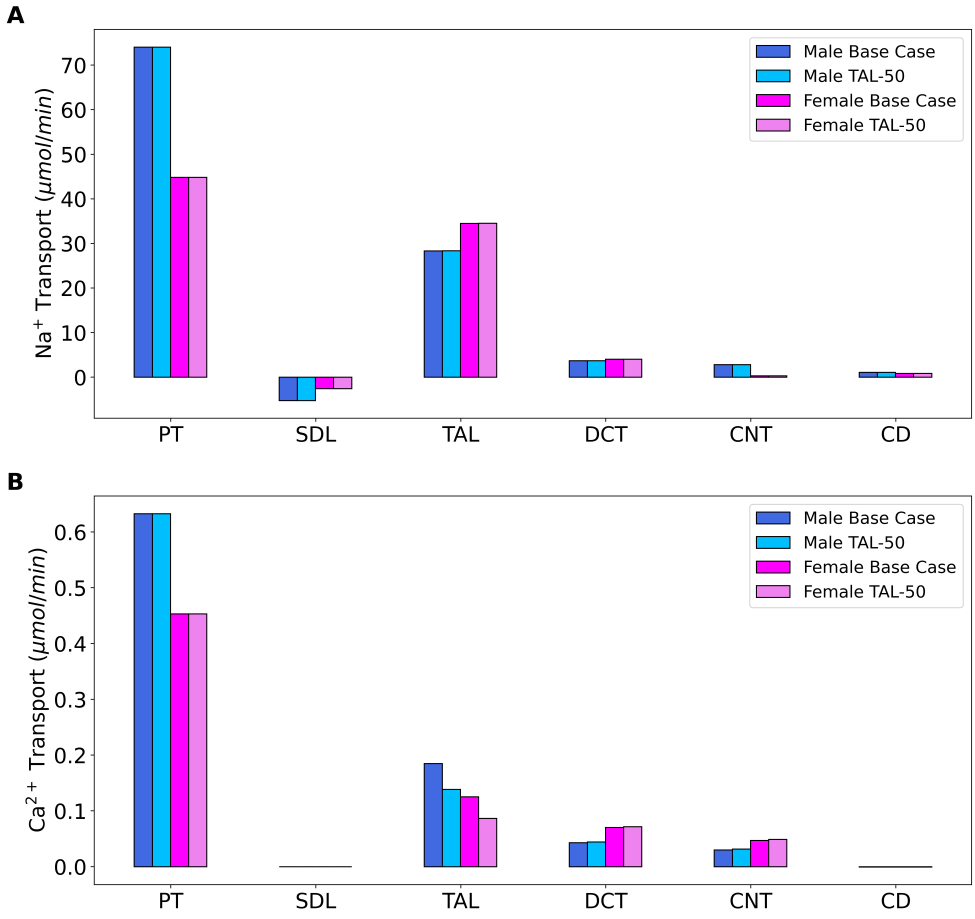

Figure 4.8: Comparison of segmental solute transport of (A) Na^+ and (B) Ca^{2+} for male and female models for the base case, and for 50% decrease in paracellular permeability if Ca^{2+} along TAL (TAL-50); PT, proximal tubule; SDL, short descending limb; TAL, thick ascending limb; DCT, distal convoluted tubule; CNT, connecting tubule; CD, cortical duct

in a reduced ΔV_{te} and water reabsorption, leading to reduced convective and electrodiffusive calcium transport in male and female models. This indicates similar calcium handling in both male and female models in this segment (see PT transport column in Table. 4.2).

The decreased Ca^{2+} reabsorption in PT compared to the baseline leads to higher calcium delivery to the subsequent segments, despite the reduction in SNGFR in both cases of inhibition in both male and female models. Along the TAL, in the male model, the competing effects of increased Na^+ and reduced NHE expressions result in a minimal change

Table 4.1: Effects of inhibiting Ca^{2+} specific proteins on calcium transport for in male and female models. Solute transport and excretion are given in μmol·min^{-1}. Percentage changes from baseline values are shown in parentheses.

	PT transport		TAL transport		DCT transport		CNT transport		Urinary excretion	
	Na^+	Ca^{2+}	Na^+	Ca^{2+}	Na^+	Ca^{2+}	Na^+	Ca^{2+}	Na^+	Ca^{2+}
					Base case					
Male	74.05	0.63	28.32	0.18	3.69	0.043	2.81	0.03	1.26	0.03
Female	44.85	0.45	34.5	0.13	4.03	0.07	0.31	0.047	1.0	0.025
TRPV5-100 (male)	74.05 (0%)	0.63 (0%)	28.32 (0%)	0.18 (0%)	3.74 (+1%)	0.0 (-100%)	2.83 (0%)	0.0 (-100%)	1.19 (-5%)	0.103 (+243%)
TRPV5-100 (female)	44.85 (0%)	0.45 (0%)	34.5 (0%)	0.13 (0%)	4.13 (+2%)	0.0 (-100%)	0.32 (+3%)	0.0 (-100%)	0.88 (-12%)	0.142 (+468%)
NCX1-100 (male)	74.05 (0%)	0.63 (0%)	28.32 (0%)	0.18 (0%)	3.7 (0%)	0.04 (-6%)	2.81 (0%)	0.019 (-36%)	1.24 (-1%)	0.044 (+46%)
NCX1-100 (female)	44.85 (0%)	0.45 (0%)	34.5 (0%)	0.13 (0%)	4.08 (+1%)	0.042 (-40%)	0.31 (0%)	0.019 (-59%)	0.92 (-8%)	0.082 (+228%)
PT-50 (male)	74.01 (0%)	0.59 (-6%)	28.32 (0%)	0.23 (+27%)	3.7 (0%)	0.043 (0%)	2.84 (+1%)	0.03 (0%)	1.29 (+2%)	0.035 (+16%)
PT-50 (female)	44.85 (0%)	0.45 (0%)	34.5 (0%)	0.13 (0%)	4.03 (0%)	0.07 (0%)	0.31 (0%)	0.047 (0%)	1.0 (0%)	0.026 (+4%)
TAL-50 (male)	74.05 (0%)	0.63 (0%)	28.36 (0%)	0.14 (-22%)	3.68 (0%)	0.044 (+2%)	2.81 (0%)	0.032 (+6%)	1.22 (-3%)	0.073 (+143%)
TAL-50 (female)	44.85 (0%)	0.45 (0%)	34.54 (0%)	0.09 (-30%)	4.02 (0%)	0.072 (+2%)	0.31 (0%)	0.049 (+4%)	0.95 (-5%)	0.06 (+140%)

in Na^+ transport. In contrast, in the female model, the competing effect leads to a more significant reduction (8% and 11% decrease for 50% and 80% inhibition, respectively) in Na^+ transport.

Furthermore, inhibiting NHE3 leads to decreased luminal NH_4^+ levels, allowing for higher binding of K^+ to NKCC2 in both male and female models. However, it is important to note that the influx of K^+ is also dependent on the influx of Na^+ via NKCC2. In the case of 80% inhibition, we observe lower Na^+ transport resulting in a decreased K^+ influx compared to 50% inhibition, for both male and female models (see TAL transport column in Table. 4.2). In the male model, this altered influx of K^+ and thus apical recycling of K^+ results in a small change in the lumen-positive ΔV_{te} along TAL, while in the female model, it leads to a more positive ΔV_{te} in both cases of inhibition. Specifically, in the male model, the change in lumen-positive ΔV_{te} results in a small change in Ca^{2+} transport for 50% inhibition and a negligible change for 80% inhibition of NHE3. On the other hand, in the female model, NHE3 inhibition results in a 15% increase in calcium transport along TAL for 50% inhibition and a 7% increase for 80% inhibition of NHE3.

Increased downstream Na^+ delivery to DCT allows for transcellular Na^+ reabsorption through other Na^+ channels and transporters. However, NHE3 inhibition leads to an in-

crease in luminal pH downstream, resulting in increased TRPV5 conductance along DCT-CNT. Nevertheless, inhibited NHE along DCT-CNT reduces the transcellular voltage gradient necessary for transcellular Ca^{2+} reabsorption, leading to a small net reduction in both cases of inhibition in both male and female models along DCT2-CNT.

The significantly decreased calcium reabsorption (as seen in the Urinary excretion column in Table. 4.2) results in a 1.76-fold increase in calcium excretion for 50% inhibition and a 2.30-fold increase for 80% inhibition in the male model, corresponding to a fractional excretion of 5.9% and 8.7%, respectively. In the female model, we observe a 1.20-fold increase in calcium excretion for 50% inhibition and a 2.04-fold increase for 80% inhibition.

Table 4.2: Effects of inhibiting Na^+ transporters on sodium and calcium transport for male and female models. Solute transport and excretion are given in μmol·min^{-1}. Percentage changes from baseline values are shown in parentheses.

	PT transport		TAL transport		DCT transport		CNT transport		Urinary excretion	
	Na^+	Ca^{2+}	Na^+	Ca^{2+}	Na^+	Ca^{2+}	Na^+	Ca^{2+}	Na^+	Ca^{2+}
Base case										
Male	74.05	0.63	28.32	0.18	3.69	0.043	2.81	0.03	1.26	0.03
Female	44.85	0.45	34.5	0.13	4.03	0.07	0.31	0.047	1.01	0.025
Na^+ Transporter Inhibitions										
NHE3-50 (male)	60.7 (-18%)	0.52 (-17%)	28.88 (+1%)	0.19 (+5%)	4.04 (+9%)	0.041 (-4%)	3.73 (+32%)	0.029 (-3%)	2.36 (+87%)	0.053 (+76%)
NHE3-50 (female)	36.81 (-17%)	0.38 (-15%)	31.49 (-8%)	0.15 (+15%)	5.27 (+30%)	0.055 (-21%)	1.59 (+412%)	0.044 (-6%)	1.66 (+66%)	0.03 (+20%)
NHE3-80 (male)	40.99 (-44%)	0.35 (-44%)	27.68 (-2%)	0.18 (0%)	4.76 (+29%)	0.043 (0%)	4.66 (+65%)	0.028 (-6%)	4.24 (+236%)	0.069 (+130%)
NHE3-80 (female)	26.83 (-40%)	0.29 (-35%)	30.38 (-11%)	0.14 (+7%)	5.87 (+45%)	0.071 (+1%)	3.51 (+1032%)	0.044 (-6%)	4.23 (+323%)	0.051 (+104%)
NKCC2-70 (male)	73.58 (0%)	0.63 (0%)	23.06 (-18%)	0.15 (-16%)	3.92 (+6%)	0.04 (-6%)	3.7 (+31%)	0.029 (-3%)	2.89 (+129%)	0.076 (+153%)
NKCC2-70 (female)	43.98 (-1%)	0.44 (-2%)	30.26 (-12%)	0.1 (-23%)	4.84 (+20%)	0.064 (-8%)	1.35 (+335%)	0.046 (-2%)	2.23 (+123%)	0.078 (+212%)
NKCC2-100 (male)	73.17 (-1%)	0.63 (0%)	5.77 (-79%)	-0.02 (back leak)	4.42 (+19%)	0.035 (-18%)	5.49 (+95%)	0.021 (-30%)	14.62 (+1060%)	0.263 (+776%)
NKCC2-100 (female)	43.16 (-3%)	0.42 (-6%)	6.87 (-80%)	-0.07 (back leak)	5.73 (+42%)	0.051 (-27%)	4.84 (+1461%)	0.036 (-23%)	19.63 (+1863%)	0.286 (+1044%)
NCC-70 (male)	74.05 (0%)	0.63 (0%)	28.32 (0%)	0.18 (0%)	2.56 (-30%)	0.045 (+4%)	3.47 (+23%)	0.027 (-10%)	1.54 (+22%)	0.031 (+3%)
NCC-70 (female)	44.85 (0%)	0.45 (0%)	34.5 (0%)	0.13 (0%)	3.04 (-24%)	0.065 (-7%)	0.9 (+190%)	0.044 (-6%)	1.16 (+16%)	0.033 (+32%)
NCC-100 (male)	74.05 (0%)	0.63 (0%)	28.32 (0%)	0.18 (0%)	1.18 (-68%)	0.042 (-2%)	4.12 (+46%)	0.023 (-23%)	2.0 (+58%)	0.037 (+23%)
NCC-100 (female)	44.85 (0%)	0.45 (0%)	34.5 (0%)	0.13 (0%)	0.71 (-82%)	0.049 (-30%)	2.4 (+674%)	0.038 (-19%)	1.69 (+69%)	0.054 (+116%)
ENaC-70 (male)	74.05 (0%)	0.63 (0%)	28.32 (0%)	0.18 (0%)	3.59 (-2%)	0.055 (+27%)	1.3 (-53%)	0.039 (+30%)	2.23 (+76%)	0.008 (-73%)
ENaC-70 (female)	44.85 (0%)	0.45 (0%)	34.5 (0%)	0.13 (0%)	3.92 (-2%)	0.084 (+20%)	-0.27 (back leak)	0.051 (+8%)	1.53 (+53%)	0.007 (-72%)
ENaC-100 (male)	74.05 (0%)	0.63 (0%)	28.32 (0%)	0.18 (0%)	3.53 (-4%)	0.058 (+34%)	-0.57 (back leak)	0.044 (+46%)	4.15 (+229%)	0.001 (-96%)
ENaC-100 (female)	44.85 (0%)	0.45 (0%)	34.5 (0%)	0.13 (0%)	3.86 (-4%)	0.088 (+25%)	-0.93 (back leak)	0.052 (+10%)	2.56 (+156%)	0.001 (-96%)

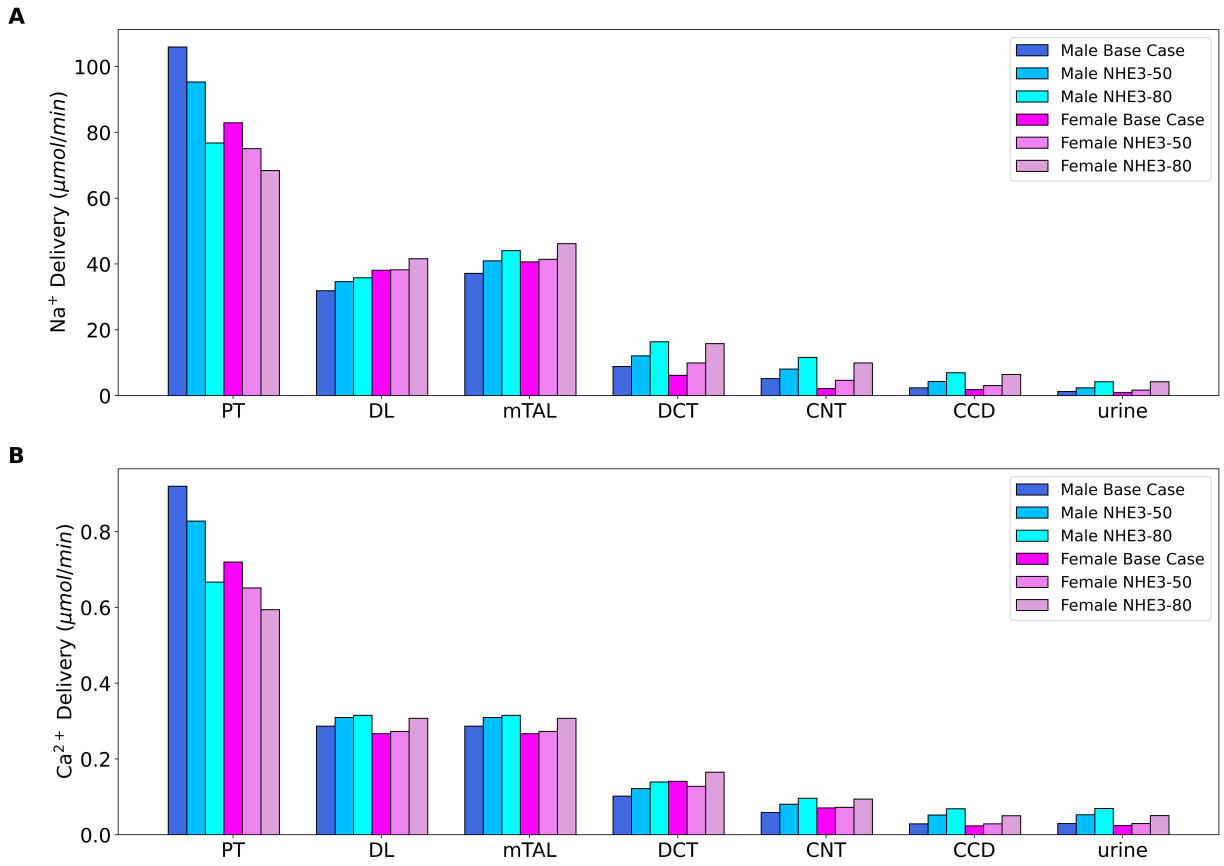

Figure 4.9: Comparison of segmental solute delivery of sodium (A) Na^+ (B) Ca^{2+} for male and female models for base case, and for 50% decrease in NHE3 activity (NHE3-50) and 80% decrease in NHE3 activity (NHE3-80); PT, proximal tubule; DL, descending limb; mTAL, medullary thick ascending limb; DCT, distal convoluted tubule; CNT, connecting tubule; CCD, cortical collecting duct.

4.2.2 NKCC2 Inhibition

The impact of inhibiting the Na^+-K^+-2Cl^- co-transporter (NKCC2), which is expressed at the apical membrane of the TAL [9], on calcium transport was investigated. NKCC2 was inhibited by 70% and 100%. Inhibiting NKCC2 significantly reduces the kidney's axial osmolarity gradient. Therefore, similar to NHE3 inhibition simulations, the medullary interstitial concentrations of Na^+, K^+, Cl^-, urea and Ca^{2+} are lowered as described in

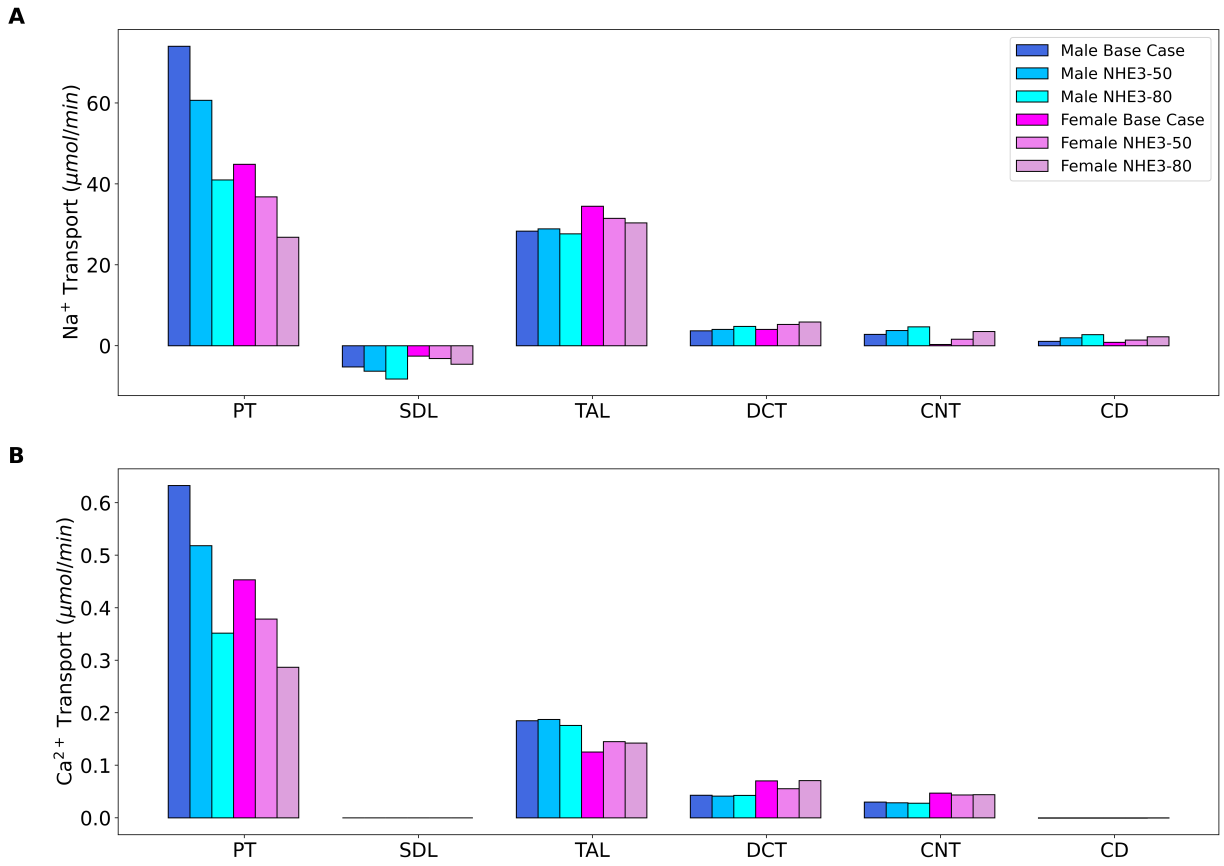

Figure 4.10: Comparison of segmental solute transport of (A) Na^+ and (B) Ca^{2+} for male and female models for base case, and for 50% decrease in NHE3 activity (NHE3-50) and 80% decrease in NHE3 (NHE3-80) activity; PT, proximal tubule; SDL, short descending limb; TAL, thick ascending limb; DCT, distal convoluted tubule; CNT, connecting tubule; CD, cortical duct.

Ref. [79]. With 100% NKCC2 inhibition, the axial cortico-medullary gradient of calcium is completely abolished, thus reducing the interstitial concentrations to 1.25 mM at the outer-inner medullary junction and papillary tip [46]. For 70% inhibition, interstitial concentrations of Na^+, K^+, Cl^-, urea and Ca^{2+} were taken to be the average of the baseline and 100% inhibition, so that at the outer-inner medullary junction and papillary tip interstitial calcium concentrations equal to 1.9 mM and 2.6 mM, respectively. NKCC2 inhibition significantly diminishes TGF response [69, 109, 152], hence no alterations to SNGFR have been made, consistent with rat experimental studies [121].

In Figs. 4.11B and 4.12B the segmental deliveries and transport of Ca^{2+} for male and female models are shown. NKCC2 inhibition does not directly impact S3 transport of Ca^{2+}. However, since medullary interstitial fluid osmolarity is reduced, it impedes the concentration gradient of select solutes (Na^+, K^+, Cl^-, urea, and Ca^{2+}). The reduction in interstitial Ca^{2+} concentration resulted in a slightly lower lumen-to-lateral innerspace Ca^{2+} concentration gradient, causing a slight decrease in Ca^{2+} transport along S3 in both male and female models (a reduction of ∼1-3%).

Along TAL, NKCC2 inhibition impairs the electrochemical gradient leading to a considerably less positive ΔV_{te} for 70% inhibition for both male and female models, reducing the paracellular transport of calcium significantly (a decrease of 21% in the male model and 23% in the female model). In the case of 100% inhibition, ΔV_{te} becomes negative along TAL, leading to a small back leak of Ca^{2+} to the lumen (see Fig. 4.12), consistent with experiments on isolated perfused cTAL mouse cells [41].

NKCC2 inhibition increases distal Na^+ delivery, which in turn facilitates Na^+ transport by NHE along the DCT-CNT. As a result, luminal pH decreases along this segment, leading to a reduced TRPV5 conductance and decreased transcellular calcium reabsorption (see DCT and CNT columns in Table. 4.2). The considerably elevated Na^+ influx results in increased intercellular Na^+ concentration, leading to a decreased Na^+ influx and Ca^{2+} efflux from the cell via NCX1. These observations are consistent in both male and female models.

The overall reduced reabsorption results in 2.53- and 8.776-fold increases in calcium excretion in the male model and 3.12- and 11.44- fold increases in calcium excretion in the female model, leading to urinary fractional excretion of 8.5% and 30% in the male model, and 10% and 37% in the female model for 70% and 100% NKCC2 inhibition, respectively.

4.2.3 NCC Inhibition

Simulations were performed to investigate the effects of inhibiting the Na^+-Cl^- cotransporter (NCC) by 70% and 100%. NCC is expressed at the apical membrane of the DCT [122] and is co-localized with TRPV5 at DCT2. Baseline interstitial concentrations were assumed for the simulations.

The segmental delivery and transport of calcium for NCC inhibitions are depicted in Figs. 4.13B and 4.14B. When NCC was inhibited by 70% and 100%, a significant reduction in Na^+ transport along DCT was observed in both male and female models (Fig. 4.14A). NCC inhibitions led to decreased Na^+ transport along DCT, resulting in an increase in luminal Na^+ concentration in this segment, which in turn increased the driving force for

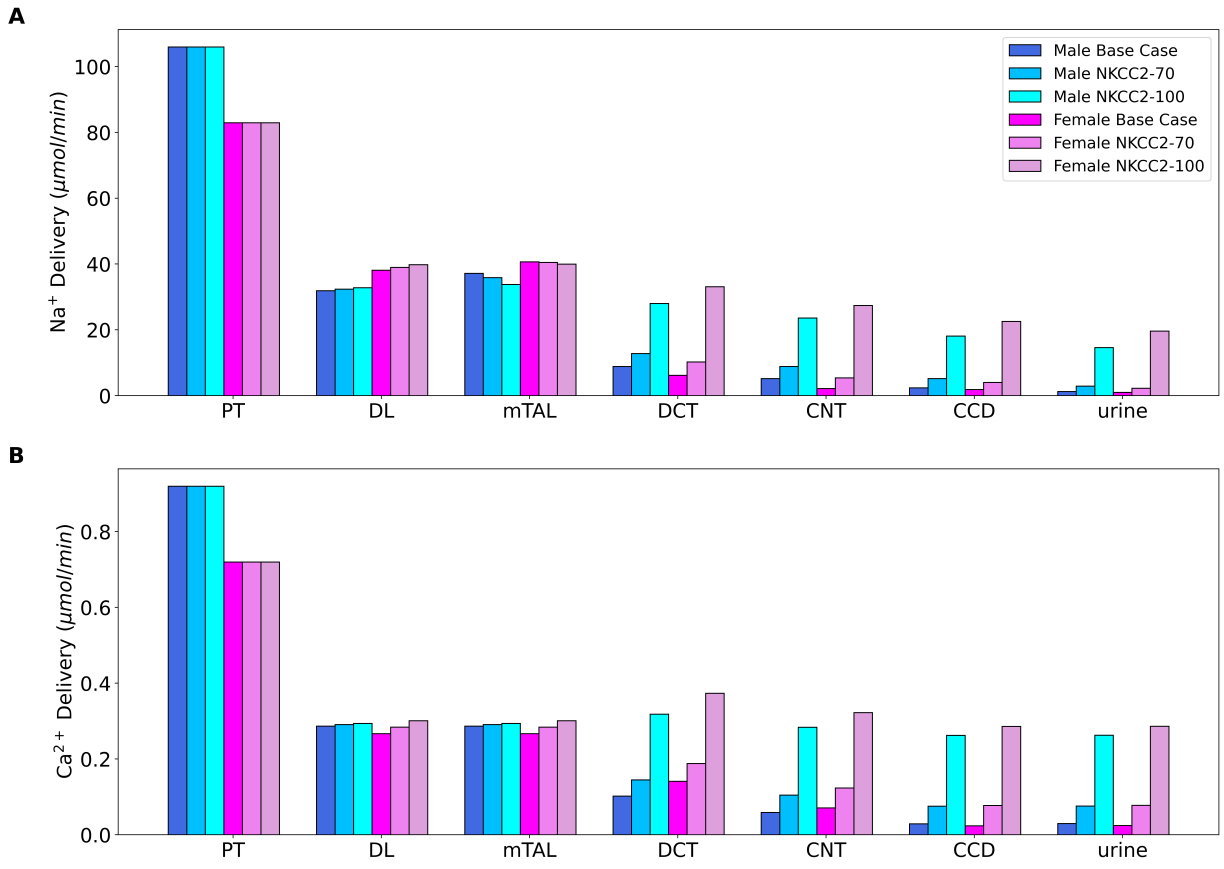

Figure 4.11: Comparison of segmental solute delivery of (A) Na^+ and (B) Ca^{2+} for male and female models for base case, and for 70% decrease in NKCC2 activity (NKCC2-70) and 100% decrease in NKCC2 activity (NKCC2-100); PT, proximal tubule; DL, descending limb; mTAL, medullary thick ascending limb; DCT, distal convoluted tubule; CNT, connecting tubule; CCD, cortical collecting duct.

Na^+ reabsorption through other apical Na^+ transporters in DCT, such as NHE2, leading to a decrease in luminal pH. Inhibition of NCC along DCT1 resulted in an increased transcellular voltage gradient; however, the co-localization of ENaC along DCT2 gradually mitigated this effect, leading to a competing effect on the transcellular voltage gradient in DCT2. In the male model, this alteration had minimal impact on calcium transport. However, in the female model, where TRPV5 expression is considerably higher than in the male model, the effects of lower pH on lowering the channel conductance were more noticeable (see Table 4.2). The increased delivery of Na^+ to CNT allowed for Na^+ reabsorption via

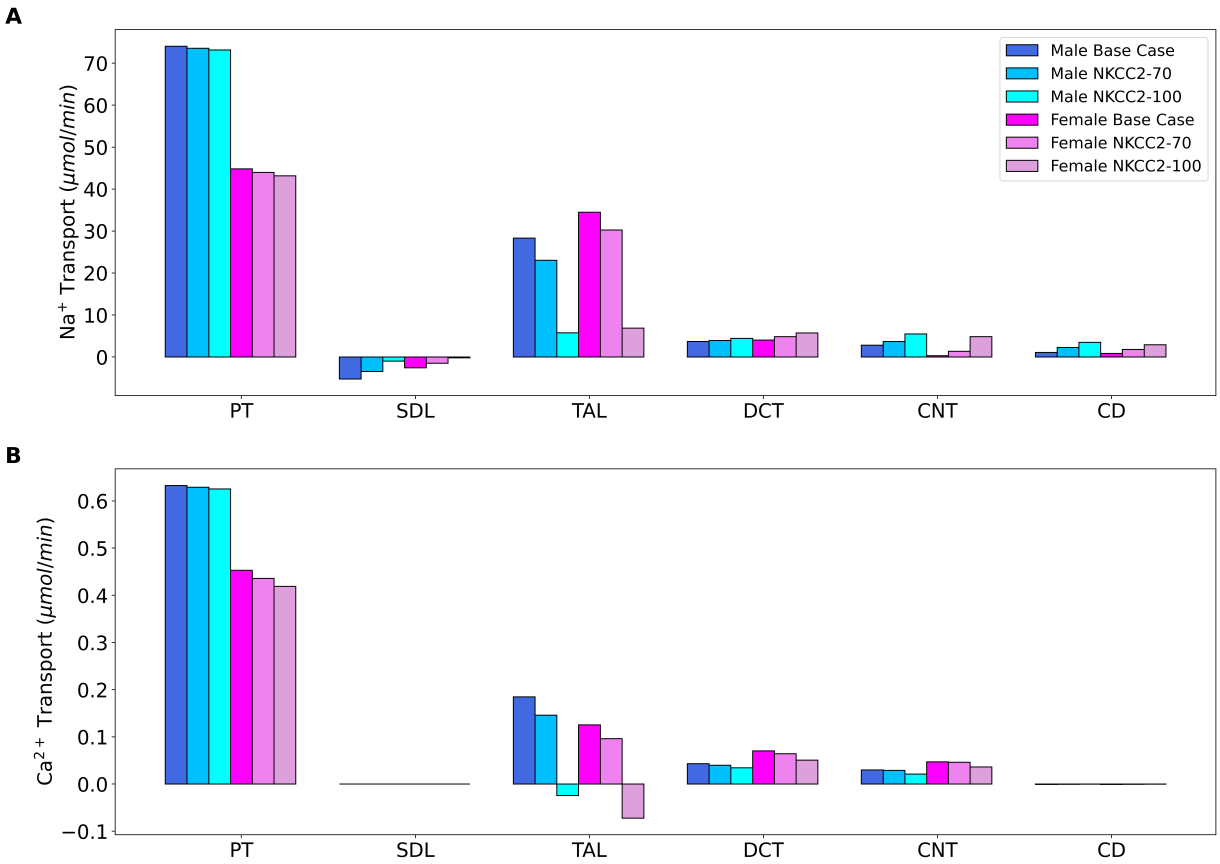

Figure 4.12: Comparison of segmental solute transport of (A) Na^+ and (B) Ca^{2+} for male and female models for base case, and for 70% decrease in NKCC2 activity (NKCC2-70) and 100% decrease in NKCC2 (NKCC2-100) activity; PT, proximal tubule; SDL, short descending limb; TAL, thick ascending limb; DCT, distal convoluted tubule; CNT, connecting tubule; CD, cortical duct.

ENaC, resulting in a less favourable voltage gradient for transcellular calcium reabsorption, as observed in both male and female models. The decreased transcellular voltage gradient, along with lower luminal pH and consequently lower TRPV5 conductance, resulted in decreased Ca^{2+} reabsorption along CNT in both male and female models (see CNT transport in Table. 4.2.

NCC inhibition results in an overall increase in urinary calcium excretion by 3% and 23% in the male model and 32% and 116% for the female model for 70% and 100% NCC inhibition, respectively.

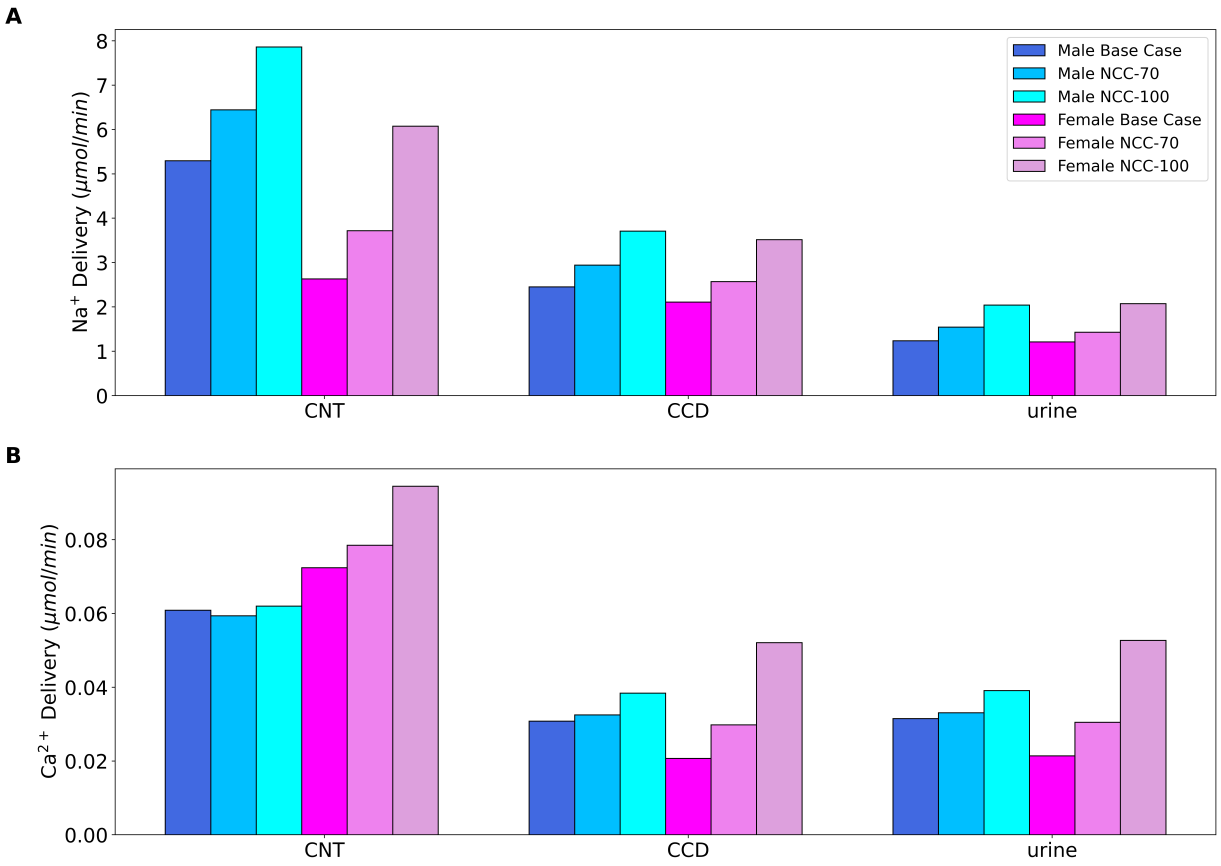

Figure 4.13: Comparison of segmental solute delivery of (A) Na^+ and (B) Ca^{2+} for male and female models for base case, and for 70% decrease in NCC activity (NCC-70) and 100% decrease in NCC activity (NCC-100); CNT, connecting tubule; CCD, cortical collecting duct.

4.2.4 ENaC Inhibition

Finally, the effects of inhibiting the epithelial Na^+ channel (ENaC) on calcium transport were investigated. ENaC is expressed at the apical membranes of DCT2, CNT, CCD, OMCD, and IMCD segments [93, 60]. Baseline interstitial concentration values were used in these simulations, and the segmental deliveries and transport of Ca^{2+} for these inhibitions are shown in Figs. 4.15B and 4.16B. In vivo experiments conducted on rats administered with amiloride revealed a sparing effect on the reabsorption of magnesium (Mg^{2+}), leading to an increase in the intracellular concentration of Mg^{2+}. Increased [Mg^{2+}] has an inhibitory

effect on TRPV5 activity by binding to its selectivity filter [88]. Since Mg^{2+} is not included in our model, we reduced TRPV5 expression by 10% for both the male and female models in the case of 100% inhibition to reflect this effect in our simulations.

Inhibition of ENaC indirectly enhances calcium reabsorption by hyperpolarizing the apical membrane, thereby increasing transcellular calcium influx via TRPV5. This effect is consistent in both male and female models. Furthermore, reduced Na^+ reabsorption along the DCT2-CNT segment results in lower intercellular sodium concentrations, leading to increased basolateral Na^+ influx through NCX1, ultimately resulting in increased Ca^{2+} efflux.

By inhibiting ENaC for 70% and 100%, the reabsorption of calcium in the DCT2-CNT segment increased considerably. Urinary fractional calcium excretion decreased to 0.43% and 0.1% in the male model (compared to baseline fractional excretion of 4.7% and 3.2%), and to 0.22% and 0.16% in the female model for 70% and 100% ENaC inhibition (compared to baseline fractional excretion of 9.7% and 6.5%), respectively. The male results are consistent with in vivo experiments on male rats administered with amiloride, which showed a considerable decrease in urinary calcium excretion [35].

4.3 Discussion

4.3.1 Ca^{2+} Specific Inhibition

The findings indicate that defects specific to Ca^{2+} in DCT2-CNT and P_{Ca}^{Para} along TAL are not compensated for downstream segments, while defect in P_{Ca}^{Para} along PT are compensated in both male and female models. Furthermore, in the female model, defects in Ca^{2+} transport along DCT2-CNT result in a higher increase in urinary excretion of Ca^{2+} compared to the male model. This can be attributed to the higher expression of TRPV5 in the DCT2-CNT of the female model. However, both male and female models exhibit similar behaviour in the case of defects in P_{Ca}^{Para}.

4.3.2 NHE3 inhibition

NHE3 inhibition has a direct effect on Na^+ reabsorption and an indirect effect on Ca^{2+} transport. NHE3 is responsible for the majority of Na^+ transport in PT and, consequently, for osmotically driven water reabsorption [95]. There have not been any microperfusion experiments outlining the effects of altering NHE3 expression. However, NHE3 null mice have

been shown to have a higher urinary calcium excretion [110]. Also in vitro experiments of over-expressed NHE3 in mice PT cells have shown higher calcium reabsorption [110]. The current model predictions have shown an increase of 77% and 153% in urinary calcium excretion in the case of 50% and 80% NHE3 inhibition in the male model and 20% and 104% in the female model, respectively. Along PT, in both male and female models, the decrease in the amount of calcium transport is in parallel with Na^+ transport. Along TAL in the male model due to the competing effects of increased Na^+ delivery and decreased NHE expression, we observe a minimal change in ΔV_{te} and therefore Ca^{2+} transport. In the female model, NHE3 inhibition results in elevated ΔV_{te} resulting in a net increase of Ca^{2+} reabsorption along this segment. NHE3 inhibition in both male and female models results in increased urinary calcium excretion for both cases of inhibition.

4.3.3 NKCC2 inhibition

Furosemide is the diuretic of choice for inhibiting NKCC2. Increased urinary loss of Ca^{2+} have been reported in human subjects and mice [84, 85], due to the effects of furosemide of diminishing the positive ΔV_{te} along TAL [39]. In the acute case of administrating furosemide in mice experiments, elevated Ca^{2+} excretion has been observed [85]. The current model predictions show a significant renal calcium loss in the case of both 70% and 100% inhibition, by mainly disrupting calcium reabsorption along TAL via diminishing the lumen-positive voltage gradient. In the case of 100% inhibition, ΔV_{te} becomes negative along TAL and we see a small back leak to the lumen, consistent with in vitro experiments on isolated cTAL mice cells [41]. The loss in calcium reabsorption will not be compensated in the DCT2-CNT segment in both male and female models, and model predictions show a significantly increased urinary calcium excretion.

4.3.4 NCC inhibition

Thiazide treatment has been shown to inhibit the Na^+-Cl^- cotransporter (NCC) and decrease urinary Ca^{2+} excretion [30, 69]. Thiazide reduces Na^+ reabsorption along the distal convoluted tubule (DCT) and increases volume excretion, leading to decreased extracellular fluid volume. As a compensatory response, micro-puncture experiments on chronic hydrochlorothiazide-treated mice have shown an upregulation in Na^+ and Ca^{2+} reabsorption along the proximal tubule (PT) due to overexpression of Na^+/H^+ exchanger 3 (NHE3) along this segment, followed by unaffected Ca^{2+} reabsorption along the DCT, resulting in an overall increase in Ca^{2+} reabsorption and hypocalcemia [107]. This effect has been ob-

served in patients with both hypo- and hyperparathyroidism, indicating its independence from parathyroid hormone (PTH) [30].

Interestingly, in our model where we do not include any alterations in Na^+ reabsorption along the PT, we predict an increase in urinary calcium excretion with thiazide treatment. This contrast between the models may be attributed to our model not reflecting the potential cross-talk between PT and DCT in the regulation of calcium handling.

4.3.5 ENaC inhibition

In vivo experiments on rats treated with amiloride have demonstrated a decrease in urinary calcium excretion [35]. ENaC inhibition induces hyperpolarization, allowing increased transcellular calcium influx via TRPV5 along DCT2-CNT. In our simulations, this effect resulted in a considerable increase in calcium reabsorption along DCT2-CNT, which is consistent in both male and female models leading to a decrease in urinary calcium excretion.

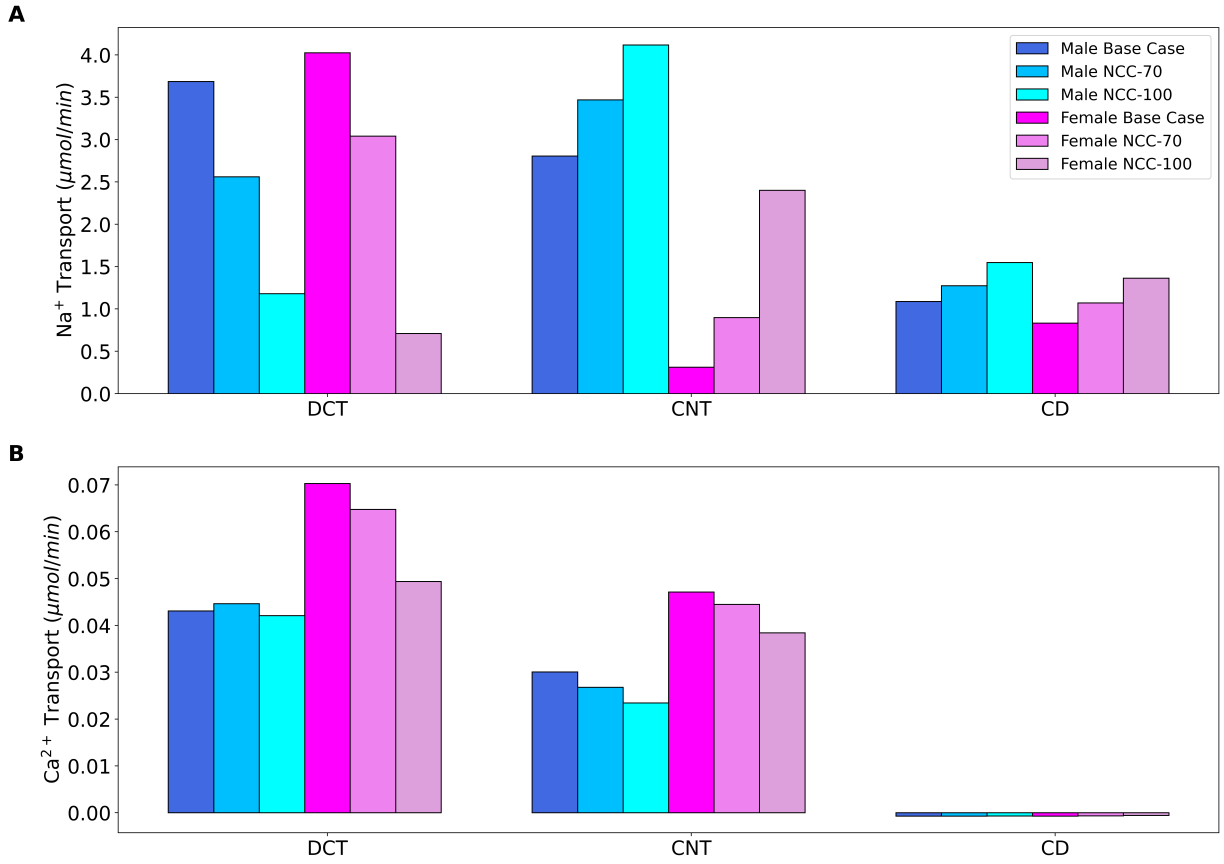

Figure 4.14: Comparison of segmental solute transport of (A) Na^+ and (B) Ca^{2+} for male and female models for base case, and for 70% decrease in NCC activity (NCC-70) and 100% decrease in NCC (NCC-100) activity; DCT, distal convoluted tubule; CNT, connecting tubule; CD, cortical duct.

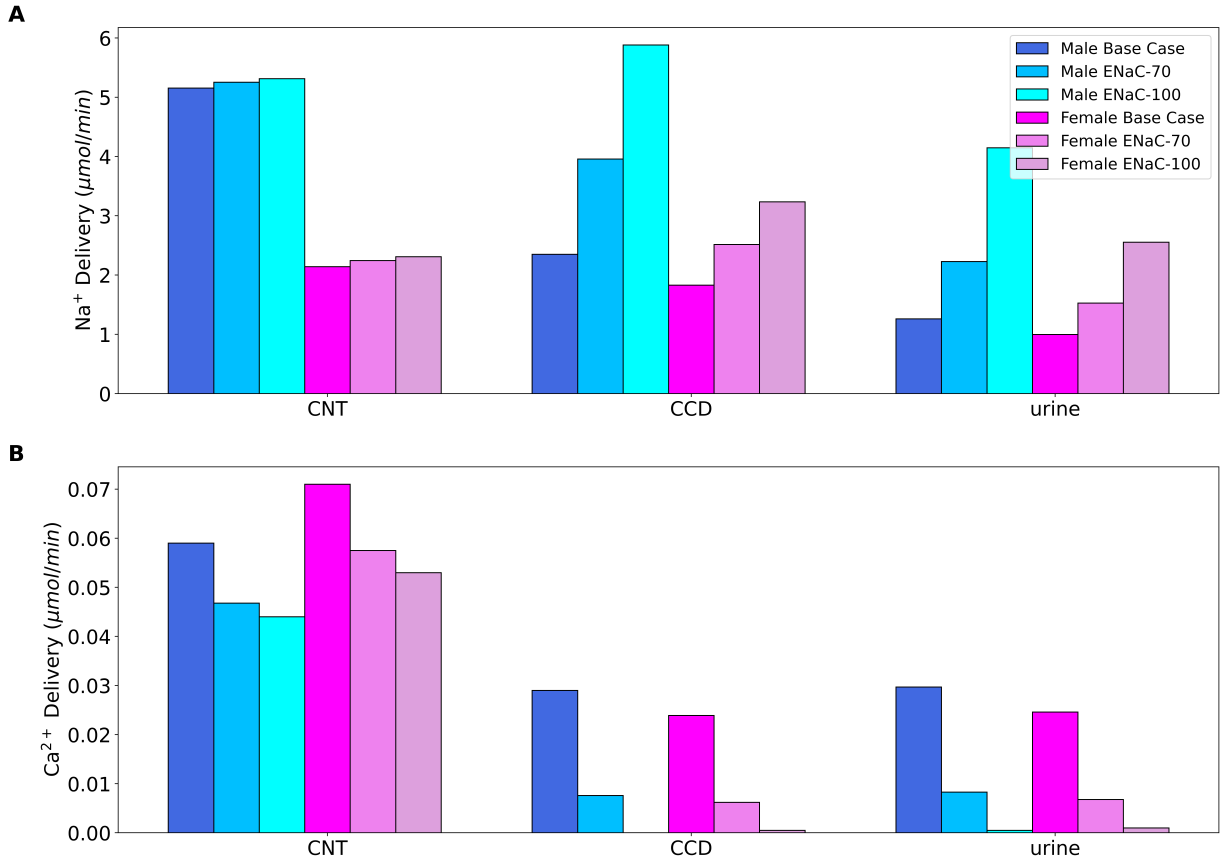

Figure 4.15: Comparison of segmental solute delivery of (A) Na^+ and (B) Ca^{2+} for male and female models for base case, and for 70% decrease in ENaC activity (ENaC-70) and 100% decrease in ENaC activity (ENaC-100); CNT, connecting tubule; CCD, cortical collecting duct.

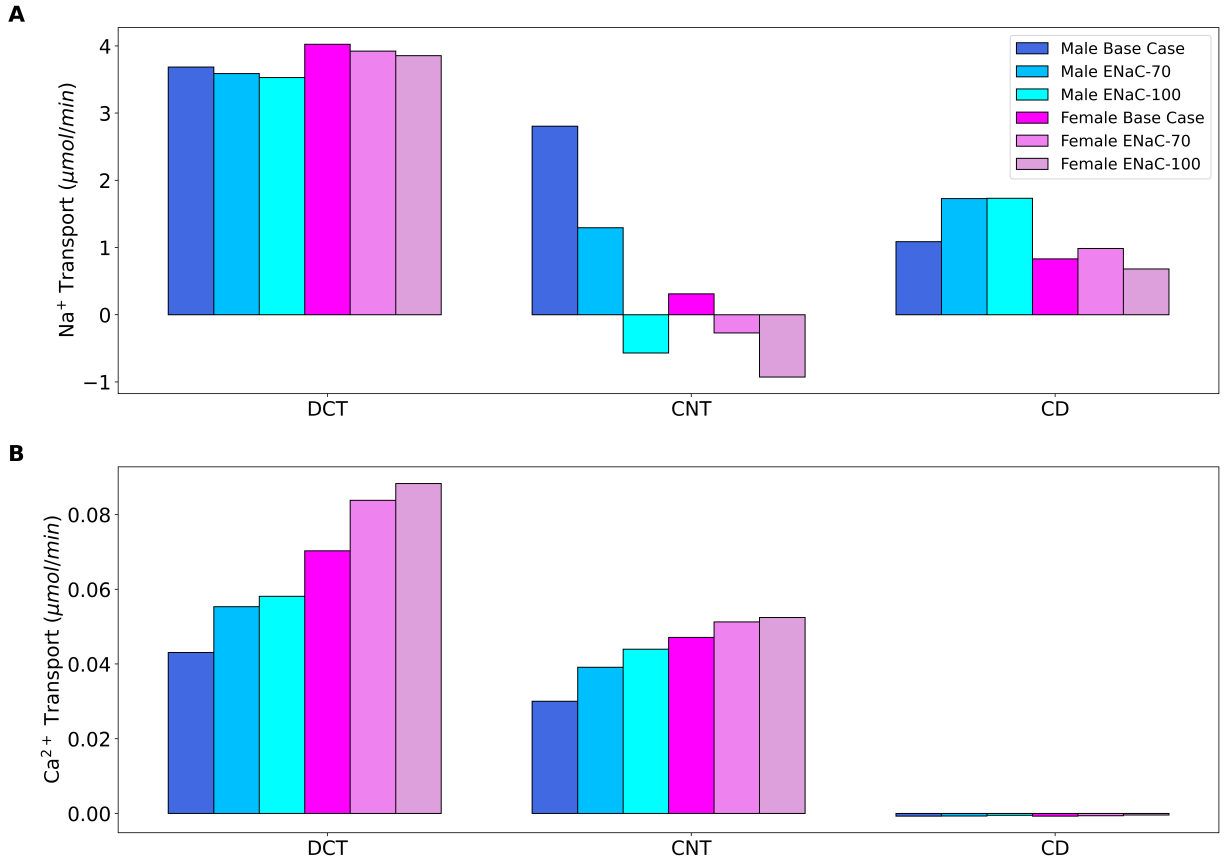

Figure 4.16: Comparison of segmental solute transport of (A) Na^+ and (B) Ca^{2+} for male and female models for base case, and for 70% decrease in ENaC activity (ENaC-70) and 100% decrease in ENaC (ENaC-100) activity; DCT, distal convoluted tubule; CNT, connecting tubule; CD, cortical duct

Chapter 5

Conclusion

Calcium is a vital mineral that plays a key role in maintaining several physiological processes, including muscle function, nerve transmission, and bone health [102]. The precise levels of ionized calcium in the body are essential for sustaining life. The kidney serves as a primary regulator of calcium excretion [127], and understanding the transport and regulation of calcium in the kidney and the differences between sexes is of high importance. Such an understanding can provide valuable insight into renal calcium handling in both males and females and enhance our knowledge of the mechanisms that govern calcium homeostasis in the body. This knowledge can lead to the identification of potential therapeutic targets and the development of new strategies to manage calcium-related disorders.

Conducting animal experiments to fully understand the complex mechanisms of calcium transport and regulation can be challenging or even impossible. In this context, *in silico* experiments provide a valuable tool to achieve a better understanding of the dynamic processes involved in calcium handling along the nephron in the kidney. Furthermore, there is limited knowledge about sex differences in renal calcium handling, which underscores the need for further research. By leveraging *in silico* experiments, we can conduct experiments that would enable us to better understand and characterize these differences.

In summary, this thesis focused on exploring the transport and regulation of calcium along the superficial nephron in male and female rat kidneys. First, we discussed the anatomy and physiology of the kidney and epithelial solute and water transport along the nephron. Then, we described the isolated renal epithelial cell models, with a specific emphasis on renal calcium transport. We identified and elaborated on the specific segments of the nephron, where calcium reabsorption occurs, and delved into the differences in renal calcium handling between male and female rat kidneys. Notably, based on animal experiments [64], there are

sex differences along the PT and DCT2-CNT, with higher transcellular and paracellular permeability to calcium in the PT, and a higher expression of TRPV5 along DCT2-CNT in the female rat kidney model compared to the male rat (see Section. 2.6).

The nephron model is then introduced, which simulates calcium transport with 15 other solutes along the superficial nephron in both male and female rat kidneys. The simulations show lower calcium reabsorption along the PT and TAL, and higher reabsorption along DCT2-CNT in the female rat kidney model compared to the male rat kidney (see Fig. 3.5B). Furthermore, the simulation results showed a higher urinary calcium excretion in the male rat kidney model compared to the female rat kidney model (see Fig. 3.4B), which is consistent with the findings from animal experiments [64].

Finally, we analyze the effects of calcium-specific and sodium-specific perturbations on renal calcium handling, uncovering insights into how these perturbations impact calcium transport and how the effects differ between male and female rat kidneys. We saw that calcium-specific inhibitions have negligible effects on sodium transport along the nephron (see Table. 4.1), whereas inhibiting sodium-specific transporters have a major effect on renal calcium transport along the superficial nephron in the male and female rat kidneys. inhibiting NHE3, NKCC2, and NCC in both male and female rats exhibit a significant increase in urinary calcium excretion in both male and female models, whereas for ENaC inhibition we saw a decrease in urinary excretion in both male and female models (see Table. 4.2.

5.1 Limitations

Recent mathematical models have advanced our understanding of renal tubular function by accurately accounting for solute and water transport, revealing insights into transport pathways, driving forces, and coupling mechanisms. Nevertheless, as noted in Ref. [146], these models have limitations that can be divided into two categories: those that result from insufficient experimental data and those that stem from the model structure itself. Given the current study's focus on renal calcium transport, we discuss the limitations of computational models of kidney function in renal calcium handling.

As discussed in Chapter 1, nephrons in the kidney can be classified as either superficial or juxtamedullary, based on the location of the glomerulus. Superficial nephrons have glomeruli located near the surface of the kidney and give rise to a shorter loop of Henle that only penetrates the outer medulla, whereas juxtamedullary nephrons have both a longer loop of Henle and penetrate deep into the renal medulla [100]. In rats, the total number of nephrons is 36,000, with only 1/3 of them being juxtamedullary nephrons

(i.e., 24,000 superficial nephrons and 12,000 juxtamedullary nephrons) [149]. Our model focuses on a single representative nephron, without differentiation between superficial and juxtamedullary nephrons, although luminal concentrations at the mTAL inlet may vary significantly with the length of Henle's loop [76, 104]. The model also assumes fixed interstitial concentration gradients along the cortico-medullary axis due to the lack of consideration of the complex architecture of the medulla.

Transport pathways that are not fully characterized pose a challenge to the development of mathematical models. For instance, in our case, we chose to use the NCX1.1 isoform, which is the predominant isoform in cardiac cells and has a known kinetic model, instead of creating a kinetic model for the NCX1.3 isoform, which is the predominant isoform in renal epithelial cells. Moreover, incorporating newly discovered proteins in specific segments of the nephron into the model can be challenging when their functional importance is unclear, such as in the case of CaSR along the nephron. In our simulations, we included the effects of CaSR along various segments, such as TAL, DCT, and CD. However, the function of CaSR along the PT is yet to be fully understood [96]. Mathematical models can generate hypotheses in such situations, but experimental validation is necessary.

Furthermore, it should be noted that model parameters are typically derived from a combination of *in vivo* and *in vitro* measurements, which can introduce heterogeneity in the model including calcium-specific parameters that need to be considered. In the context of renal calcium handling in female models, there are still uncertainties regarding the direct effects of steroid hormones and other sex-specific differences between male and female rat kidneys [70]. Further animal experiments are required to fully elucidate sex differences in terms of calcium-specific protein expressions in the male and female rat kidneys. Finally, the model does not represent the circadian rhythms that are known to be exhibited by GFR and renal transporter abundance [142, 78].

5.2 Future Work

Our present study on renal calcium handling paves the way for potential future investigations, some of which are outlined below:

Multi Nephron Model. The current model of renal calcium handling is based on the dynamics of calcium transport in the superficial nephron. However, as noted above, the nephron population in the kidney is heterogeneous, with differences in structure and function between the superficial and juxtamedullary nephrons. Therefore, to obtain a more comprehensive understanding of renal calcium handling, the current model can be extended

to include juxtamedullary nephrons, as was done in Refs [66, 65, 81]. To investigate the heterogeneity in calcium transport and regulation in the nephron population.

Magnesium Transport. Since magnesium transport and regulation along the nephron is closely related to calcium [114], it is would be worthwhile to extend the current model to represent the dynamics of renal magnesium handling and its interactions with calcium transport.

Effects of Diabetes in Renal Calcium Handling. The effects of diabetes on renal calcium handling have been observed in clinical trials [99], animal experiments [15], and previous models of epithelial solute and water transport in diabetic rats [82]. In diabetes the kidney undergoes several changes such as hyperfiltration (e.g., SNGFR goes up), tubular hypertrophy, and alterations in renal transporter abundance as previously investigated in renal epithelial solute transport models [82, 81], resulting in increased sodium excretion. As calcium transport is closely linked to sodium transport, alterations in sodium handling in diabetes impact renal calcium handling as well. Moreover, studies in streptozotocin-induced diabetic rats have shown changes in protein expression, such as increased expression of TRPV5 [86]. Therefore, investigating renal calcium handling in male and female rats with diabetes could provide further insights into the complex interactions between diabetes and renal calcium handling.

Effects of Pregnancy in Renal Calcium Handling. During pregnancy, there are significant changes in hormone levels, along with structural changes such as hyperfiltration, tubular hypertrophy, and alternations in transporter abundance in the kidney which can affect renal calcium handling. For example, the hormone estrogen can increase the activity of calcium transporters in the kidneys, leading to increased calcium reabsorption [57]. On the other hand, the hormone progesterone can decrease calcium reabsorption by promoting calcium excretion [113]. Moreover, during lactation, there is an increased demand for calcium to support milk production [72], which can further affect renal calcium handling. Thus, further investigation is needed to better understand the mechanisms underlying pregnancy-related changes in renal calcium handling, and the current model can be extended to explore these effects.

Whole Body Calcium Homeostasis. The regulation of calcium homeostasis is a complex process that involves multiple feedback mechanisms and interactions between different organs such as the intestine, the kidneys and the bones. Therefore, a comprehensive understanding of whole-body calcium regulation requires a systems-level approach that integrates the renal calcium handling model with other models of calcium transport and regulation in the body. Such a model could help to elucidate the role of the intestine and bones in maintaining calcium balance and provide insights into the pathogenesis of calcium-

related disorders, such as osteoporosis and hypercalcemia. Furthermore, this integrated model could be used as a tool to facilitate the development of new therapeutic strategies for the treatment of these conditions by identifying key targets for intervention in the complex network of calcium regulation.

References

[1] ZALMAN S Agus, PJ Chiu, and MARTIN Goldberg. Regulation of urinary calcium excretion in the rat. *American Journal of Physiology-Renal Physiology*, 232(6):F545–F549, 1977.

[2] ZALMAN S Agus, LAURENCE B Gardner, LAURENCE H Beck, and MARTIN Goldberg. Effects of parathyroid hormone on renal tubular reabsorption of calcium, sodium, and phosphate. *American Journal of Physiology-Legacy Content*, 224(5):1143–1148, 1973.

[3] Zalman S Agus, Fuad N Ziyadeh, and Ellie Kelepouris. Mechanisms of calcium transport in the thick ascending limb of the loop of henle. *Phosphate and Mineral Homeostasis*, pages 171–175, 1986.

[4] R Todd Alexander and Henrik Dimke. Molecular mechanisms underlying paracellular calcium and magnesium reabsorption in the proximal tubule and thick ascending limb. *Annals of the New York Academy of Sciences*, 2022.

[5] Michele D Alexandre, Qun Lu, and Yan-Hua Chen. Overexpression of claudin-7 decreases the paracellular cl–conductance and increases the paracellular na+ conductance in llc-pk1 cells. *Journal of cell science*, 118(12):2683–2693, 2005.

[6] Maria Almeida, Michaël R Laurent, Vanessa Dubois, Frank Claessens, Charles A O'Brien, Roger Bouillon, Dirk Vanderschueren, and Stavros C Manolagas. Estrogens and androgens in skeletal physiology and pathophysiology. *Physiological reviews*, 97(1):135–187, 2017.

[7] Robert J Alpern and Steven C Hebert. *Seldin and Giebisch's The Kidney: Physiology & Pathophysiology 1-2*. Elsevier, 2007.

[8] Morimasa Amemiya, Jan Loffing, Marius Lötscher, Brigitte Kaissling, Robert J Alpern, and Orson W Moe. Expression of nhe-3 in the apical membrane of rat renal proximal tubule and thick ascending limb. *Kidney international*, 48(4):1206–1215, 1995.

[9] Gustavo R Ares, Paulo S Caceres, and Pablo A Ortiz. Molecular regulation of nkcc2 in the thick ascending limb. *American Journal of Physiology-Renal Physiology*, 301(6):F1143–F1159, 2011.

[10] JOHN R Asplin, NEIL S Mandel, and FL Coe. Evidence of calcium phosphate supersaturation in the loop of henle. *American Journal of Physiology-Renal Physiology*, 270(4):F604–F613, 1996.

[11] JOHN R Asplin, NEIL S Mandel, and FL Coe. Evidence of calcium phosphate supersaturation in the loop of henle. *American Journal of Physiology-Renal Physiology*, 270(4):F604–F613, 1996.

[12] John C Atherton. Regulation of fluid and electrolyte balance by the kidney. *Anaesthesia & Intensive Care Medicine*, 7(7):227–233, 2006.

[13] John C. Atherton. Regulation of fluid and electrolyte balance by the kidney. *Anaesthesia Intensive Care Medicine*, 7(7):227–233, 2006. Renal.

[14] Mei Bai, Steven Quinn, Sunita Trivedi, Olga Kifor, Simon HS Pearce, Martin R Pollak, Karen Krapcho, Steven C Hebert, and Edward M Brown. Expression and characterization of inactivating and activating mutations in the human ca2+ o-sensing receptor. *Journal of Biological Chemistry*, 271(32):19537–19545, 1996.

[15] George L Bakris, Vivian A Fonseca, Kumar Sharma, and Ernest M Wright. Renal sodium–glucose transport: role in diabetes mellitus and potential clinical implications. *Kidney international*, 75(12):1272–1277, 2009.

[16] Silvana Bazúa-Valenti, Lorena Rojas-Vega, María Castañeda-Bueno, Jonatan Barrera-Chimal, Rocío Bautista, Luz G Cervantes-Pérez, Norma Vázquez, Consuelo Plata, Adrián R Murillo-de Ozores, Lorenza González-Mariscal, et al. The calcium-sensing receptor increases activity of the renal ncc through the wnk4-spak pathway. *Journal of the American Society of Nephrology*, 29(7):1838–1848, 2018.

[17] John F Bertram, Rebecca N Douglas-Denton, Boucar Diouf, Michael D Hughson, and Wendy E Hoy. Human nephron number: implications for health and disease. *Pediatric nephrology*, 26:1529–1533, 2011.

[18] Camila Nogueira Alves Bezerra, Adriana Castello Costa Girardi, Luciene Regina Carraro-Lacroix, and Nancy Amaral Rebouças. Mechanisms underlying the long-term regulation of nhe3 by parathyroid hormone. *American Journal of Physiology-Renal Physiology*, 294(5):F1232–F1237, 2008.

[19] Lindsay M Biga, Sierra Dawson, Amy Harwell, Robin Hopkins, Joel Kaufmann, Mike LeMaster, Philip Matern, Katie Morrison-Graham, Devon Quick, and Jon Runyeon. *Anatomy & physiology*. OpenStax/Oregon State University, 2020.

[20] RJM Bindels, PLM Ramakers, JA Dempster, A Hartog, and CH Van Os. Role of na+/ca 2+ exchange in transcellular ca 2+ transport across primary cultures of rabbit kidney collecting system. *Pflügers Archiv*, 420:566–572, 1992.

[21] Martha L Blair. Sex-based differences in physiology: what should we teach in the medical curriculum? *Advances in physiology education*, 31(1):23–25, 2007.

[22] Markus Bleich, Qixian Shan, and Nina Himmerkus. Calcium regulation of tight junction permeability. *Annals of the New York Academy of Sciences*, 1258(1):93–99, 2012.

[23] Olivier Bonny and Aurélie Edwards. Calcium reabsorption in the distal tubule: regulation by sodium, ph, and flow. *American Journal of Physiology-Renal Physiology*, 304(5):F585–F600, 2013.

[24] Rachell E Booth, John P Johnson, and James D Stockand. Aldosterone. *Advances in physiology education*, 2002.

[25] Sandor Boros, René JM Bindels, and Joost GJ Hoenderop. Active ca 2+ reabsorption in the connecting tubule. *Pflügers Archiv-European Journal of Physiology*, 458:99–109, 2009.

[26] Sheerazed Boulkroun, Cathi Le Moellic, Marcel Blot-Chabaud, Nicolette Farman, and Nathalie Courtois-Coutry. Expression of androgen receptor and androgen regulation of ndrg2 in the rat renal collecting duct. *Pflügers Archiv*, 451:388–394, 2005.

[27] JAMES E Bourdeau and RHONDA J Hellstrom-Stein. Voltage-dependent calcium movement across the cortical collecting duct. *American Journal of Physiology-Renal Physiology*, 242(3):F285–F292, 1982.

[28] JE Bourdeau and MB Burg. Voltage dependence of calcium transport in the thick ascending limb of henle's loop. *American Journal of Physiology-Renal Physiology*, 236(4):F357–F364, 1979.

[29] JE Bourdeau and MB Burg. Effect of pth on calcium transport across the cortical thick ascending limb of henle's loop. *American Journal of Physiology-Renal Physiology*, 239(2):F121–F126, 1980.

[30] Arnold S Brickman, Shaul G Massry, Jack W Coburn, et al. Changes in serum and urinary calcium during treatment with hydrochlorothiazide: studies on mechanisms. *The Journal of clinical investigation*, 51(4):945–954, 1972.

[31] Edward M Brown, Gerardo Gamba, Daniela Riccardi, Michael Lombardi, Robert Butters, Olga Kifor, Adam Sun, Matthias A Hediger, Jonathan Lytton, and Steven C Hebert. Cloning and characterization of an extracellular ca2+-sensing receptor from bovine parathyroid. *Nature*, 366(6455):575–580, 1993.

[32] David A Bushinsky, Krystof J Neumann, John Asplin, and Nancy S Krieger. Alendronate decreases urine calcium and supersaturation in genetic hypercalciuric rats. *Kidney international*, 55(1):234–243, 1999.

[33] David A Bushinsky, Krystof J Neumann, John Asplin, and Nancy S Krieger. Alendronate decreases urine calcium and supersaturation in genetic hypercalciuric rats. *Kidney international*, 55(1):234–243, 1999.

[34] Jing Chen, Anita T Layton, and Aurélie Edwards. A mathematical model of o2 transport in the rat outer medulla. i. model formulation and baseline results. *American Journal of Physiology-Renal Physiology*, 297(2):F517–F536, 2009.

[35] LINDA S Costanzo. Comparison of calcium and sodium transport in early and late rat distal tubules: effect of amiloride. *American Journal of Physiology-Renal Physiology*, 246(6):F937–F945, 1984.

[36] LINDA S Costanzo and ERICH E Windhager. Calcium and sodium transport by the distal convoluted tubule of the rat. *American Journal of Physiology-Renal Physiology*, 235(5):F492–F506, 1978.

[37] Joshua N Curry and Alan SL Yu. Paracellular calcium transport in the proximal tubule and the formation of kidney stones. *American Journal of Physiology-Renal Physiology*, 316(5):F966–F969, 2019.

[38] Marie Céleste de Jesus Ferreira, Cécile Hélies-Toussaint, Martine Imbert-Teboul, Claire Bailly, Jean-Marc Verbavatz, Anne-Christine Bellanger, and Danielle Chabardes. Co-expression of a ca2+-inhibitable adenylyl cyclase and of a ca2+-sensing receptor in the cortical thick ascending limb cell of the rat kidney: Inhibition

of hormone-dependent camp accumulation by extracellular ca2+. *Journal of Biological Chemistry*, 273(24):15192–15202, 1998.

[39] Georges Deschenes, Monika Wittner, ANTONIO DI STEFANO, Sylvie Jounier, and Alain Doucet. Collecting duct is a site of sodium retention in pan nephrosis: a rationale for amiloride therapy. *Journal of the American Society of Nephrology*, 12(3):598–601, 2001.

[40] John Devane and Michael P Ryan. The effects of amiloride and triamterene on urinary magnesium excretion in conscious saline-loaded rats. *British journal of pharmacology*, 72(2):285, 1981.

[41] A Di Stefano, N Roinel, C De Rouffignac, and M Wittner. Transepithelial ca2+ and mg2+ transport in the cortical thick ascending limb of henle's loop of the mouse is a voltage-dependent process. *Kidney and Blood Pressure Research*, 16(4):157–166, 1993.

[42] A Di Stefano, M Wittner, R Nitschke, R Braitsch, R Greger, C Bailly, C Amiel, N Roinel, and C De Rouffignac. Effects of parathyroid hormone and calcitonin on na+, cl-, k+, mg 2+ and ca 2+ transport in cortical and medullary thick ascending limbs of mouse kidney. *Pflügers Archiv*, 417:161–167, 1990.

[43] Sandra Donnelly. Why is erythropoietin made in the kidney? the kidney functions as a critmeter. *American journal of kidney diseases*, 38(2):415–425, 2001.

[44] Sophie Doublier, Enrico Lupia, Paola Catanuto, Simone Periera-Simon, Xiaomei Xia, Ken Korach, Mariana Berho, Sharon J Elliot, and Michael Karl. Testosterone and 17β-estradiol have opposite effects on podocyte apoptosis that precedes glomerulosclerosis in female estrogen receptor knockout mice. *Kidney international*, 79(4):404–413, 2011.

[45] D.L. Eaton and E.P. Gallagher. 1.01 - general overview of toxicology. In Charlene A. McQueen, editor, *Comprehensive Toxicology (Second Edition)*, pages 1–46. Elsevier, Oxford, second edition edition, 2010.

[46] Aurélie Edwards. Regulation of calcium reabsorption along the rat nephron: a modeling study. *American Journal of Physiology-Renal Physiology*, 308(6):F553–F566, 2015.

[47] Aurélie Edwards and Olivier Bonny. A model of calcium transport and regulation in the proximal tubule. *American Journal of Physiology-Renal Physiology*, 315(4):F942–F953, 2018.

[48] Mary K Findley and Michael Koval. Regulation and roles for claudin-family tight junction proteins. *IUBMB life*, 61(4):431–437, 2009.

[49] Kevin K Frick, John R Asplin, Murray J Favus, Christopher Culbertson, Nancy S Krieger, and David A Bushinsky. Increased biological response to 1, 25 (oh) 2d3 in genetic hypercalciuric stone-forming rats. *American Journal of Physiology-Renal Physiology*, 304(6):F718–F726, 2013.

[50] Kevin K Frick, John R Asplin, Murray J Favus, Christopher Culbertson, Nancy S Krieger, and David A Bushinsky. Increased biological response to 1, 25 (oh) 2d3 in genetic hypercalciuric stone-forming rats. *American Journal of Physiology-Renal Physiology*, 304(6):F718–F726, 2013.

[51] Peter A Friedman. Codependence of renal calcium and sodium transport. *Annual Review of Physiology*, 60(1):179–197, 1998.

[52] Peter A Friedman. Mechanisms of renal calcium transport. *Nephron Experimental Nephrology*, 8(6):343–350, 2000.

[53] Peter A Friedman. Renal calcium metabolism. *The kidney: physiology and pathophysiology*, 3:1749–1789, 2000.

[54] RP Garay and PJ Garrahan. The interaction of sodium and potassium with the sodium pump in red cells. *The Journal of Physiology*, 231(2):297–325, 1973.

[55] Dimitra Gkika, Yu-Juei Hsu, Annemiete W Van Der Kemp, Sylvia Christakos, René J Bindels, and Joost G Hoenderop. Critical role of the epithelial ca2+ channel trpv5 in active ca2+ reabsorption as revealed by trpv5/calbindin-d28k knockout mice. *Journal of the American Society of Nephrology*, 17(11):3020–3027, 2006.

[56] Yuchun Gu. Effects of [ca2+] i and ph on epithelial na+ channel activity of cultured mouse cortical collecting ducts. *Journal of Experimental Biology*, 211(19):3167–3173, 2008.

[57] Ho-Jae Han, Yeune-Hee Lee, and Soo-Hyun Park. Estradiol-17β-bsa stimulates ca2+ uptake through nongenomic pathways in primary rabbit kidney proximal tubule cells: Involvement of camp and pkc. *Journal of Cellular Physiology*, 183(1):37–44, 2000.

[58] Ramy M Hanna, Rebecca S Ahdoot, Kamyar Kalantar-Zadeh, Lena Ghobry, and Ira Kurtz. Calcium transport in the kidney and disease processes. *Frontiers in Endocrinology*, page 1721, 2022.

[59] Erich Heinz. Mechanics and energetics of biological transport. 2012.

[60] Warren G Hill, Michael B Butterworth, Huamin Wang, Robert S Edinger, Jonathan Lebowitz, Kathryn W Peters, Raymond A Frizzell, and John P Johnson. The epithelial sodium channel (enac) traffics to apical membrane in lipid rafts in mouse cortical collecting duct cells. *Journal of Biological Chemistry*, 282(52):37402–37411, 2007.

[61] Joost GJ Hoenderop, Dominik Müller, ANNEMIETE WCM VAN DER KEMP, Anita Hartog, Makoto Suzuki, Kenichi Ishibashi, Masashi Imai, Fred Sweep, Peter HGM Willems, CAREL H VAN OS, et al. Calcitriol controls the epithelial calcium channel in kidney. *Journal of the American Society of Nephrology*, 12(7):1342–1349, 2001.

[62] Jianghui Hou, Madhumitha Rajagopal, and Alan SL Yu. Claudins and the kidney. *Annual review of physiology*, 75:479–501, 2013.

[63] Wendy E Hoy, Michael D Hughson, John F Bertram, Rebecca Douglas-Denton, and Kerstin Amann. Nephron number, hypertension, renal disease, and renal failure. *Journal of the American Society of Nephrology*, 16(9):2557–2564, 2005.

[64] Yu-Juei Hsu, Henrik Dimke, Joost PH Schoeber, Shih-Che Hsu, Shih-Hua Lin, Pauling Chu, Joost GJ Hoenderop, and René JM Bindels. Testosterone increases urinary calcium excretion and inhibits expression of renal calcium transport proteins. *Kidney international*, 77(7):601–608, 2010.

[65] Rui Hu, Alicia A McDonough, and Anita T Layton. Functional implications of the sex differences in transporter abundance along the rat nephron: modeling and analysis. *American Journal of Physiology-Renal Physiology*, 317(6):F1462–F1474, 2019.

[66] Rui Hu, Alicia A McDonough, and Anita T Layton. Sex differences in solute transport along the nephrons: effects of na+ transport inhibition. *American Journal of Physiology-Renal Physiology*, 319(3):F487–F505, 2020.

[67] Thomas J Hund and Yoram Rudy. Rate dependence and regulation of action potential and calcium transient in a canine cardiac ventricular cell model. *Circulation*, 110(20):3168–3174, 2004.

[68] Couse Jf. Tissue distribution and quantitative analysis of estrogen receptor-alpha (eralpha) and estrogen receptor-beta (erbeta) messenger ribonucleic acid in the wild-type and eralpha-knockout mouse. *Endocrinology*, 138:4613–4621, 1997.

[69] PA Johnston and ST Kau. The effect of loop of henle diuretics on the tubuloglomerular feedback mechanism. *Methods and findings in experimental and clinical pharmacology*, 14(7):523–529, 1992.

[70] Rougin Khalil, Na Ri Kim, Ferran Jardi, Dirk Vanderschueren, Frank Claessens, and Brigitte Decallonne. Sex steroids and the kidney: role in renal calcium and phosphate handling. *Molecular and Cellular Endocrinology*, 465:61–72, 2018.

[71] PAUL Kofuji, WJ Lederer, and DH Schulze. Na/ca exchanger isoforms expressed in kidney. *American Journal of Physiology-Renal Physiology*, 265(4):F598–F603, 1993.

[72] Christopher S Kovacs. Calcium and bone metabolism during pregnancy and lactation. *Journal of mammary gland biology and neoplasia*, 10:105–118, 2005.

[73] Rajiv Kumar, Peter J Tebben, and James R Thompson. Vitamin d and the kidney. *Archives of biochemistry and biophysics*, 523(1):77–86, 2012.

[74] Girishkumar Kaitholil Kumaran and Israel Hanukoglu. Identification and classification of epithelial cells in nephron segments by actin cytoskeleton patterns. *The FEBS Journal*, 287(6):1176–1194, 2020.

[75] William E Lassiter, Carl W Gottschalk, and Margaret Mylle. Micropuncture study of renal tubular reabsorption of calcium in normal rodents. *American Journal of Physiology-Legacy Content*, 204(5):771–775, 1963.

[76] Anita T Layton. A mathematical model of the urine concentrating mechanism in the rat renal medulla. i. formulation and base-case results. *American Journal of Physiology-Renal Physiology*, 300(2):F356–F371, 2011.

[77] Anita T Layton, Aurélie Edwards, Anita T Layton, and Aurélie Edwards. Transport across tubular epithelia. *Mathematical Modeling in Renal Physiology*, pages 155–183, 2014.

[78] Anita T Layton and Michelle L Gumz. Sex differences in circadian regulation of kidney function of the mouse. *American Journal of Physiology-Renal Physiology*, 323(6):F675–F685, 2022.

[79] Anita T Layton, Kamel Laghmani, Volker Vallon, and Aurélie Edwards. Solute transport and oxygen consumption along the nephrons: effects of na+ transport inhibitors. *American Journal of Physiology-Renal Physiology*, 311(6):F1217–F1229, 2016.

[80] Anita T Layton and Harold E Layton. A computational model of epithelial solute and water transport along a human nephron. *PLoS computational biology*, 15(2):e1006108, 2019.

[81] Anita T Layton and Volker Vallon. Sglt2 inhibition in a kidney with reduced nephron number: modeling and analysis of solute transport and metabolism. *American Journal of Physiology-Renal Physiology*, 314(5):F969–F984, 2018.

[82] Anita T Layton, Volker Vallon, and Aurélie Edwards. Predicted consequences of diabetes and sglt inhibition on transport and oxygen consumption along a rat nephron. *American Journal of Physiology-Renal Physiology*, 310(11):F1269–F1283, 2016.

[83] Christian Le Grimellec, Nicole Roinel, Francois Morel, P Philippe, and P Malorey. Simultaneous mg, ca, p, k, na and cl analysis in rat tubular fluid: I. during perfusion of either inulin or ferrocyanide. *Pflügers Archiv*, 340:181–196, 1973.

[84] WP Leary, AJ Reyes, RD Wynne, and K Van der Byl. Renal excretory actions of furosemide, of hydrochlorothiazide and of the vasodilator flosequinan in healthy subjects. *Journal of international medical research*, 18(2):120–141, 1990.

[85] Chien-Te Lee, Hung-Chun Chen, Li-Wen Lai, Kim-Chong Yong, and Yeong-Hau H Lien. Effects of furosemide on renal calcium handling. *American Journal of Physiology-Renal Physiology*, 293(4):F1231–F1237, 2007.

[86] CT Lee, YH H Lien, LW Lai, JB Chen, CR Lin, and HC Chen. Increased renal calcium and magnesium transporter abundance in streptozotocin-induced diabetes mellitus. *Kidney international*, 69(10):1786–1791, 2006.

[87] Jae Wook Lee, Chung-Lin Chou, and Mark A Knepper. Deep sequencing in microdissected renal tubules identifies nephron segment–specific transcriptomes. *Journal of the American Society of Nephrology*, 26(11):2669–2677, 2015.

[88] Jason Lee, Seung-Kuy Cha, Tie-Jun Sun, and Chou-Long Huang. Pip2 activates trpv5 and releases its inhibition by intracellular mg2+. *The Journal of general physiology*, 126(5):439–451, 2005.

[89] DAVID LEPPLA, RICHARD BROWNE, KATHY HILL, and CHARLES YC PAK. Effect of amiloride with or without hydrochlorothiazide on urinary calcium and saturation of calcium salts. *The Journal of Clinical Endocrinology & Metabolism*, 57(5):920–924, 1983.

[90] Joseph Levy, James R Gavin III, and James R Sowers. Diabetes mellitus: a disease of abnormal cellular calcium metabolism? *The American journal of medicine*, 96(3):260–273, 1994.

[91] Qianyi Li, Alicia A McDonough, Harold E Layton, and Anita T Layton. Functional implications of sexual dimorphism of transporter patterns along the rat proximal tubule: modeling and analysis. *American Journal of Physiology-Renal Physiology*, 315(3):F692–F700, 2018.

[92] YH Li. S. g regory. 1974. diffusion of ions in sea water and in deep-sea sediments. *Geochim. Cosmochim. Acta*, 38:703–714, 1974.

[93] Johannes Loffing and Christoph Korbmacher. Regulated sodium transport in the renal connecting tubule (cnt) via the epithelial sodium channel (enac). *Pflügers Archiv-European Journal of Physiology*, 458:111–135, 2009.

[94] Johannes Loffing, Dominique Loffing-Cueni, Victor Valderrabano, Lea Klausli, Steven C Hebert, Bernard C Rossier, Joost GJ Hoenderop, René JM Bindels, and Brigitte Kaissling. Distribution of transcellular calcium and sodium transport pathways along mouse distal nephron. *American Journal of Physiology-Renal Physiology*, 281(6):F1021–F1027, 2001.

[95] John N Lorenz, Patrick J Schultheis, Timothy Traynor, Gary E Shull, and Jurgen Schnermann. Micropuncture analysis of single-nephron function in nhe3-deficient mice. *American Journal of Physiology-Renal Physiology*, 277(3):F447–F453, 1999.

[96] Alexandre Loupy, Suresh Krishna Ramakrishnan, Bharath Wootla, Régine Chambrey, Renaud de La Faille, Soline Bourgeois, Patrick Bruneval, Chantal Mandet, Erik Ilso Christensen, Hélène Faure, et al. Pth-independent regulation of blood calcium concentration by the calcium-sensing receptor. *The Journal of clinical investigation*, 122(9):3355–3367, 2012.

[97] Lois Lockard MacKay and Eaton M MacKay. Factors which determine renal weight: Ii. age. *American Journal of Physiology-Legacy Content*, 83(1):191–195, 1927.

[98] B Mandon, E Siga, N Roinel, and C De Rouffignac. Ca 2+, mg 2+ and k+ transport in the cortical and medullary thick ascending limb of the rat nephron: influence of transepithelial voltage. *Pflügers Archiv*, 424:558–560, 1993.

[99] S Michael Mauer, Michael W Steffes, and David M Brown. The kidney in diabetes. *The American journal of medicine*, 70(3):603–612, 1981.

[100] Charlene McQueen. *Comprehensive toxicology*. Elsevier, 2017.

[101] Shunsuke Miura, Akiomi Yoshihisa, Mai Takiguchi, Takeshi Shimizu, Yuichi Nakamura, Hiroyuki Yamauchi, Shoji Iwaya, Takashi Owada, Makiko Miyata, Satoshi Abe, et al. Association of hypocalcemia with mortality in hospitalized patients with heart failure and chronic kidney disease. *Journal of Cardiac Failure*, 21(8):621–627, 2015.

[102] Matthias B Moor and Olivier Bonny. Ways of calcium reabsorption in the kidney. *American Journal of Physiology-Renal Physiology*, 310(11):F1337–F1350, 2016.

[103] Matthias B Moor and Olivier Bonny. Ways of calcium reabsorption in the kidney. *American Journal of Physiology-Renal Physiology*, 310(11):F1337–F1350, 2016.

[104] Robert Moss and S Randall Thomas. Hormonal regulation of salt and water excretion: a mathematical model of whole kidney function and pressure natriuresis. *American Journal of Physiology-Renal Physiology*, 306(2):F224–F248, 2014.

[105] KAREN Munger and CHRISTINE Baylis. Sex differences in renal hemodynamics in rats. *American Journal of Physiology-Renal Physiology*, 254(2):F223–F231, 1988.

[106] RC Ng, Diane Rouse, Wadi N Suki, et al. Calcium transport in the rabbit superficial proximal convoluted tubule. *The Journal of clinical investigation*, 74(3):834–842, 1984.

[107] Tom Nijenhuis, Volker Vallon, Annemiete WCM van der Kemp, Johannes Loffing, Joost GJ Hoenderop, René JM Bindels, et al. Enhanced passive ca 2+ reabsorption and reduced mg 2+ channel abundance explains thiazide-induced hypocalciuria and hypomagnesemia. *The Journal of clinical investigation*, 115(6):1651–1658, 2005.

[108] BE CHRISTOPHER NORDIN, ALLAN G NEED, HOWARD A MORRIS, MICHAEL HOROWITZ, and WILLIAM G ROBERTSON. Evidence for a renal calcium leak in postmenopausal women. *The Journal of Clinical Endocrinology & Metabolism*, 72(2):401–407, 1991.

[109] Mona Oppermann, Diane Mizel, Soo Mi Kim, Limeng Chen, Robert Faulhaber-Walter, Yuning Huang, Cuiling Li, Chuxia Deng, Josie Briggs, Jurgen Schnermann, et al. Renal function in mice with targeted disruption of the a isoform of the na-k-2cl co-transporter. *Journal of the American Society of Nephrology*, 18(2):440–448, 2007.

[110] Wanling Pan, Jelena Borovac, Zachary Spicer, Joost G Hoenderop, René J Bindels, Gary E Shull, Michael R Doschak, Emmanuelle Cordat, and R Todd Alexander. The epithelial sodium/proton exchanger, nhe3, is necessary for renal and intestinal calcium (re) absorption. *American Journal of Physiology-Renal Physiology*, 302(8):F943–F956, 2012.

[111] Allein Plain, Wanling Pan, Deborah O'Neill, Megan Ure, Megan R Beggs, Maikel Farhan, Henrik Dimke, Emmanuelle Cordat, and R Todd Alexander. Claudin-12 knockout mice demonstrate reduced proximal tubule calcium permeability. *International journal of molecular sciences*, 21(6):2074, 2020.

[112] Martin R Pollak, Susan E Quaggin, Melanie P Hoenig, and Lance D Dworkin. The glomerulus: the sphere of influence. *Clinical Journal of the American Society of Nephrology*, 9(8):1461–1469, 2014.

[113] JC Prior. Progesterone as a bone-trophic hormone. *Endocrine Reviews*, 11(2):386–398, 1990.

[114] Gary A Quamme. Renal magnesium handling: new insights in understanding old problems. *Kidney international*, 52(5):1180–1195, 1997.

[115] Marcus Quinkler, Iwona J Bujalska, Kirren Kaur, Claire U Onyimba, Sabine Buhner, Bruno Allolio, Susan V Hughes, Martin Hewison, and Paul M Stewart. Androgen receptor–mediated regulation of the α-subunit of the epithelial sodium channel in human kidney. *Hypertension*, 46(4):787–798, 2005.

[116] S Ramakrishnan, A Loupy, A Edwards, DA Bushinsky, and P Houillier. Genetic hypercalciuria stone-forming rats have a decrease in paracellular permeability to calcium in the cortical thick ascending limb. *J Am Soc Nephrol*, 23:43A, 2012.

[117] Kirsten Y Renkema, Ana Velic, Henry B Dijkman, Sjoerd Verkaart, Annemiete W Van Der Kemp, Marta Nowik, Kim Timmermans, Alain Doucet, Carsten A Wagner, Rene J Bindels, et al. The calcium-sensing receptor promotes urinary acidification to prevent nephrolithiasis. *Journal of the American Society of Nephrology: JASN*, 20(8):1705, 2009.

[118] Kirsten Y Renkema, Ana Velic, Henry B Dijkman, Sjoerd Verkaart, Annemiete W van der Kemp, Marta Nowik, Kim Timmermans, Alain Doucet, Carsten A Wagner, Rene J Bindels, et al. The calcium-sensing receptor promotes urinary acidification to prevent nephrolithiasis. *Journal of the American Society of Nephrology*, 20(8):1705–1713, 2009.

[119] Daniela Riccardi, Martin Traebert, Donald T Ward, Brigitte Kaissling, Jürg Biber, Steven C Hebert, and Heini Murer. Dietary phosphate and parathyroid hormone alter the expression of the calcium-sensing receptor (car) and the na+-dependent p i transporter (napi-2) in the rat proximal tubule. *Pflügers Archiv*, 441:379–387, 2000.

[120] ANTONINO S RocHA, JB Magaldi, JP Kokko, et al. Calcium and phosphate transport in isolated segments of rabbit henle's loop. *The Journal of clinical investigation*, 59(5):975–983, 1977.

[121] GIULIO ROMANO, GRAZIA FAVRET, EDDA FEDERICO, and ETTORE BARTOLI. The site of action of furosemide. *Pharmacological Research*, 37(5):409–419, 1998.

[122] Monica B Sandberg, Arvid B Maunsbach, and Alicia A McDonough. Redistribution of distal tubule na+-cl- cotransporter (ncc) in response to a high-salt diet. *American Journal of Physiology-Renal Physiology*, 291(2):F503–F508, 2006.

[123] JM Sands, M Naruse, M Baum, I Jo, SC Hebert, EM Brown, HW Harris, et al. Apical extracellular calcium/polyvalent cation-sensing receptor regulates vasopressin-elicited water permeability in rat kidney inner medullary collecting duct. *The Journal of clinical investigation*, 99(6):1399–1405, 1997.

[124] JM Sands, M Naruse, M Baum, I Jo, SC Hebert, EM Brown, HW Harris, et al. Apical extracellular calcium/polyvalent cation-sensing receptor regulates vasopressin-elicited water permeability in rat kidney inner medullary collecting duct. *The Journal of clinical investigation*, 99(6):1399–1405, 1997.

[125] Patricia A Schenck, Dennis J Chew, Larry A Nagode, Thomas J Rosol, et al. Disorders of calcium: hypercalcemia and hypocalcemia. *Fluid, electrolyte, and acid-base disorders in small animal practice*, 4:120–94, 2006.

[126] Benjamin Schoener and Judith Borger. Erythropoietin stimulating agents. In *StatPearls [Internet]*. StatPearls Publishing, 2022.

[127] Donald W Seldin. Renal handling of calcium. *Nephron*, 81(Suppl. 1):2–7, 1999.

[128] Lesley A Stevens, Josef Coresh, Tom Greene, and Andrew S Levey. Assessing kidney function—measured and estimated glomerular filtration rate. *New England Journal of Medicine*, 354(23):2473–2483, 2006.

[129] J Strieter, JOHN L Stephenson, GERHARD Giebisch, and ALAN M Weinstein. A mathematical model of the rabbit cortical collecting tubule. *American Journal of Physiology-Renal Physiology*, 263(6):F1063–F1075, 1992.

[130] Wadi N Suki. Calcium transport in the nephron. *American Journal of Physiology-Renal Physiology*, 237(1):F1–F6, 1979.

[131] AM Sun, Y Liu, LD Dworkin, Chung Ming Tse, Mark Donowitz, and KP Yip. Na+/h+ exchanger isoform 2 (nhe2) is expressed in the apical membrane of the medullary thick ascending limb. *The Journal of membrane biology*, 160:85–90, 1997.

[132] Yuanhua Tang and John L Stephenson. Calcium dynamics and homeostasis in a mathematical model of the principal cell of the cortical collecting tubule. *The Journal of general physiology*, 107(2):207–230, 1996.

[133] Magali Tournus, Nicolas Seguin, Benoît Perthame, S Randall Thomas, and Aurélie Edwards. A model of calcium transport along the rat nephron. *American Journal of Physiology-Renal Physiology*, 305(7):F979–F994, 2013.

[134] Yusuke Tsukamoto, Satoshi Saka, and Michiyo Saitoh. Parathyroid hormone stimulates atp-dependent calcium pump activity by a different mode in proximal and distal tubules of the rat. *Biochimica et Biophysica Acta (BBA)-Biomembranes*, 1103(1):163–171, 1992.

[135] Shuichi Tsuruoka, David A Bushinsky, and George J Schwartz. Defective renal calcium reabsorption in genetic hypercalciuric rats. *Kidney international*, 51(5):1540–1547, 1997.

[136] Shuichi Tsuruoka, David A Bushinsky, and George J Schwartz. Defective renal calcium reabsorption in genetic hypercalciuric rats. *Kidney international*, 51(5):1540–1547, 1997.

[137] Karl J Ullrich, Bodil Schmidt-Nielsen, Roberta O'Dell, Gundula Pehling, Carl W Gottschalk, William E Lassiter, and Margaret Mylle. Micropuncture study of composition of proximal and distal tubular fluid in rat kidney. *American Journal of Physiology-Legacy Content*, 204(4):527–531, 1963.

[138] Volker Vallon, Jan-Robert Schwark, Kerstin Richter, and Max Hropot. Role of na+/h+ exchanger nhe3 in nephron function: micropuncture studies with s3226, an inhibitor of nhe3. *American Journal of Physiology-Renal Physiology*, 278(3):F375–F379, 2000.

[139] Luciana C Veiras, Adriana CC Girardi, Joshua Curry, Lei Pei, Donna L Ralph, An Tran, Regiane C Castelo-Branco, Nuria Pastor-Soler, Cristina T Arranz, SL Alan, et al. Sexual dimorphic pattern of renal transporters and electrolyte homeostasis. *Journal of the American Society of Nephrology*, 28(12):3504–3517, 2017.

[140] Miriam A Wallace. Anatomy and physiology of the kidney. *AORN journal*, 68(5):799–820, 1998.

[141] WH Wang, MING Lu, and STEVEN C Hebert. Cytochrome p-450 metabolites mediate extracellular ca (2+)-induced inhibition of apical k+ channels in the tal. *American Journal of Physiology-Cell Physiology*, 271(1):C103–C111, 1996.

[142] Ning Wei, Michelle L Gumz, and Anita T Layton. Predicted effect of circadian clock modulation of nhe3 of a proximal tubule cell on sodium transport. *American Journal of Physiology-Renal Physiology*, 315(3):F665–F676, 2018.

[143] ALAN M Weinstein. A mathematical model of the rat proximal tubule. *American Journal of Physiology-Renal Physiology*, 250(5):F860–F873, 1986.

[144] Alan M Weinstein. Mathematical models of tubular transport. *Annual review of physiology*, 56(1):691–709, 1994.

[145] Alan M Weinstein. A kinetically defined na+/h+ antiporter within a mathematical model of the rat proximal tubule. *The Journal of general physiology*, 105(5):617–641, 1995.

[146] Alan M Weinstein. Mathematical models of renal fluid and electrolyte transport: acknowledging our uncertainty. *American Journal of Physiology-Renal Physiology*, 284(5):F871–F884, 2003.

[147] Alan M Weinstein. A mathematical model of rat distal convoluted tubule. ii. potassium secretion along the connecting segment. *American Journal of Physiology-Renal Physiology*, 289(4):F721–F741, 2005.

[148] Alan M Weinstein. A mathematical model of rat ascending henle limb. iii. tubular function. *American Journal of Physiology-Renal Physiology*, 298(3):F543–F556, 2010.

[149] Alan M Weinstein. A mathematical model of rat proximal tubule and loop of henle. *American Journal of Physiology-Renal Physiology*, 308(10):F1076–F1097, 2015.

[150] Alan M Weinstein, Sheldon Weinbaum, Yi Duan, Zhaopeng Du, QingShang Yan, and Tong Wang. Flow-dependent transport in a mathematical model of rat proximal tubule. *American Journal of Physiology-Renal Physiology*, 292(4):F1164–F1181, 2007.

[151] M Wittner, A Di Stefano, P Wangemann, R Nitschke, R Greger, C Bailly, C Amiel, N Roinel, and C De Rouffignac. Differential effects of adh on sodium, chloride, potassium, calcium and magnesium transport in cortical and medullary thick ascending limbs of mouse nephron. *Pflügers Archiv*, 412(5):516–523, 1988.

[152] Fred S Wright, Jürgen Schnermann, et al. Interference with feedback control of glomerular filtration rate by furosemide, triflocin, and cyanide. *The Journal of clinical investigation*, 53(6):1695–1708, 1974.

[153] Yufeng Xu, Xiaoying Wang, and Xuexiang Jiang. Relationship between the renal apparent diffusion coefficient and glomerular filtration rate: preliminary experience. *Journal of Magnetic Resonance Imaging: An Official Journal of the International Society for Magnetic Resonance in Medicine*, 26(3):678–681, 2007.

[154] Li Yuan-Hui and Sandra Gregory. Diffusion of ions in sea water and in deep-sea sediments. *Geochimica et Cosmochimica Acta*, 38(5):703–714, 1974.

[155] MI Zhang and ROGER G O'Neil. Regulated calcium channel in apical membranes renal proximal tubule cells. *American Journal of Physiology-Cell Physiology*, 271(5):C1757–C1764, 1996.